Fabrication and Characterization of White Light Emission Organic Light-Emitting Devices

by

Han-Jen Yang

Department of Electrical and Computer Engineering
McGill University, Montreal

February 2006

A thesis submitted to McGill University in partial fulfillment of the requirements of the degree of Master of Engineering

Your file Votre référence
ISBN: 978-0-494-25019-8
Our file Notre référence
ISBN: 978-0-494-25019-8

Abstract

Organic light emitting devices (OLED) based on small molecule materials capable of white light emission have been fabricated and electrical and optical performance of devices was characterized. The fabricated OLEDs utilize one hole transport material, *N*, *N*′-diphenyl-*N*, *N*′-bis(3-methylphenyl)-1, 1′-biphenyl-4, 4′-diamine [TPD], and three light emitting materials including 4, 4′-bis(2, 2′-diphenylvinyl)-1, 1′-biphenyl [DPVBi], Tris-(1-phenylisoquinolinato-N) iridium (III) [$Ir(piq)_3$], and tris- (8-hydroxyquinoline) aluminium [Alq_3] to achieve the color blending close to the white light. The overall OLED configuration is in a multi-layer stacking structure. A total of 6 different OLED layer thickness configurations were implemented to investigate the effect of the layer thickness parameters. In one particular configuration, the CIE color coordinates range from (0.357,0.358) at 140.4 cd/m^2 to (0.303,0.360) at 1321.7 cd/m^2, which indicates adequate color stability in the medium to high luminance range. The luminance value of 1321.7 cd/m^2 at the current density of 64.9 mA/cm^2 and the operating voltage of 14 V indicates that the device is capable of producing a relatively high level of brightness while operating at relatively low operating voltage and low driving current density.

Résumé

Des diodes électroluminescentes organiques (OLED) faites de matériaux composés de petites molécules ont été fabriqués. Les OLEDs sont capables d'émettre de la lumière blanche et ont été caractérisés par des mesures électriques et optiques. Ces dispositifs sont fait d'un matériau de porteurs positifs qui contient N, *N*′-diphenyl-*N*, *N*′-bis(3-methylphenyl)-1, 1′-biphenyl-4, 4′-diamine [TPD] et de trois autres matériaux électroluminescent soient 4, 4′-bis(2, 2′-diphenylvinyl)-1, 1′-biphenyl [DPVBi], Tris-(1-phenylisoquinolinato-N) iridium (III) [$Ir(piq)_3$], et tris- (8-hydroxyquinoline) aluminium [Alq_3]. La structure générale des dispositifs est un empilement multicouche de matériaux organiques. Les diodes fabriquées avec les matériaux ont une couleur proche de la lumière blanche. Au total, six configurations différentes d'épaisseurs de couches de matériaux OLED ont été étudiées afin d'analyser les effets liés à l'épaisseur. Avec une configuration particulière, les coordonnées de couleurs CIE varient entre (0.357, 0.358) à un niveau de luminance de 140.4 cd/m^2 et (0.303,0.360) à 1321.7 cd/m^2. Ces résultats indiquent que une bonne stabilité sun la gamme de moyenne à forte lumincence. Un niveau de luminance de 1321.7 cd/m^2 est obtenu avec une densité de courant de 64.9 mA/cm^2 et tension une de 14 V. En conclusion, le dispositif est capable de produire un

haut niveau de luminosité avec une faible tension d'opération et une faible densité de courant.

Acknowledgements

First and the most important of all, I would like to express my sincere appreciations to my supervisor, Dr. Ishiang Shih, for his exceptional guidance, knowledgeable advices, and thoughtful considerations throughout this research work. Also, I would like to thank all my colleagues for their assistance, valuable advices, and thoughtful discussions during this research work.

Great appreciation also goes to Steven Xiao at Organic Vision and Steve Qiu at CIS Scientific for their helpful discussions, kind patience, and support. Not to mention all the help they have given me while I was doing my measurements.

I would also like to thank both Hung-Pao Yang and Jeanne Shih for translating the abstract into French and the revision of the French abstract.

Last but not the least, I would like to thank my friends and family for their unconditional and complete support and encouragements.

Table of Contents

Abstract i

Résumé ii

Acknowledgements iv

Table of Contents v

Chapter 1 Introduction 1

1.1 Overview of Organic Light-Emitting Devices 1

1.2 Research Objectives 4

Chapter 2 Fundamentals of Organic Light-Emitting Devices 8

2.1 Overview 8

2.2 Basic Electronic Structure of π–conjugated Organic Materials 8

2.3 Basic Structure of OLED 11

2.4 Basic Operation of OLED 14

2.5 Light Emission Process in OLED 16

2.6 Degradation Mechanisms 21

2.7 Realization of White OLED 22

2.7.1 Organic material selection 22

2.7.2 Electrode contact material selection 30

2.7.3 Proposed OLED structure 32

2.8 Summary 34

Chapter 3 Fabrication of Organic Light-Emitting Devices 38

3.1 Overview 38

3.2 Preparations of Fabrication 41

3.2.1 Experimental setup 41

3.2.2 Calibration of film thickness monitor 47

3.3 Fabrication Procedure 50

3.3.1 Process flow chart 50

3.3.2 Substrate preparation 52

3.3.3 ITO electrode patterning 53

3.3.4 Thermal vacuum deposition of the organic material 55

3.3.5 Thermal evaporation of top metal contact 60

3.4 Summary 61

Chapter 4 Device Characterization 63

4.1 Overview 63

4.2 Measurement setup 64

4.3 Current-voltage characteristics 68

4.4 Device Luminance 71

4.4.1 Luminous flux 71

4.4.2 Lambertian emission 74

4.4.3 Luminous intensity 76

4.4.4 Calculation of attenuation ratio γ 78

4.4.5 Luminance 79

4.4.6 Device Luminance 80

4.5 Luminous Efficiency 85

4.6 External Quantum Efficiency 88

4.7 CIE Color Coordinates 92

4.7.1 Color-matching functions and XYZ tristimulus values 93

4.7.2 CIE color coordinates 98

4.7.3 CIE chromaticity diagram and CIE standard illuminants 99

4.7.4 Device CIE color coordinates 101

4.8 Conclusions 115

Chapter 5 Conclusions and Future Work **120**

5.1 Thesis Summary 120

5.2 Future Work 123

Chapter 1

Introduction

1.1 Overview of Organic Light-Emitting Devices

Organic light-emitting devices (OLEDs) have attracted great interests and have rapidly developed ever since the first functional demonstration was reported by Tang and Van Slyke almost two decades ago [1-1]. Commercial OLED displays are now available and are being used in mobile device applications such as mobile phone, mp3 player, and others. Large-size full-color OLED display prototypes fabricated by various companies for applications such as computer monitor and television have also been demonstrated. Research prototypes for flexible display application have also been reported and demonstrated [1-2]. The projected roadmap for OLED is very promising for a wide variety of applications [1-3].

Tremendous amount of research effort has been devoted to OLED displays as OLEDs have wide-ranging potential applications due to their intrinsic feature of wide-angle viewing, high contrast, fast response, low power consumption, and light weight. Besides these, OLEDs also have several other notable advantages when

compared to other display technology: (1) possible lower cost and relative ease of fabrication, (2) chemical tunability of the organic materials used in OLED, and (3) flexibility of the OLED.

The large-scale implementation of the synthesis and production process of organic materials is usually easier and less expensive than inorganic materials. The existing silicon-based semiconductor device fabrication processes require expensive equipments and facilities such as ultra-high vacuum, clean rooms and high-temperature furnaces. Contrarily, the fabrication of organic semiconductor devices utilizes simpler methods such as spin coating, ink-jet printing and simple vacuum deposition. The relative ease of fabrication methods employed by OELDs also implies easier and less costly production scale-up for the large-size devices. For organic materials, the electrical and optical properties are related to the molecular composition and crystal structure of the material. This means that the alteration of electrical and optical properties such as energy band gap characteristics, charge carrier mobility, light absorption spectrum, and light emission spectrum can possibly be achieved by chemically tuning the molecular structure of the materials. The typical OLEDs usually have a total active layer thickness in the order of a few hundred nanometers and are light weight. The thin and light-weight nature of the OLEDs is especially advantageous for mobile applications. The active material

composition of an OLED is also very suitable for flexible substrates. The flexible nature of OLED makes it one of the known leading candidates for the flexible display applications. Of course, the OLED is not without its shortcomings. Improvements still need to be achieved on various aspects such as power-efficiency, luminescent efficiency, and packaging to reduce device degradation. The packaging and encapsulation issue is very critical in order to minimize the effects of several factors such as the high sensitivity of the materials toward environment, non-linear degradation behavior over the device lifetime, and material lifetime. If the effects of these factors are not minimized, the reliability and stability of OLED performance over time will be greatly hampered.

Among the various activities in the OLED field, the research on white OLED (WOLED) has received special attention due to the potential application of this technology for general solid-state lighting applications and backlight in flat-panel displays. The challenges facing WOLED technology are mainly due to the limited wavelength band of light emission from typical organic materials, which at most only covers about one third of the visible spectrum. Presently, in order to produce light emission in the blue, green, or red portion of the visible spectrum, OLEDs must be fabricated using materials prepared by chemical tuning with a variety of molecular structures and their derivatives. No single organic material capable of efficient emission

across the entire visible spectrum has been developed so far. For producing high-quality white light, it is necessary to have a device capable of producing efficient broad-spectrum emission covering the entire visible spectrum. For this reason, WOLEDs typically require incorporating multiple light emitting organic materials in order to achieve broadband emission spanning across the entire visible spectrum. Due to the necessity of multiple organic light emitting materials in the WOLED, a number of design approaches on device structure have been explored and experimented [1-4].

1.2 Research Objectives

The main objective of this research project is to fabricate a functional white OLED using selected materials and design structure. The three specific objectives are: (1) to identify and implement an OLED design which leads to successful realization of the multi-color OLEDs which in turn, produce colors close to a white light source, (2) to evaluate the electrical and optical properties of the devices, and (3) to identify and fine tune the device layer thickness to have the closest white color emission.

Identification of OLED design involves the selection of organic semiconducting materials for the OLED, the design of the OLED structure, and the development of a

fabrication processes. As mentioned earlier in this chapter, light emission from typical organic materials does not cover the entire visible spectrum. Hence, multiple light emission materials are often required to produce broad-spectrum light emission close to white color. Three well-known small molecule organic semiconductor materials for OLEDs, *N*, *N*′-diphenyl-*N*, *N*′-bis(3-methylphenyl)-1, 1′-biphenyl-4, 4′-diamine [TPD], tris- (8-hydroxyquinoline) aluminium [Alq3], and 4, 4′-bis(2, 2′-diphenylvinyl)-1, 1′-biphenyl [DPVBi] are chosen for the present work because of their relatively good performance and good availability. TPD is used as hole transport material; DPVBi is used as the light emitting material for the blue photoluminescence; and Alq3 is used as both the light emitting material for the green photoluminescence and the electron transport material. Additionally, one organic phosphorescent material, tris- (1-phenylisoquinolinato -N) iridium (III) [Ir(piq)3], is chosen as the red light emitting material. The above selection of light-emitting organic materials covers the three primary colors and should theoretically produce broad-spectrum light emission close to the white color, if mixed in the proper ratio. With the selection of the above-mentioned materials, multiple emissive layer stacking structure OLED configuration design is best suited as there are two electroluminescent materials. Lastly, the realization of the OLEDs cannot be accomplished without the development of a complete fabrication procedure.

Device characterization is required to examine the electrical and optical properties of the fabricated OLEDs. Two major measurements are performed in the present work: current-voltage characteristics and emission spectrum measurements. Further analysis is also performed on the raw data obtained to determine other device characteristics such as device brightness, device efficiency, and emission color. With such data in hand, the OLED configuration with emission color closest to the white color can be easily identified for possible further fine-tuning of the devices.

This thesis contains five chapters. The first chapter covers an introduction to organic light emitting devices and the research objectives. Chapter 2 briefly describes the basic operations and construction principles of the organic light emitting devices, and a description of the light emission mechanism. The material selection and the implemented OLED structure are also discussed in chapter 2. Chapter 3 provides information on the fabrication of the OLED, which includes the experimental setup and the fabrication procedure. Chapter 4 covers the device characterization on both the device electrical properties and optical properties. The derivations of various device characteristics such as luminance, luminous efficiency, external quantum efficiency, emission spectra, and CIE color coordinates and their analysis are also discussed in the chapter 4. The final chapter, chapter 5, provides the summary of the thesis and possible future research activities.

[1-1] C.W. Tang and S.A. Van Slyke, *Appl. Phys. Lett.* **1987**, *51*, 913.

[1-2] Gregory P. Crawford ed., *Flexible Flat Panel Displays*, John Wiley & Sons, West Sussex, England, **2005**.

[1-3] J.N. Bardsley, *IEEE Journal on Selected Topics in Quantum Electronics* **2004**, *10*, no. 1, 3.

[1-4] B.W. D'Andrade and S.R. Forrest, *Adv. Mater.* **2004**, *16*, *No. 18*, 1585.

Chapter 2

Fundamentals of Organic Light-Emitting Devices

2.1 Overview

The fundamentals of organic light emitting devices (OLEDs) include the basics of organic materials, the basic structures of OLEDs, the basic operation mechanism of OLED such as charge carrier injection and transport, the degradation mechanism of the OLEDs, and most importantly, the light-emitting process. This chapter will attempt to provide a brief discussion on each aspect of the OLED fundamentals. A more detailed description of each above-mentioned aspect can be found in books such as *Organic light-emitting devices : a survey*, edited by Joseph Shinar (2004) [2-1].

2.2 Basic Electronic Structure of π–conjugated Organic Materials

Most luminescent organic materials are π–conjugated compounds, which are materials in which single and double or single and triple bonds alternate throughout

molecules or the polymer backbone. The first bond of a double or triple bond is a sigma bond and the rest are π bonds. In other words, the second bond and third bond of a double or triple bond are π bonds. π bonds are formed from the overlapping atomic p_z or p_y orbitals. Due to the overlap of the π orbital wave functions of adjacent carbon atoms, the electrons occupying π orbitals are relatively delocalized. The delocalized π-bonding systems give rise to energy bands, which are similar to those in an inorganic semiconductor material. The occupied π ortibal, comprised of hole transport states, is analogous to the valence band. The unoccupied π* orbital, comprised of electron transport states, is analogous to the conduction band. The highest occupied molecular π orbital (HOMO) is analogous to the valence band edge and the lowest unoccupied molecular π orbital (LUMO) is analogous to the conduction band edge. The gap between HOMO and LUMO is analogous to the energy band gap. Figure 2-1 shows the delocalized π-bonding system in a benzene ring chemical structure and also the energy band and the HOMO and LUMO energy levels in a π–conjugated material.

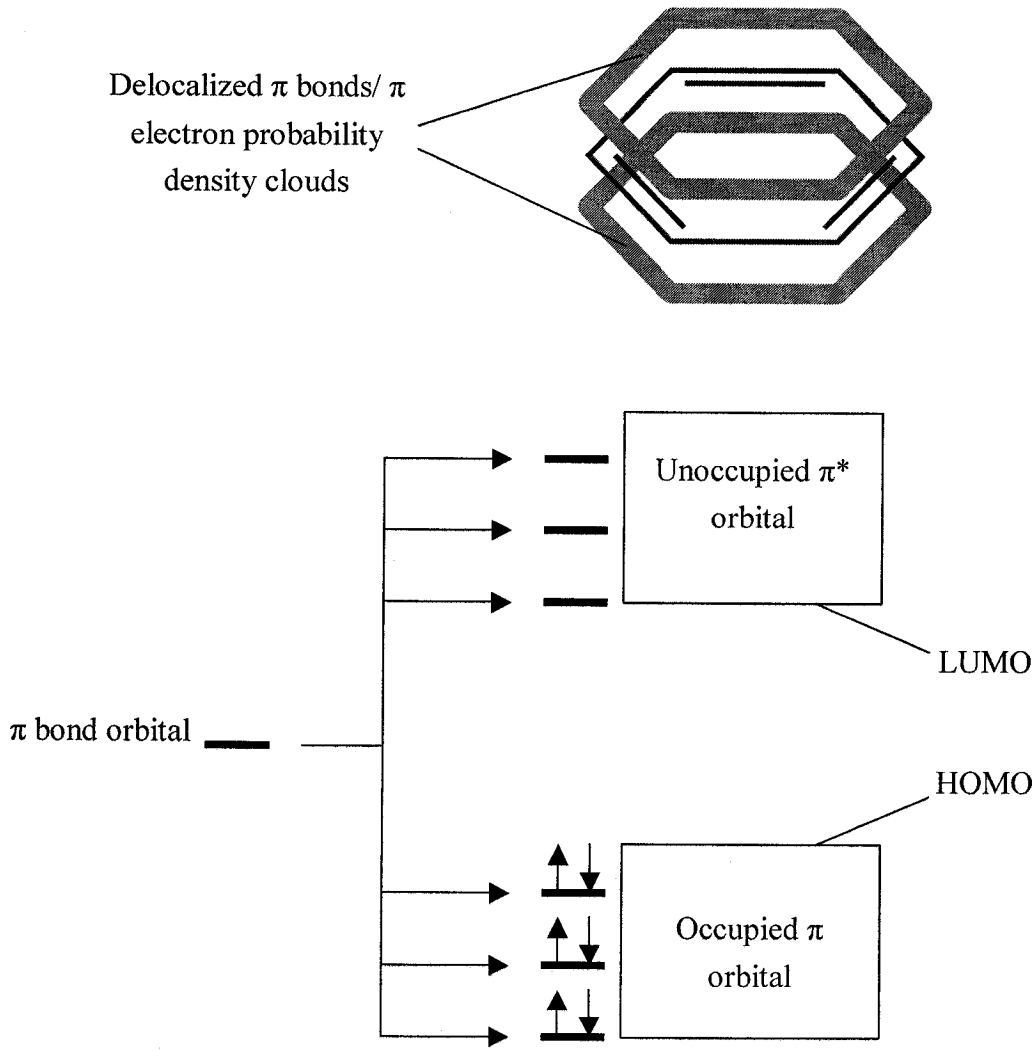

Figure 2-1: (top) A diagram showing the delocalized π bonds in a benzene ring chemical structure; (bottom) A schematic diagram showing the energy bands along with HOMO and LUMO energy levels in a π–conjugated organic material.

Like valence band and conduction band edges in an inorganic semiconductor, HOMO and LUMO energy levels create energy barrier in a multi-layer semiconductor device if the HOMO and LUMO between each layer are misaligned. The energy barrier has negative implications on device performances just like in an inorganic semiconductor

device. The distance of the energy gap between HOMO and LUMO is also important due its direct correlation to the emission spectrum of the material. The discussion on the light emission mechanism of OLED will be covered in section 2.4

2.3 Basic Structure of OLED

In the very early days of the OLED research, single layer OLEDs was the predominant structure design used. Today, the most common basic structure of OLEDs is either a DC-biased bi-layer or multi-layer OLED due to their superior performances over the single layer OLED variant. Multi-layer OLEDs are, in essence, extensions from the basic bi-layer structure. The multi-layer OLED design provides a simple way of improving and fine-tuning various OLED performance characteristics via the adjustments of only structural parameters such as layer composition, layer order and layer thickness. The basic structure of a bi-layer OLED is shown in Figure 2-2.

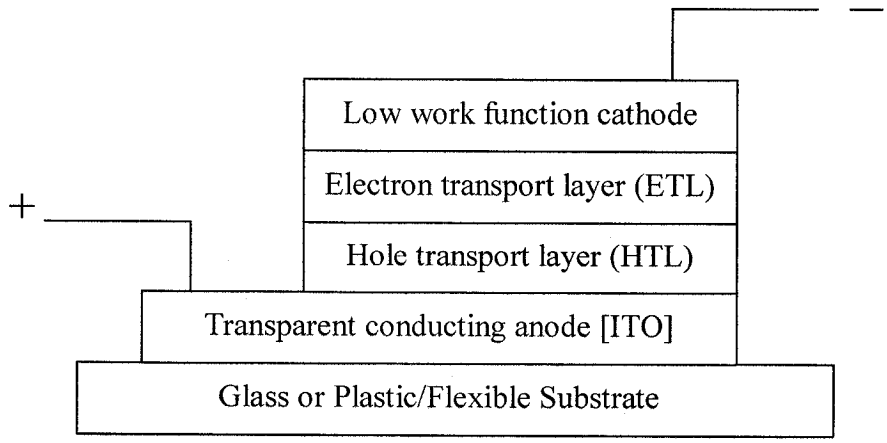

Figure 2-2: Basic structure of a bi-layer OLED containing a hole transport layer (HTL) and an electron transport layer (ETL).

The device is built on the surface of a glass substrate or a flexible transparent substrate like plastic. The first layer above the substrate is a transparent conducting anode, which must be a high work function material in order to provide best energy level alignment with the HOMO of first organic material layer. The anode material is typically indium tin oxide (ITO) for glass substrate or a conducting polymer like doped PEDOT such as PEDOT:PSS for flexible substrates. The multi-layer small molecule organic materials or polymer films are deposited on the transparent anode. As mentioned earlier, the proper multilayer structures show performances superior to the single layer structure due to the capability of lowering the barrier for charge injection from anode or cathode and the capability to control the location of the electron hole recombination region by

altering the charge balance between electrons and holes. In the two-layer OLED structure, the layer deposited on the anode side would generally be a good hole transport material and provides the function of the hole transport layer (HTL). Similarly, the layer deposited on the cathode side would generally be a good electron transport material since it provides the function of the electron transport layer (ETL). In a typical bi-layer OLED, the ETL is usually also the emitting layer. In a typical multi-layer OLED, the emitting layers are usually sandwiched between the HTL and the ETL. The cathode is typically a low-to-medium work function metal such as calcium, aluminum, or magnesium/silver alloy. For transparent OLEDs or top emission OLEDs, other transparent low work function materials are used to allow the light emission from the topside. The appropriate selection of high work function anode material and hole transport material should benefit the proper alignment between HOMO energy level in HTL and the anode work function level. Thus, the potential energy barrier issue could be reduced by avoiding a large mismatch of energy levels. Similarly, the appropriate selection of low work function cathode material and the electron transport material should benefit the proper alignment between LUMO energy level in ETL and the cathode work function level. The multi-layer OLED structure extends the basic two-layer OLED structure by incorporating more specialized ETL, specialized HTL or specialized emitting layers. Those specialized

ETL and HTL usually have a specific purpose such as charge blocking, charge transport promotion, interface improvement and also, to improve the device performance.

2.4 Basic Operation of OLED

In the basic operation of an OLED, holes are injected from the anode and electrons are injected from the cathode when the device is under bias. The charge carriers transport from one electrode to another through the organic materials. During such process, if the charge carrier density is sufficiently high in the organic materials, it will be more probable that the other type of charge carrier will likely to pass within the capture radius for collisions of at least one charge. The recombination of electrons and holes will result in the formation of neutral excited states, which are either singlet exciton or triplet exciton. The light emission is due to the radiative transitions from the neutral excited states to the ground states. Figure 2-3 illustrates the basic operation of an OLED at a bias voltage V, which shows the carrier actions in OLED such as carrier injection, carrier transport, and carrier recombination – leading to the emission of light.

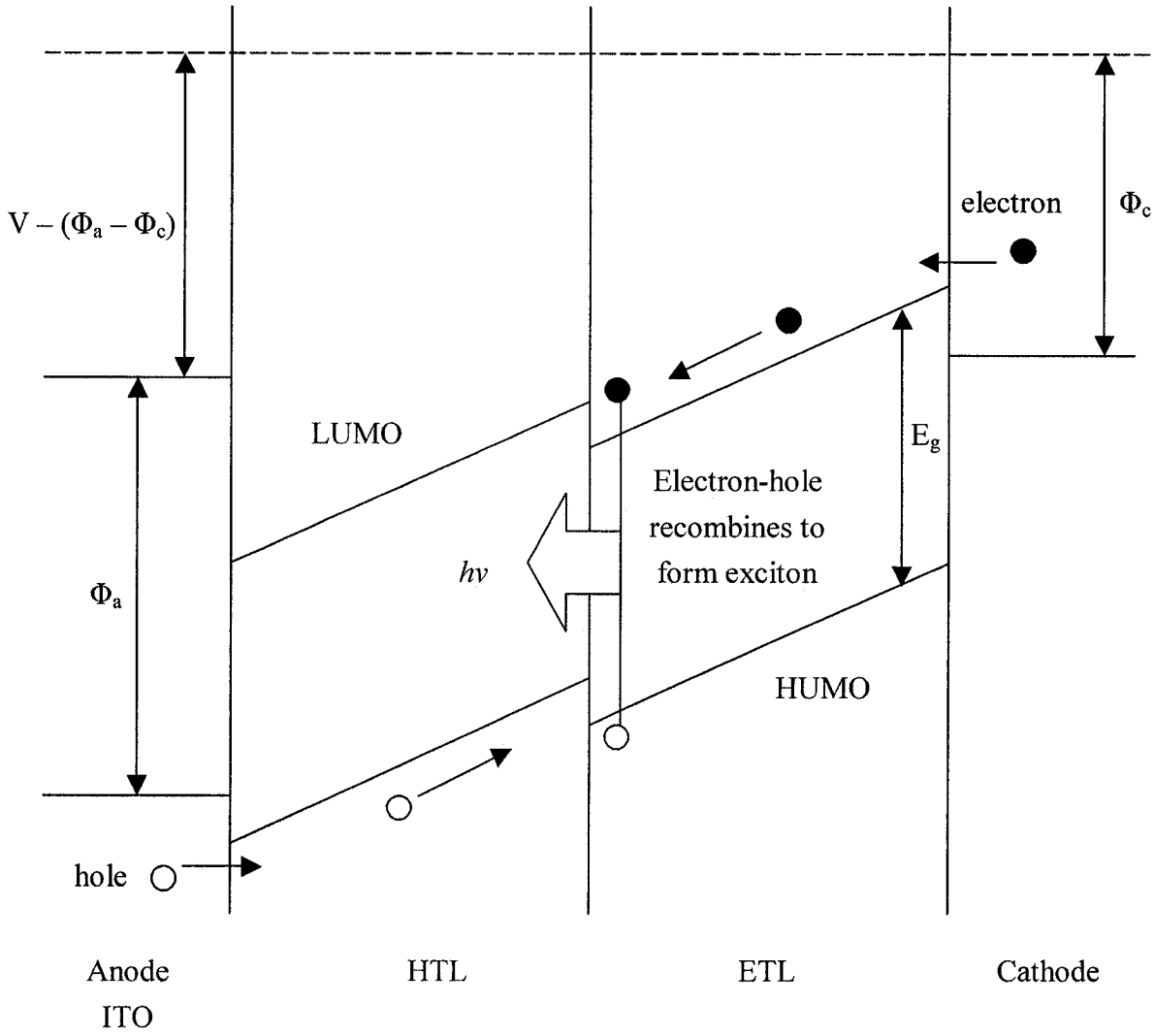

Figure 2-3: A band diagram showing the basic operation of an OLED at a bias V with cathode work function Φ_c, anode work function Φ_a, and energy gap E_g in the electron transport layer/light emitting layer.

The carrier injection and transport mechanism in organic semiconductors is different from inorganic semiconductors, which have free moving charge carriers. The carrier injection in organic semiconductors is achieved through hopping from delocalized states in the metal to localized states in the organic layer. The carrier transport is achieved

through inter-site hopping of charge carriers between localized energy states, which are created from delocalized π-bond. The actual transition rate from one site to another depends on the site energy difference and the distance between the sites. The carriers may hop to a site with a higher energy only upon absorbing a phonon of appropriate energy. As a result, the probability of transition to a localized state with higher energy is decreased. It should also be noted that the energy states involved in the hopping transport of carriers are not fixed to the exact HOMO and LUMO levels. Instead, the energy states form narrow bands around the HOMO and LUMO levels. The width of these bands of states is determined by the intermolecular interactions and by the level of disorder.

2.5 Light Emission Process in OLED

As mentioned earlier, when electrons and holes recombine in the light emitting organic materials, neutral excited states, which are also known as excitons, form. The light emitted from OLEDs is generated from the de-excitation of excitons. The spin-symmetry of an exciton determines its probability of radiative recombination and also its multiplicity. Spin-symmetric excitons with a total spin of S=1, in which both electrons spin up or down, have a multiplicity of three and are known as triplets.

Spin-antisymmetric excitons with a total spin of S=0, in which two electrons have opposite spin direction or said to be spin-paired, have a multiplicity of one and are known as singlets. According to spin statistics, three triplets are generated for every singlet generation during electrical excitation. Since the ground state of most organic molecules is typically spin-antisymmetric which means ground states are singlet states, only relaxations of singlet excitons conserve spin and generate light emission by fluorescence. Light emission is also possible by phosphorescence, which is the forbidden relaxation of a triplet state to the ground singlet state and a slow radiative decay. Phosphorescence is forbidden by the quantum mechanical selection rules, which means that the phosphorescence process has very low probability of occurrence in ordinary organic materials and occurs more slowly, allowing other processes such as quenching to occur. As a result, the energy in triplet excitons is usually wasted and not contributing to light emission. Combining with the previously-mentioned singlet to triplet ratio of 1 to 3, OLEDs relying solely on fluorescence emission mechanism would only have the theoretical limit of 25% for maximum possible electroluminescence efficiency. However, phosphorescence may be enhanced by the presence of a heavy metal atom with strong spin-orbit coupling which mixes the single and triplet states [2-2]. Thus, obtaining high efficiency emission in OLED is possible by enhancing phosphorescence. OLEDs

exploiting phosphorescence process, first pioneered by Baldo *et al.* [2-3], has become an increasingly popular design due to the improved efficiency over the non-phosphorescent OLEDs. Figure 2-4 shows a schematic representation of the elementary processes for charge carrier recombination, formation of molecular excitons, exciton relaxation process, and external emission. Figure 2-5 shows a schematic representation of pathways for exciton decay.

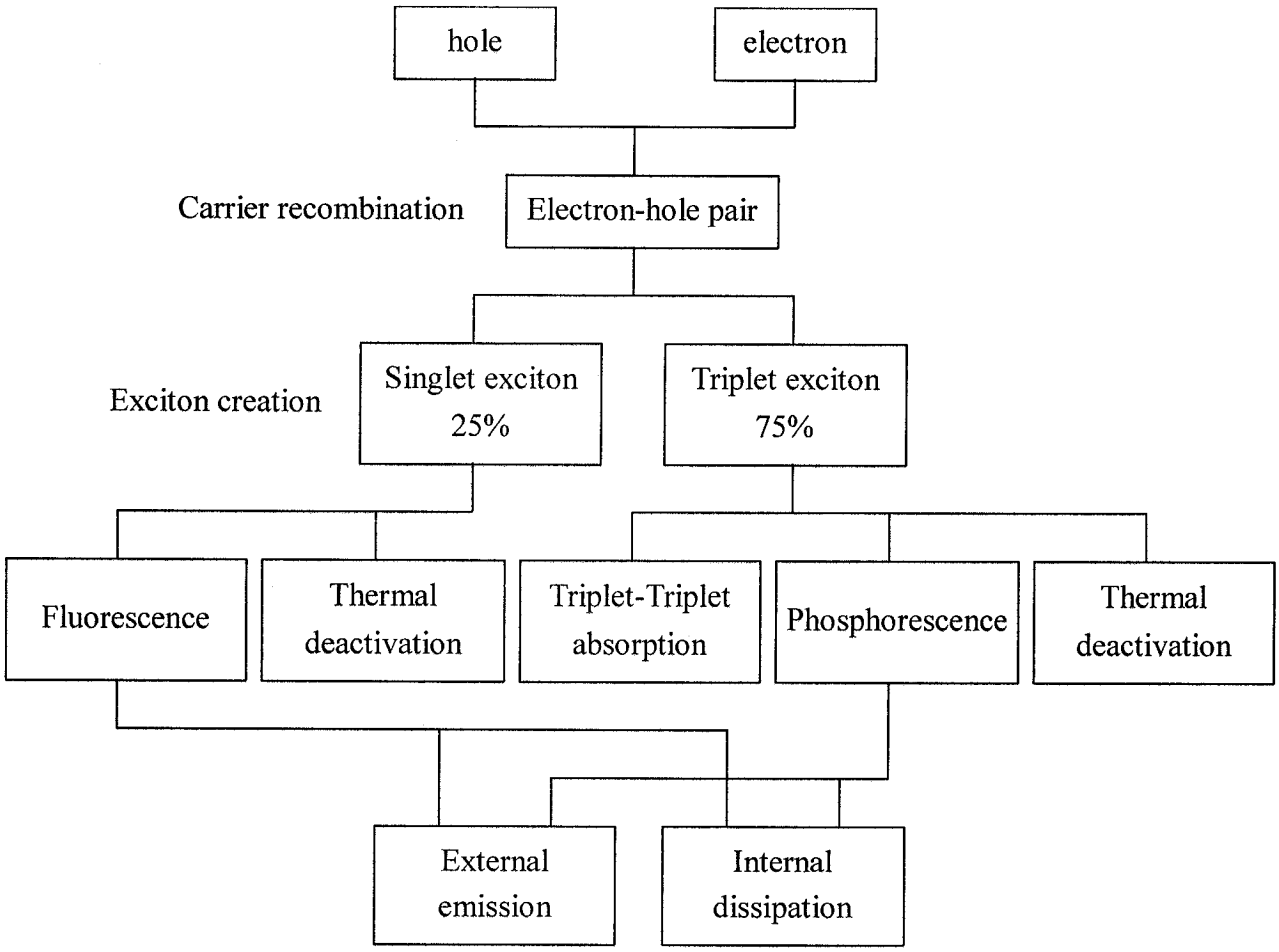

Figure 2-4: A schematic representation of the elementary processes for charge carrier recombination, formation of molecular excitons, exciton relaxation process, and external emission [2-1].

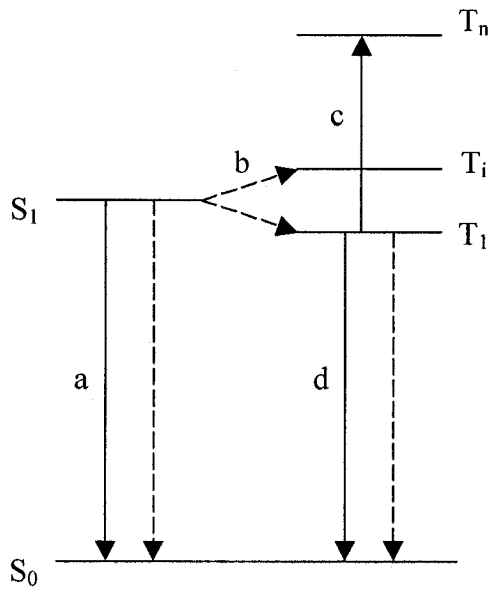

Figure 2-5: A schematic representation of pathways for exciton decay. Solid arrows represent radiative processes, corresponding to absorption or emission of light. Dashed arrows represent non-radiative process. S_0 is the ground (singlet) state; S_1 is the first excited singlet state; T_1 is the first excited triplet state; and T_i and T_n are higher triplet states. Process (a) is fluorescence; (b) is intersystem crossing (ISC); (c) is photo-induced triplet-triplet absorption; and (d) is phosphorescence. [2-4]

As mentioned earlier, the electroluminescent intensity and efficiency depends on the rate of exciton generation, which is directly tied to the electron-hole recombination rate. Also, the recombination probability is depending on carrier density in the particular organic material. As a result, electroluminescent characteristics such as intensity and efficiency can be modified or fine-tuned by controlling the recombination current. It has been shown that electron-hole recombination current could be controlled by introducing

charge-blocking layers, by varying layer thickness, and by adjusting dopant concentrations [2-5 to 2-7]. The ability to adjust electroluminescent characteristics in an emission layer is extremely beneficial for a multiple emissive layer OLED design where a specific mixture of color can be achieved by controlling the recombination current in each individual emission layer. Figure 2-6 provides a schematic diagram showing current flow components inside an OLED. It should be noted that the ratio of recombination current flow to total current flow is the charge balance factor, which is tied to the definition of internal quantum efficiency. The details on OLED efficiency are discussed in chapter 4.

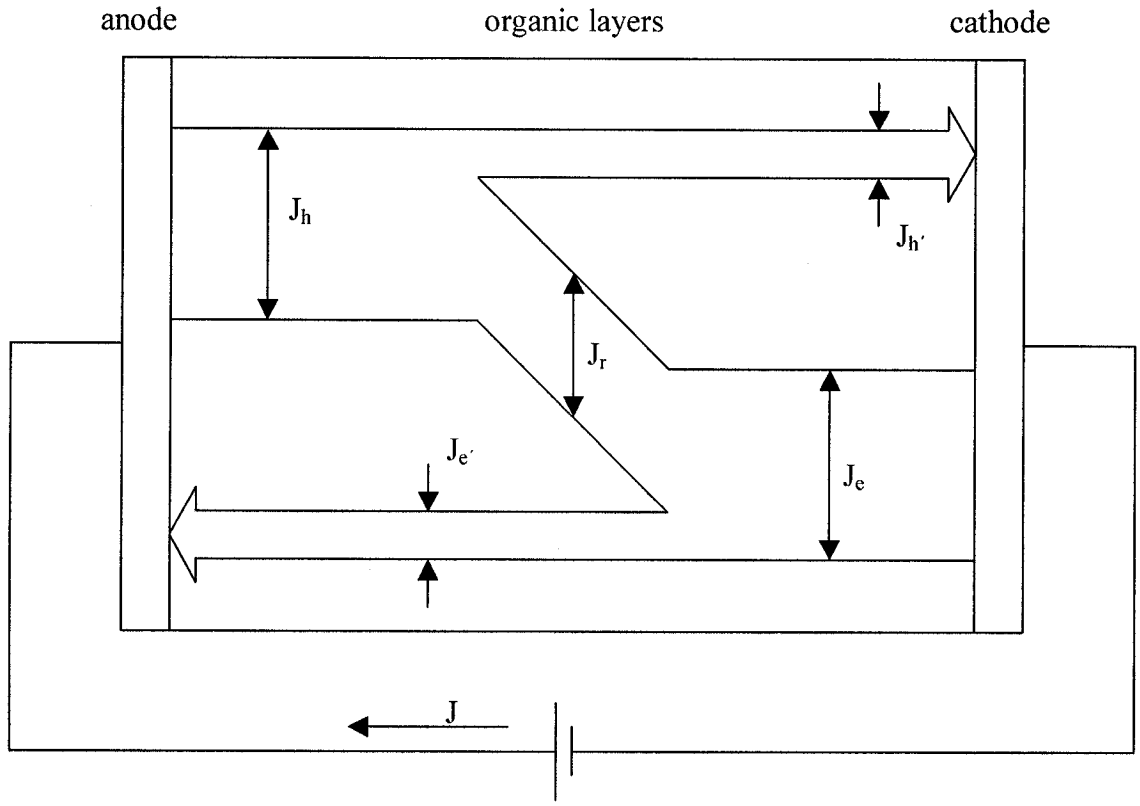

$$J = J_h + J_{e'} = J_e + J_{h'}$$
$$J_r = J_h - J_{h'} = J_e - J_{e'}$$

Figure 2-6: A schematic diagram showing current flow components inside an OLED. J_h and J_e are net hole and electron current density. J_r is the component of recombination current density. $J_{h'}$ and $J_{e'}$ are the hole and electron current density without recombination [2-1].

2.6 Degradation Mechanisms

Two of the key issues of OLED for large-scale application are its stability and reliability. Numerous research efforts have concentrated on the identifications of degradation mechanisms and the improvements of reliability and lifetime of OLEDs [2-8

to 2-10]. Degradation mechanism such as dark spot formation, recrystallization, and general sensitivity of organic materials toward water and oxygen are the possible causes for device failure. The most common degradation mechanisms are summarized in several articles [2-11]. Dark spot is a localized non-emissive defect on the device, which is possibly caused by cathode pinhole formation. Recrystallization is one of the main degradation mechanisms in OLEDs based on amorphous organic layers which will slowly recrystallize when the temperature of the organic layer reaches its glass transition temperature value. Also, an organic material, by its own nature, is suspected to oxidation and reaction with water and oxygen. As a result, extra care in passivation and packaging are necessary in order to ensure the reliability of OLEDs.

2.7 Realization of White OLED

2.7.1 Organic material selection

The emission spectrum from typical organic materials is limited to narrowband, which at most only covers about one third of the visible spectrum. Generally, the emission profile is not flat, but rather peaked at a certain wavelength. It is noted that no single organic material is capable of efficient emission across the entire visible spectrum.

To produce high-quality white light, it is necessary to have a device capable of producing efficient broad-spectrum emission covering the entire visible spectrum. Table 2-1 illustrates the colors of the visible light spectrum and their corresponding wavelength intervals.

Table 2-1: The colors of the visible light spectrum and their corresponding wavelength intervals.

Color	Wavelength interval
Red	~625-740 nm
Orange	~590-625 nm
Yellow	~565-590 nm
Green	~500-565 nm
Cyan	~485-500 nm
Blue	~440-485 nm
Violet	~380-440 nm

For this reason, white OLED typically requires incorporating multiple light emitting organic materials in order to achieve broadband emission spanning across the entire visible spectrum. The simplest solution is to incorporate and mix proper amounts of organic light emitting materials each corresponding to one of the three primary colors – blue, green, and red. While it is also possible to incorporate more emitting materials than just three in order to achieve the truly flat emission profile across the spectrum and to closely simulate the daylight emission spectrum, such method is not without its drawbacks. Figure 2-7 presents the daylight emission spectrum defined by the CIE

illuminant D50 and D65. The obvious drawbacks of using too many emitting materials are increased fabrication complexity, increased difficulty of fine-tuning device performance, and lower device reliability where device failure can simply be caused by the failure of a specific material in the device. In general, white OLED design is typically based on the tri-color principle.

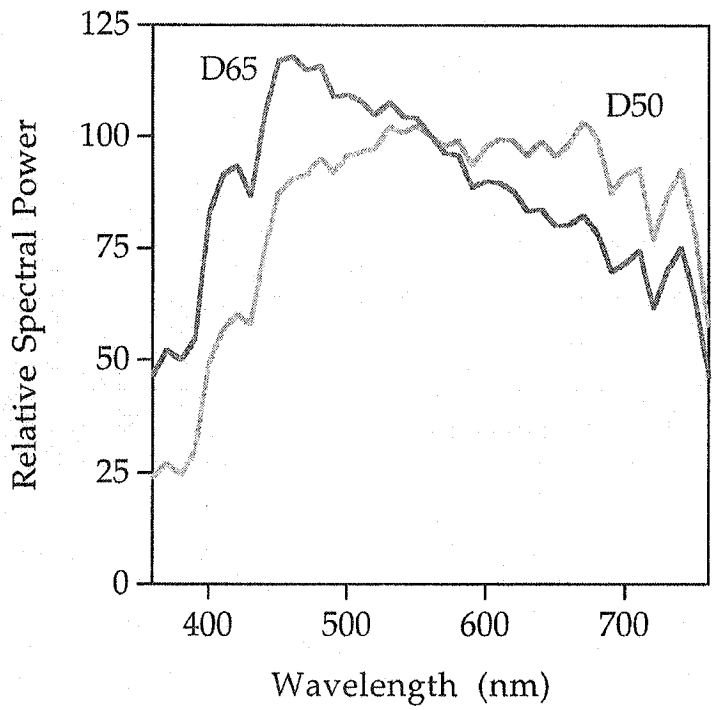

Figure 2-7: Average daylight emission spectrum defined by the CIE illuminant D50 and D65 where CIE illuminant D65 represents an average daylight with a CCT of 6,504K and D50 represents an average daylight with a CCT of 5,003 K. [2-12]

The organic materials used in OLED can be categorized into two main groups: small molecule and polymer. The differences between the two groups are the chemical structure and molecular weight. Small molecule materials typically have a fixed chemical structure

where each individual molecule has the same structure as opposed to polymers, which have varying number of repeating units in its chemical structure. Although the chemical structure stays the same, every individual polymer molecule will have slightly different molecular structures depending on the number of the repeating units in the specific polymer molecule or, in other words, depending on how long the polymer chain is. Due to the repeating units in the polymer chemical structure, polymers usually have much heavier molecular weight than the small molecule materials and the molecular weight of each individual polymer molecule also depends on the number of repeating units in the specific molecule itself. Besides chemical structure and molecular weight, there is also one major difference in material property - the sensitivity to heat. Polymers generally crosslink or decompose upon heating whereas small molecule materials have higher tolerance toward heating. This poses restrictions on the use of thermal vacuum evaporation deposition technique in conjunction with polymer materials and makes small molecule material the only material compatible with vacuum evaporation deposition processes.

OLED based on small molecule materials tends to have better performance than the polymer based OLED counterparts. Also, small molecule materials are compatible with the thermal vacuum evaporation technique. Thermal vacuum evaporation technique has

the advantage in which the device performance can be fine-tuned by precisely controlling and varying material layer thicknesses. On the other hand, the strength of the polymer based OLED lies in the cheaper production method utilizing solution processing. Due to the above-mentioned reasons, the organic materials chosen in this work will be small molecule type materials to take full advantage of the superior performance of small molecule OLED and the ability to fine tune the device via adjusting its layer thickness.

N, *N*′-diphenyl-*N*, *N*′-bis(3-methylphenyl)-1, 1′-biphenyl-4, 4′-diamine [TPD] has been used extensively as hole transport material in OLED fabrication since the early days. TPD is also one of the very first materials used in conjunction with Alq_3 to produce the first functional OLED emitting green light. Not only the long history of TPD makes it one of the most widely available and widely used hole transport materials, but the performance of TPD is still very comparable to the more recent hole transport materials such as NPB, except for its stability. For the above reasons, TPD is chosen to be used as the hole transport material for this work. The molecular structure of TPD is shown in Figure 2-8(a).

Tris- (8-hydroxyquinoline) aluminium [Alq_3] is probably one of the most widely used small molecule emitter materials. Ever since it was used in the pioneering work by Tang and van Slyke [2-13], Alq_3 has been extensively used in OLED research. Despite

being one of the earliest developed OLED materials, Alq_3 still provides a relatively good green fluorescence performance. Besides being used as green light emitting materials, Alq_3 has also been used solely as an electron transport material in contact with cathode and used as a host material for lower-gap emitter guest molecules. According to the manufacturer information, the photoluminescence maximum of Alq_3 occurs at 515 nm, which would give the light emission appearance of slightly light green color. The molecular structure of TPD is shown in Figure 2-8(b).

4, 4′-bis(2, 2′-diphenylvinyl)-1, 1′-biphenyl [DPVBi] is the blue emitting material used in this work due to its good performance and good availability. DPVBi was first used by Tokailin *et al.* [2-14] to produce a good performance blue light emission OLED. Since then, DPVBi has become one of the more popular blue fluorescent materials used in OLED design. According to the manufacturer information, the photoluminescence maximum of DPVBi occurs at 443 nm, which would give the light emission appearance of slightly light blue color. The molecular structure of TPD is shown in Figure 2-8(c).

Tris-(1-phenylisoquinolinato-N) iridium (III) [$Ir(piq)_3$] is the red emitting material used. Unlike the other light emitting materials used in this work, $Ir(piq)_3$ is a phosphorescent material, which should exhibit a higher emission efficiency. Such advantage of the phosphorescent material would also imply that the phosphorescent

material layer thickness does not need to be as thick as the fluorescent material layer to have the same luminous intensity. According to the manufacturer information, the photoluminescence maximum of $Ir(piq)_3$ occurs at 616 nm, which would give the light emission appearance of orange-red color. The molecular structure of TPD is shown in Figure 2-8(d). Table 2-2 summarizes the physical, electrical, and optical properties of the organic materials selected for this thesis project.

Table 2-2: Physical, electrical, and optical properties of organic materials used in this thesis project. Unless noted otherwise, all information is supplied by the material provider, Organic Vision.

Name	TPD	Alq_3	DPVBi	$Ir(piq)_3$
Molecular Formula	$C_{38}H_{32}N_2$	$C_{27}H_{18}AlN_3O_3$	$C_{40}H_{33}$	$C_{45}H_3N_3Ir$
Molecular Weight	516.7 g/mol	459.4 g/mol	510.7 g/mol	804.98 g/mol
LUMO	2.5 eV [2-15]	3.0 eV [2-16]	2.8 eV [2-16]	2.45 eV [2-17]
HOMO	5.6 eV [2-15]	5.6 eV [2-16]	5.9 eV [2-16]	4.8 eV [2-17]
Energy gap (LUMO to HOMO)	3.1 eV	2.6 eV	3.1 eV	2.35 eV
Photoluminescence Max	—	515 nm	443 nm	616 nm
Absorption Max	352 nm	389 nm	350 nm	250 nm
Appearance	White powder	Bright yellow powder	Light yellow powder	Red powder

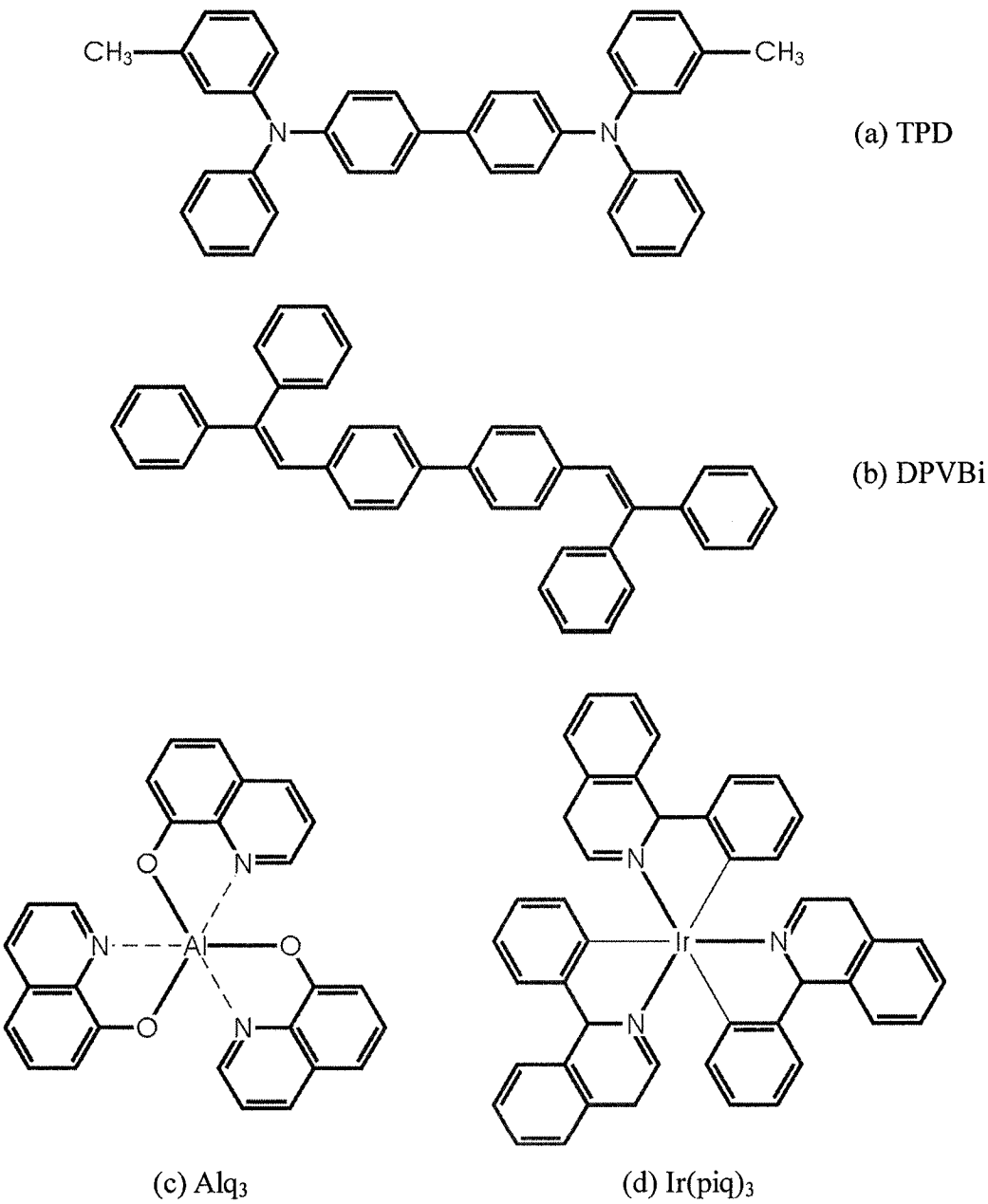

Figure 2-8: Molecular structure of the materials used in the experiment: (a) TPD (b) DPVBi (c) Alq_3 (d) $Ir(piq)_3$. [2-15 to 2-17]

2.7.2 Electrode contact material selection

The selection of electrical contact materials is as important as the selection of the organic materials due to the possible energy barrier issue introduced by mismatched work functions and the material energy levels. Ideally, ohmic contacts between both electrodes and their respective neighbor organic layers are most desirable as the carriers can travel through the interface without encountering any potential barriers. As mentioned earlier in this chapter, energy barrier could cause negative impacts on device performance such as reduced efficiency and the necessity of higher driving voltage. In practice, energy barrier should be lowered as much as possible if not outright eliminated all together.

As the OLED structure is of vertical stacking design with light emission mainly exiting in the vertical direction, at least one transparent electrode is required for strong light emission. Otherwise, the light would only be able to exit from the enclosing edge surfaces of the device, not from the top or the bottom side of the device. Indium tin oxide (ITO) is selected as the anode because of its high optical transmission coefficient in the visible spectrum, good conductivity, low sheet resistance with values of 20 to 30 Ω/sq and high work function value which would provide good energy level match to the HOMO level of the hole transport material. High transmission coefficient (typically

above 80%) in the visible spectrum ensures a small percentage lost of luminous intensity from the OLED through ITO layer. Good conductivity and low sheet resistance are the standard requirements for electrode material, which guarantee minimal power loss in the electrode. Typically, ITO has a high work function value of 4.7 eV, which should match relative well with the HOMO levels of most hole transport materials. For example, hole transport materials such as TPD and NPB both have HOMO levels of 5.6 eV [2-1].

Magnesium (Mg) and silver (Ag), which are both opaque metals, are a good choice for a composite layer for the cathode due to four reasons: (1) the low work function value of magnesium (3.66 eV) provides good energy level match with the LUMO energy level of the electron transport material, (2) the excellent conductivity of silver, (3) their ease of deposition by thermal vacuum evaporation, and also (4) good chemical stability of silver (Ag does not easily react with oxidizing agents). The magnesium/silver cathode used for OLED is not a pure alloy. Rather, it is more of a distinct two composite layer cathode. The bottom layer, in contact with the electron transport material, is mainly magnesium with very little silver. This mixture takes the full advantage of the low work function value of magnesium. The top layer, covering up the topside of OLED, is made of mainly silver and very little magnesium. This mixture takes the full advantage of the excellent conductivity of silver and the shielding effect from the silver as a stable metal.

2.7.3 Proposed OLED structure

Given the specific materials chosen for this work, the proposed device structure design is the vertical multilayer stacking structure. The overall OLED structure is glass-substrate/ITO/TPD/DPVBi/Ir(piq)$_3$/Alq$_3$/MgAg. The hole transport material, TPD, is positioned right on top of the ITO anode. The order of the light emission layers will be first DPVBi, then Ir(piq)$_3$, and finally Alq$_3$. As mentioned earlier, Alq$_3$ is also a good electron transport material so that Alq$_3$ is positioned right next to the cathode. Since emission from all three light emitting materials is desired, the DPVBi and Ir(piq)$_3$ layers sandwiched between TPD and Alq$_3$ should be sufficiently thin so that a sufficiently high amount of holes reach the Alq$_3$ layer and trigger the light emission process in Alq$_3$. Figure 2-9 shows the structural construct of the white OLED fabricated in this study while Figure 2-10 illustrates the energy level diagram of both the electrode work function and the LUMO/HOMO levels of the organic layers in the fabricated OLEDs.

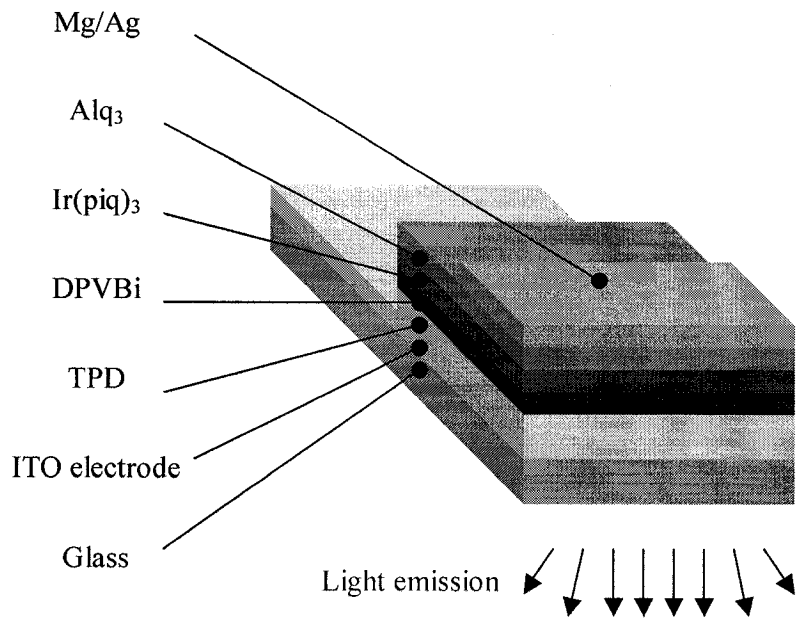

Figure 2-9: 3D diagram showing the structural construct (glass/ITO/TPD/ DPVBi/Ir(piq)$_3$/Alq$_3$/MgAg) of the OLEDs fabricated in this work.

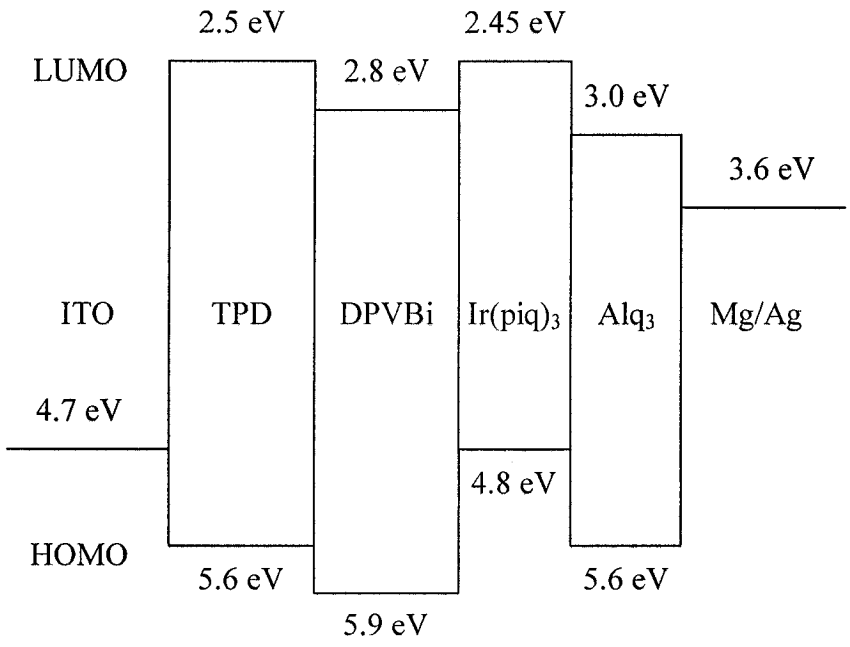

Figure 2-10: An energy level diagram showing the work functions of the anode (ITO) and the cathode (Mg/Ag) and LUMO/HOMO levels of the organic material layers (TPD/DPVBi/Ir(piq)$_3$/Alq$_3$) in the fabricated OLEDs.

2.8 Summary

In this chapter, the basic concepts of the organic light emitting devices are examined. Basic electronic structure of the organic semiconductor material, basic OLED structure, basic operation of OLED/carrier transport mechanism in OLED, and light emitting mechanism of OLED have all been discussed. Unlike the inorganic semiconductor, the carriers in organic materials are not free-moving charge carriers, but rather transport via site hopping. Also unlike the inorganic light emitting devices, the light emission process and the emission efficiency are strongly tied to the excited states produced from the recombination of charge carriers. The typical fluorescent organic material emission process relies on the relaxation from excited singlet states to the ground states and this only accounts for roughly one fourth of the total excited states. Light emission process in phosphorescent organic material, on the other hand, utilizes not only the excited singlet states but also the excited triplet states. This means that the phosphorescent material would likely have better emission efficiency. Energy level match up between each layers in a OLED is important as the existence of energy barrier will likely increase the difficulty of carrier transport and, as a result, reduce the device performance.

In the second half of the chapter, the organic materials used in this project and the

corresponding device structure have been discussed. In order to successfully produce broad-spectrum light emission with a color close to white, multiple light emitting materials must be employed. The design strategy is to utilize strong light emitting materials in each of the three primary color spectra – blue, green, and red and to mix the light emission from each material. The final resulting color is to be fine-tuned by varying the layer thickness. The following chapter, chapter 3, will describe the fabrication processes and the experimental setup.

[2-1] Joseph Shinar ed., *Organic light-emitting devices : a survey*, AIP Press, New York, **2004**.

[2-2] M.A. Baldo, M.E. Thompson, S.R. Forrest, *Nature* **2000**, *403*, 750.

[2-3] M.A. Baldo, D.F. O'Brien, Y. You, A. Shoustikov, S. Sibley, M.E. Thompson, S.R. Forrest, *Nature* **1998**, *395*, 151.

[2-4] R.H. Fried, R.W. Gymer, A.B. Holmes, J.H. Burroughes, R.N. Marks, C. Taliani, D.D.C. Bradley, D.A. Dos Santos, J.L. Bredas, M. Logdlund, W.R. Salaneck, *Nature* **1999**, *397*, 121.

[2-5] Z.G. Liu, H. Nazare, *Syth. Met.* **2000**, *111*, 47.

[2-6] R.H. Jordan, A. Dodabalapur. M. Strukelij, T.M. Miller, *Appl. Phys. Lett.* **1996**, *68*, 1192.

[2-7] B.W. D'Andrade, M.E. Thompson, S.R. Forrest, *Adv. Mater.* **2002**, *14*, 147.

[2-] J. Shen, D. Wang, E. Langlois, J. Yang, *Proc. SPIE* **2001**, *4105*, 236.

[2-] Z.D. Popovic, H. Aziz, *IEEE Journal of Selected Topics in Quantum Electronics* **2002**, *8*, No. 2, 362.

[2-] P.E. Burrows, V. Bulovic, S.R. Forrest, L.S. Sapochak, D.M. McCarty, M.E. Thompson, *Appl. Phys. Lett.* **1994**, *65*, No. 23, 2922.

[2-8] Y. Sato, S. Ichinosawa, H. Kanai, *IEEE Journal of Selected Topics in Quantum Electronics* **1998**, *4*, No. 1, 40.

[2-] Mark D. Fairchild, *Color Appearance Model*, Addison-Wesley, Reading, Massachusetts, **1998**.

[2-9] C.W. Tang and S.A. Van Slyke, *Appl. Phys. Lett.* **1987**, *51*, 913.

[2-10] H. Tokailin, M. Matsuura, H. Higashi, C. Hosokawa, T. Kusumoto, *Proc. SPIE* **1993**, *1910*, 38.

[2-11] H. Murata, C.D. Merritt, Z.H. Kafafi, *IEEE Journal of selected topics in quantum electronics* **1998**, *4*, No. 1, 119.

[2-12] G. Li and J. Shinar, *Appl. Phys. Lett.* **2003**, *83*, 5359.

[2-13] T.H. Kim, H.K. Lee, O.O. Park, B.D. Chin, S.H. Lee, J.K. Kim, *Adv. Funct. Mater.* **2006**, *0000*, no. 0, 1.

Chapter 3

Fabrication of Organic Light-Emitting Devices

3.1 Overview

Thermal vacuum evaporation and wet-coating techniques are the two major methods currently used for the fabrication of organic light-emitting device (OLED). Thermal vacuum evaporation is used for deposition of small molecule materials and wet-coating technique is used for the deposition of polymer-based organic materials. A brief overview of the OLED fabrication methods and a comparison of the methods can be found in several references [3-1, 3-2].

Thermal vacuum evaporation of small molecule materials is usually performed in a high-vacuum chamber at a pressure of 10^{-6} Torr or less. Figure 3-1(a) illustrates a schematic diagram of the thermal vacuum evaporation technique. One of the advantages of thermal vacuum evaporation over other deposition methods is that a precise layer thickness control can be achieved. This is especially beneficial for the consistent

fabrication of multi-layer OLEDs where reproducible layer thickness is required. As discussed in chapter 2, the performance of OLED is greatly influenced by layer composition and layer thickness. The ability to control precise layer thickness is also advantageous for optimizing OLED. A major appeal of vacuum deposition techniques to the industry is that the existing vacuum equipments could be utilized. Of course, thermal vacuum evaporation techniques are not without their drawbacks. First, thermal evaporation can only be applied to small molecule organic materials as polymers generally crosslink or decompose upon heating. Second, the throughput of vacuum evaporation is lower than other fabrication techniques. Also, the cost associated with running vacuum equipment is higher than either spin-coating or ink-jet printing.

Wet-coating techniques, also referred as solution-processed techniques, include spin-coating, ink-jet printing, and other wet casting techniques such as screen printing and micro-stamping. The difference between spin-coating and ink-jet printing is that spin-coating is used for large area film deposition and ink-jet printing is used for localized film deposition. As such, ink-jet printing provides the opportunity of patterning while depositing materials that spin-coating could not. Spin-coating may also face the additional difficulty for the application on large size display backplane, while in-jet printing could be easily integrated into reel-to-reel processes for the large batch flexible

display manufacturing. The recent development of the ink-jet printing process is covered by Carter *et al.* [3-3]. The obvious limitation of the wet-coating techniques is that the materials must be soluble. This not only limits the wet-coating techniques to polymer materials, but also imposes restrictions on the nature of polymers and the side-groups attached to the polymer backbone. Another drawback is that when a multi-layer structure is required, the solvent for each layer material must be carefully chosen so that the previously deposited film will not be re-dissolved. For spin-coating, even though the thickness of the deposited films may be controlled by concentration of the polymer in the solution, the spin rate, and the spin-coating temperature, the precise control of the layer thickness is still difficult and the real-time thickness monitoring during deposition is impossible. Besides, it is also difficult to fabricate uniform thick films using spin-coating methods. Figure 3-1(b) and (c) present schematic diagrams of both the spin-coating and ink-jet printing techniques.

We now describes the experimental setup used to realize OLED fabrication by the vacuum deposition method and the complete procedure for constructing multi-layer OLED device structures.

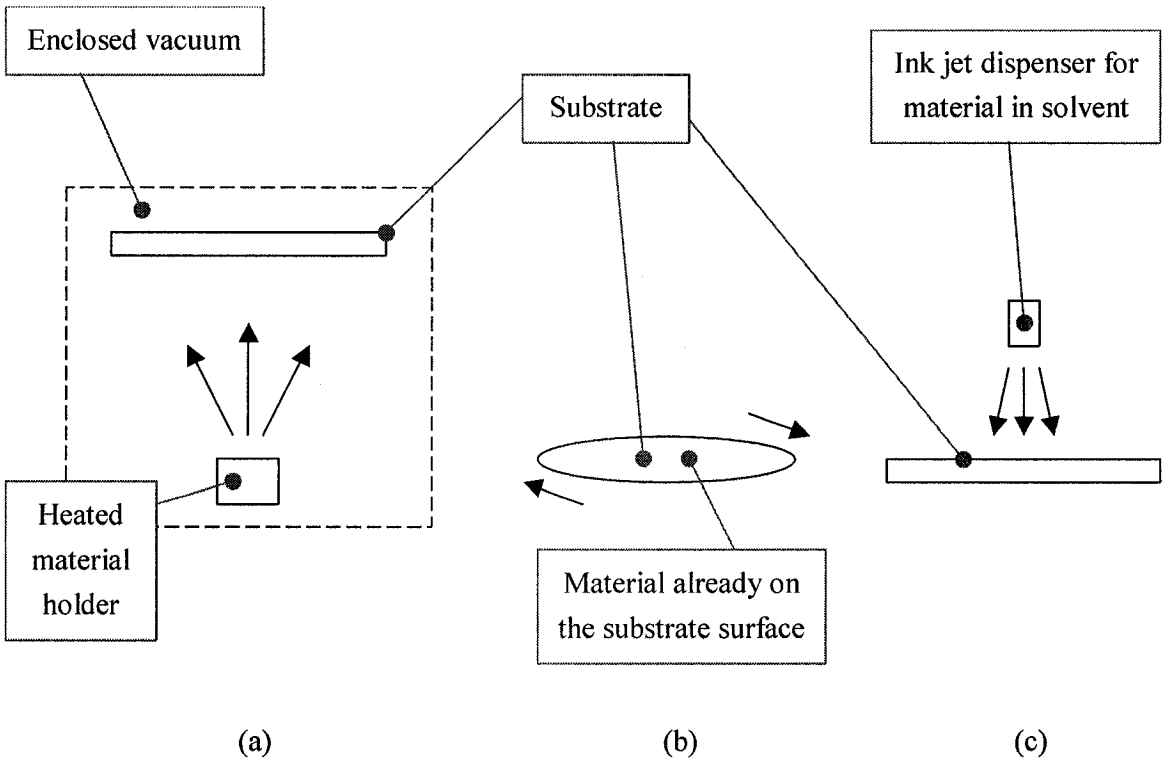

Figure 3-1: Schematic diagrams of (a) thermal vacuum evaporation, (b) spin-coating, and (c) ink-jet printing.

3.2 Preparations of Fabrication

3.2.1 Experimental setup

Vacuum deposition of the organic materials and filament evaporation of the metal electrode are performed in the laboratory using an Edward model E12E3 vacuum system. The ultimate vacuum pressure in the vacuum chamber of the system is less than $1x10^{-6}$ Torr. The mean free path of a gas molecule, which is an important parameter of vacuum

deposition, is the average distance of the molecule travels before it collides with another molecule. The mean free path, λ, of oxygen at different pressures is shown in Table 3-1. The deposition of the organic materials and metal electrode is performed in the same vacuum chamber so both steps could be done sequentially without the need of opening up the chamber. The vacuum chamber is equipped with a high-current source for thermal evaporation of the metal electrode, two temperature control systems for organic material deposition, and a Sloan model OMNI 3 Film Thickness Monitor which provides real-time film thickness monitoring capability.

The metal layer evaporation is performed with a molybdenum (Mo) metal boat holding source metal and with high current applied through it. There are two temperature control systems for the deposition of organic materials and each temperature control system comprises a temperature control unit, a type-K thermalcouple, and a heating element. Each temperature control system is connected to a graphite boat used as a thermal conductive container for the organic material. With this setup, two different kinds of organic material layers can be deposited without the need of opening up the vacuum chamber. The Sloan model OMNI 3 Film Thickness Monitor allows real-time film thickness monitoring during the material deposition. The film thickness monitoring is achieved by measuring the oscillating frequency of the embedded quartz crystal on the

sensor head.

Table 3-1: Values of mean free path of oxygen gas molecule at room temperature at different pressures.

Pressure	Temperature	Mean free path
760 Torr	297 K	1.76×10^{-8} m
1×10^{-3} Torr	297 K	1.34×10^{-2} m
1×10^{-6} Torr	297 K	13.39 m

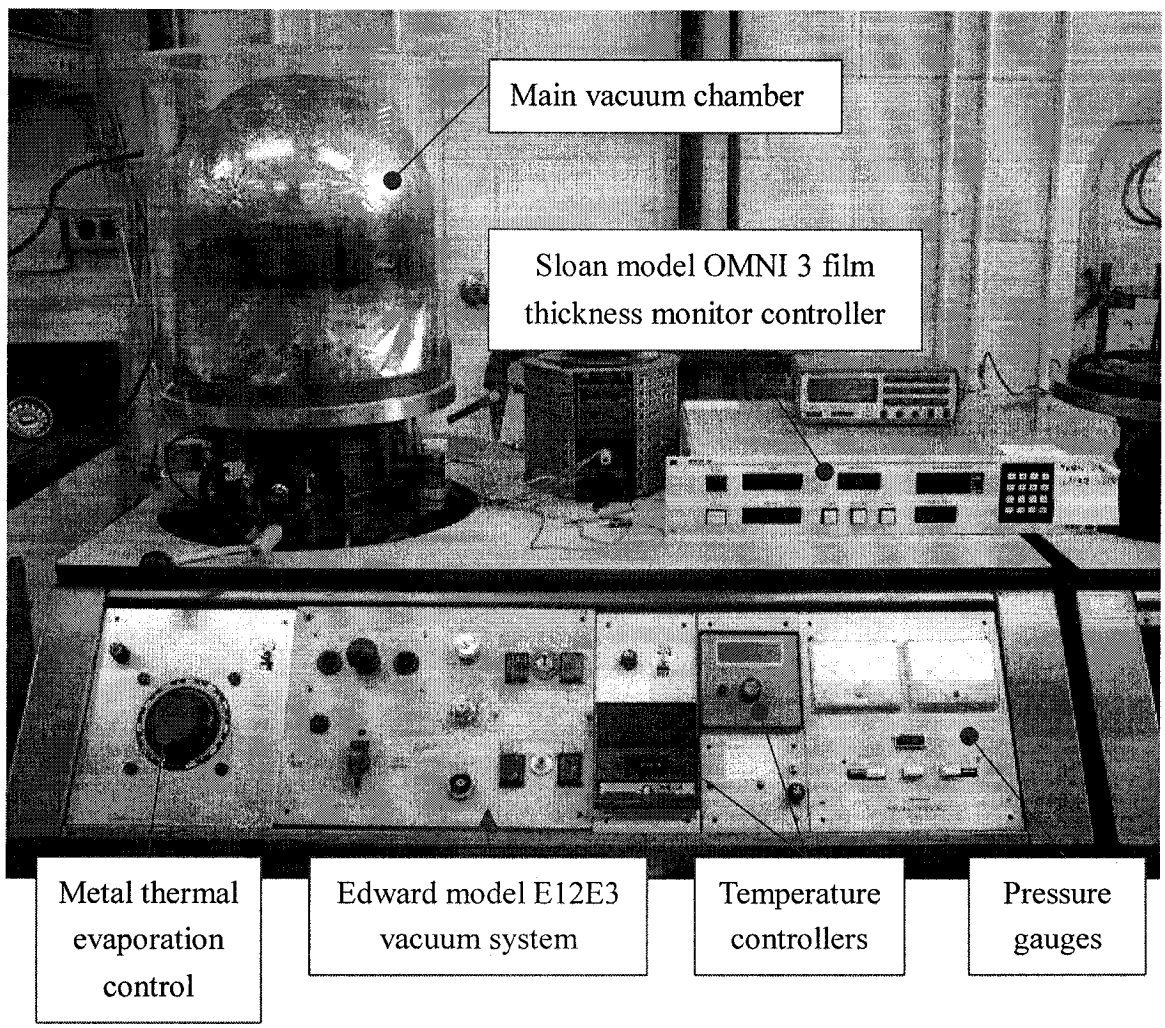

Figure 3-1: A photograph showing the Edward model E12E3 vacuum system with controllers for fabricating OLEDs.

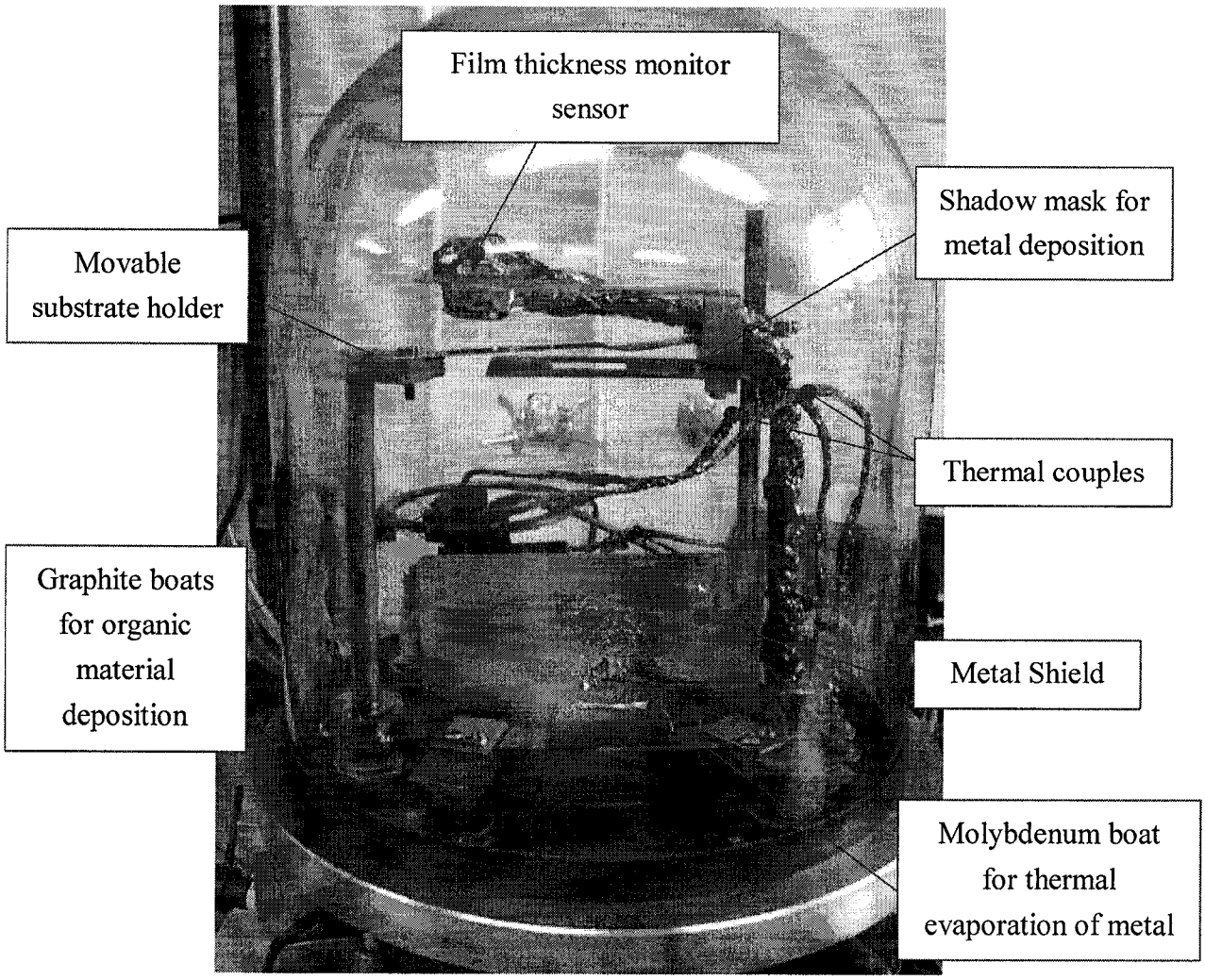

Figure 3-2: A photograph showing the vacuum chamber setup for thermal vacuum evaporation of organic materials and metal contact deposition

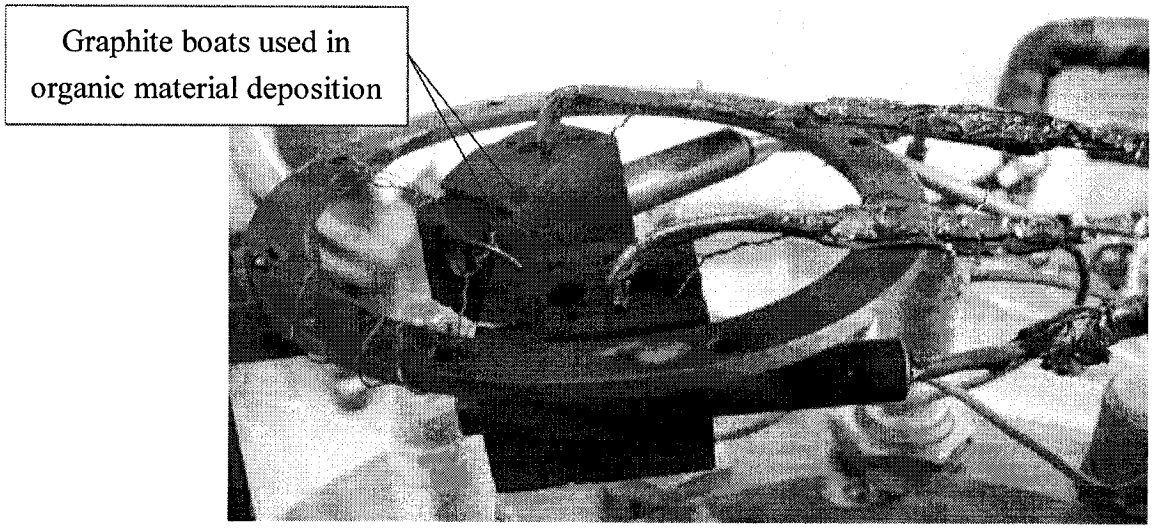

Figure 3-3: Custom-made graphite boats used as both material containers and heating elements in organic film deposition.

The vacuum chamber shown in Figure 3-2 can be separated by the metal shield into two zones. The behind-the-shield zone, which consists of graphite boats, thermalcouples, and thickness monitor sensor is dedicated to organic layer deposition and the front zone, which consists of a shadow mask and a Mo boat, is devoted to thermal evaporation of the metal contacts. The aluminum shadow mask is used to pattern the metal contact during thermal evaporation of the metals and the thermalcouples are used as temperature probes for the two temperature controller units. The shield separating the two zones is made of aluminum and its primary function is to reduce possible cross contamination of materials between the two zones. For example, any accidental deposition of metal onto the two graphite boats would be considered as extremely undesirable. The two graphite boats,

which act as both the materials containers and the heating elements for the organic material are suspended within a metal O-ring connected to a rotary shaft. The rotary shaft allows about 90 degrees of horizontal movement and its purpose is to allow selective direct alignment between the selected graphite boat and the film thickness monitor sensor. During the deposition of each organic material, the corresponding graphite boat is positioned directly below the thickness monitor sensor, as this would allow the most accurate reading of the deposited film thickness. The substrate holder is also connected to a similar rotary shaft, which allows the substrate position switching depending on the stage of the deposition process. The rotary shaft allows about 120 degrees of horizontal movement. When organic materials are to be deposited onto the substrate, the movable substrate holder will be moved into the behind-the-shield zone and placed in the proximity of the thickness monitor sensor. During metal contact deposition, the movable substrate holder will then be moved into the front zone and be placed directly above the shadow mask and the Mo boat. As for the rest of the time, the substrate will be hidden behind the solid part of the shadow mask, which would act as a shield against the unwanted heat radiation and unwanted material deposition during heat-up and cool-down processes.

3.2.2 Calibration of film thickness monitor

As discussed in chapter 2, since the film thickness has a strong influence on various performance characteristics of the organic semiconductor device, the film thickness of the different layers in the fabricated OLED needs to be precisely monitored and controlled. Thus, the task of calibrating the film thickness monitor to give accurate layer thickness data reading is quite critical. For the purpose of the experiment, separate calibration process is performed for each organic material in order to make the layer thickness information as accurate as possible.

The calibration is performed utilizing both the film thickness monitor and a JOEL model 6100 scanning electron microscope (SEM). Each organic material is deposited onto a clean n-type silicon substrate. The reason of using silicon substrate instead of the glass substrate is to provide better SEM image contrast between deposited material and the substrate since the doped silicon substrate is more conducting than the organic semiconductor materials. The silicon substrate is pre-cleaned using acetone (ACE) and DI water in the ultrasonic bath. With the thickness monitor set at the default settings, organic material deposition is performed at a base pressure of roughly $1x10^{-6}$ Torr until the thickness reaches a preset number under default setting. The deposited silicon substrate is

then fractured and its cross-section examined by the JOEL model 6100 SEM to determine the real film thickness. With the true film thickness determined by the SEM, this data is compared with the reading taken under default thickness setting so that the ratio between the two can be calculated and the proper thickness monitor setting for each individual type of materials can be devised. As a side note, the deposition rate varies with type of material, deposition temperature, the distance of the substrate from the boat, and amount of organic material in the boat. Moreover, the material used for each deposition is typically less than 10 mg and fresh material is used for each experiment. Table 3-1 presents key parameters used in the calibration of the film thickness monitor. Figure 3-4 and 3-5 presents the SEM photographs showing the cross section of the organic thin film.

Table 3-1: Key parameters used in the calibration of film thickness monitor.

Organic material	Distance from substrate to graphite boat (mm)	Distance from film thickness monitor to substrate (mm)	Base vacuum chamber pressure (Torr)	Graphite boat temperature range during material deposition (°C)	Temperature controller accuracy (°C)
TPD	85	10	$< 1x10^{-6}$	210	+/-2
DPVBi	85	10	$< 1x10^{-6}$	220	+/-2
Alq3	85	10	$< 1x10^{-6}$	280	+/-2
$Ir(piq)_3$	85	10	$< 1x10^{-6}$	300-330	+/-2

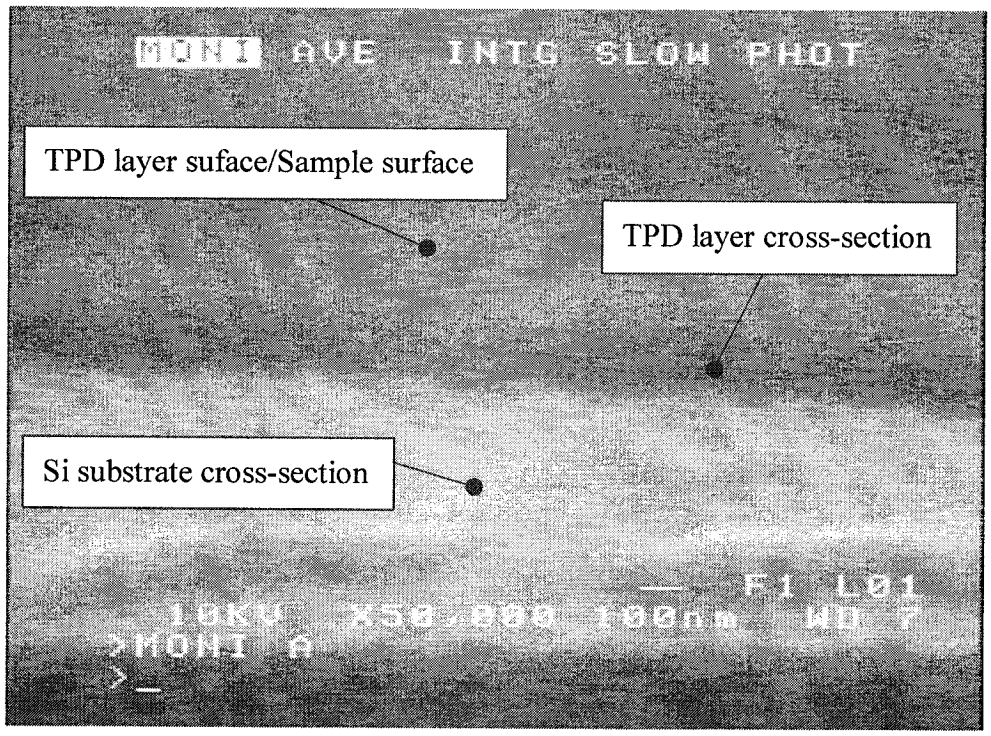

Figure 3-4: A SEM photograph showing the cross section of a vacuum deposited TPD film with a thickness of 144 nm.

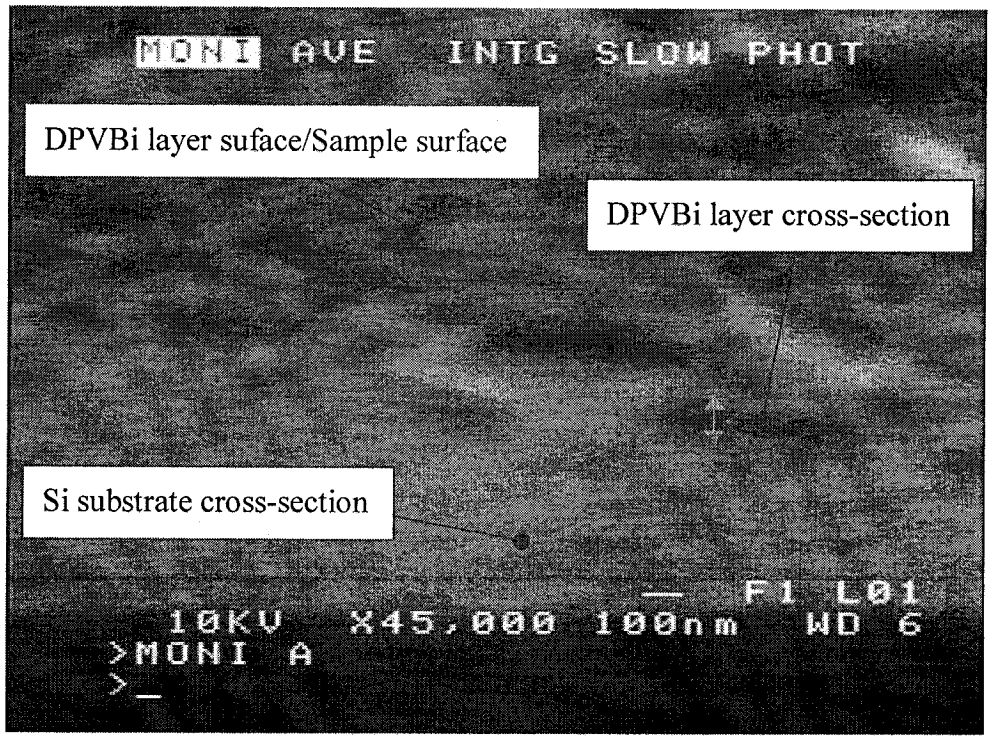

Figure 3-5: A SEM photograph showing the cross section of a vacuum deposited DPVBi film with a thickness of 112 nm.

3.3 Fabrication Procedure

3.3.1 Process flow chart

The flow chart in Figure 3-6 summarizes the key steps in the OLED fabrication procedure used in the present work.

The large size commercial ITO-coated glass plate is first cut into the smaller pieces with the size that can be easily processed in the laboratory. The ITO substrates are then cleaned with acetone in an ultrasonic bath. A photolithography process followed by an etching process is utilized to pattern the ITO coating on the substrate into the desired electrode size. Once the patterned ITO substrate is ready, it is mounted onto the substrate holder in the main vacuum chamber of the organic material deposition system. After the evacuation of the chamber, the multi-layer organic material deposition is accomplished in the order of TPD, DPVBi, $Ir(piq)_3$, and then Alq_3. Finally, the fabrication of the OLED is completed with the deposition of the top metal contacts by thermal evaporation through the aluminum shadow mask.

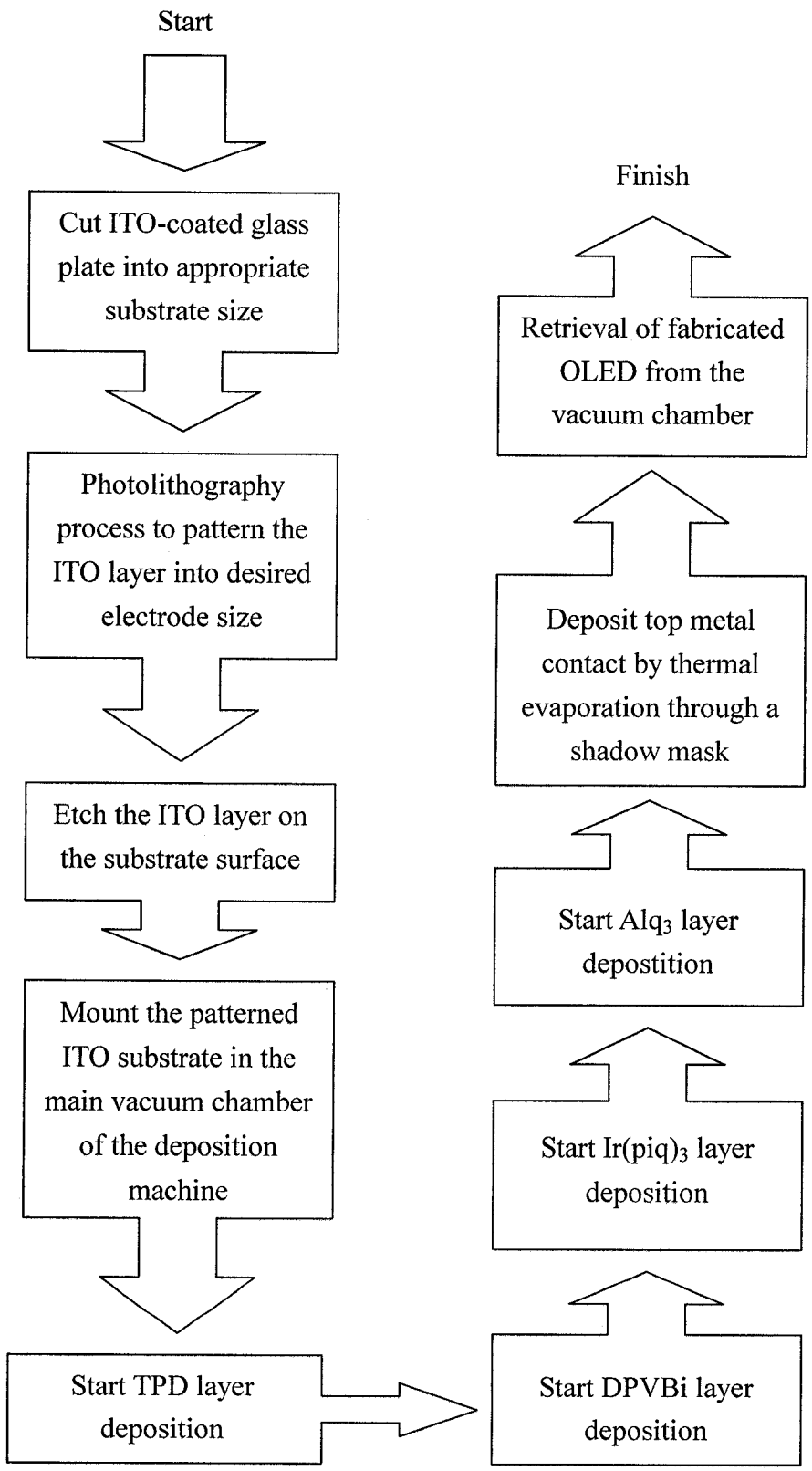

Figure 3-6: A general flow chart summarizes key steps in fabricating white OLEDs.

3.3.2 Substrate preparation

The substrates used in the experiments are the ITO-coated glass obtained from Applied Films. The sheet resistance of the ITO film is measured to be about 20 to 30 Ω/sq. The average thickness of the ITO film is ranging from roughly 120 to 150 nm with the maximum ITO film thickness not exceeding 200 nm. The obtained ITO-coated glass panel has the size of 30 cm by 30 cm and its size is too large to be processed in the laboratories. Therefore, the ITO-coated glass is cut into smaller pieces, typically with size of 10 mm by 30 mm, in order to be able to be processed in our laboratories.

Since the cleanliness of the ITO film plays an important role in determining the fabrication yield and the performance of the fabricated devices, the ITO-coated substrate is cleaned repeatedly to ensure maximum possible cleanliness and the consistent ITO cleanliness among all ITO substrates. The cleaning procedure of the ITO-coated substrate includes ultrasonic agitation of the substrates immersed in a solvent such as acetone (ACE). After the ultrasonic bath agitation in the solvents, the substrate is then rinsed thoroughly with de-ionized (DI) water for a few minutes. Afterward, the substrate is baked dried at 90°C for 10 minutes.

3.3.3 ITO electrode patterning

For the purpose of the experiment consistency, the dimensions of the device are precisely controlled by controlling the sizes of both the ITO electrode and top metal contact. The dimensions of the device itself are targeted to be 2 mm by 3 mm for a surface area of 6 mm^2 for a single OLED. The dimensions of ITO electrode are designed to be 2 mm by 24 mm with a spacing of 1mm between each ITO electrode. The creation of ITO pattern is accomplished by using photolithography process. This lithography process is detailed below:

1) Apply Shipley AZ-1827 photoresist onto the substrate by spin coating
2) Pre-bake the photoresist at 90°C for 10 minutes
3) Align the photomask and expose the photoresist to the UV light. The UV system (Oriel Corp. Model 87100 Mask Aligner, UV exposure system) is set at 300W and the exposure time is set to 300 seconds.
4) Develop the photoresist using Shipley Microposit Developer.
5) Post-bake the photoresist at 120°C for 20 to 25 minutes.
6) Cool the substrate to room temperature in a Pyrex dish.

After the patterns have been created on the photoresist, the substrate is now ready to

be etched using the ITO etching solution, which is a specific mixture of 21 ml of HCl, 0.534g of $Fe_2Cl_3 \cdot 6H_2O$, and 100ml of H_2O. The substrate is immersed into the warmed ITO etching solution (the temperature is controlled at 50°C) and the etching process takes roughly 15 minutes. The exact etching time will of course depend on the actual thickness of the ITO film on the substrate and other factors. The etched substrate is then rinsed in warm running tap water (~ 40°C) for 20 minutes to remove any residual etching solution. Figure 3-6 shows the completed patterned ITO substrate after the etching process. To remove the photoresist, the substrate is immersed in ACE and followed by rinsing thoroughly with DI water for a few minutes. Finally, the patterned substrate is baked-dried at 90°C for 10 minutes to remove any possible residual H_2O left on the surface the ITO substrate. The drying process is necessary due to the fact that organic materials deposited onto the substrate are suspect to the degradation caused by H_2O.

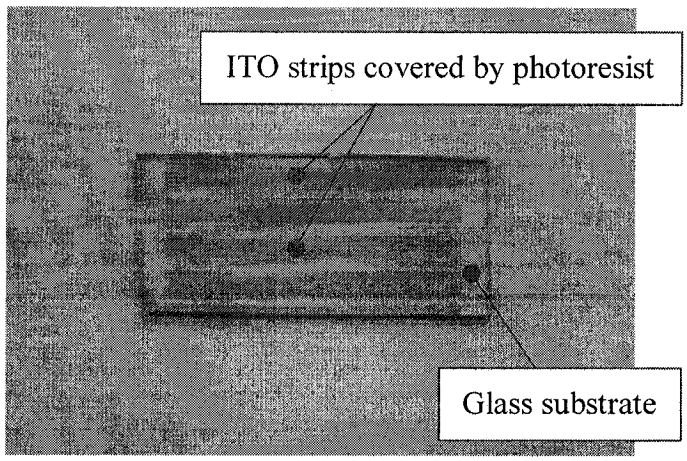

Figure 3-6: A photograph showing the etched ITO strips on a glass substrate with photoresist covering the ITO.

3.3.4 Thermal vacuum deposition of the organic material

The patterned ITO-coated substrate is first mounted with the ITO side facing downward on the substrate holder of the vacuum chamber before starting chamber evacuation toward the desired pressure. Once the desired vacuum pressure of less than 10^{-6} Torr is reached, the thermal evaporation of the material is performed. The procedure for depositing each organic material is basically the same and the only difference is in the deposition temperature setting of each material. The heating system attached to the graphite boat used for organic material deposition is switched on first. The sample is initially shielded from both the undesired material deposition and the heat radiation by a metal mask. Once the desired deposition temperature has been reached, the sample is moved into position by adjusting the rotary shaft connected to the substrate holder. The thickness monitor is used to perform the real-time thickness measurement of the deposited organic thick film. Once the target thickness has been reached, the sample is moved away from the source and again shielded behind the metal mask. The heating system is then switched off and the graphite boat is allowed to cool down to near room temperature before another deposition cycle. After the deposition cycle is repeated as many times as the structure requires to, the device is completed with a layer of metal

contact formed by thermal evaporation. The vacuum chamber is only opened when the device structure requires more material variety than the capability of the vacuum chamber. The vacuum chamber could only accommodate a maximum of two different kinds of organic material at any given time, so the vacuum chamber will need to be opened if more than two organic materials are needed to create the devices. Table 3-2 shows the key parameters used in the deposition of organic materials.

Table 3-2: Key parameters used in the deposition of organic materials.

Organic material	Base vacuum chamber pressure (Torr)	Graphite boat temperature during deposition / Controller set point (°C)	Temperature controller accuracy (°C)	Typical average deposition rate (Å/s)
TPD	$< 1x10^{-6}$	210	+/-2	~3.5
DPVBi	$< 1x10^{-6}$	220	+/-2	2.0~3.0
Alq3	$< 1x10^{-6}$	280	+/-2	~3.0
$Ir(piq)_3$	$< 1x10^{-6}$	330	+/-2	3.0~3.5

The deposition temperature is chosen based on the following criteria: the typical average deposition rate at the temperature set-point should be higher than 2.0 Å/s if possible, but without risking overheating the materials. The reasons behind this criterion are that: first, deposition rate should be sufficiently high so that the deposition time is not too long while the substrate is being exposed to the possible heat radiation coming from

the heating elements and, second, the temperature should not be too high so that the materials in the graphite boat are not being over heated, causing changes in the material molecular structure or properties.

Figure 3-7(a) shows a flow chart for organic material deposition process. At first, three organic materials, TPD, DPVBi, and $Ir(piq)_3$ are deposited in sequence respectively. To bypass the limitation of a maximum number of two organic materials may be deposited without the need of opening vacuum chamber and deposit three material at one time, DPVBi and $Ir(piq)_3$ share the same graphite boat and are deposited in sequence at different temperature since the evaporation temperature is drastically different between the two materials. In effect, when DPVbi starts to evaporate and deposit onto the substrate at the temperature of 220°C, $Ir(piq)_3$ is only merely heated up and thus not evaporating. Once all DPVbi has been evaporated, which process could easily be confirmed by the thickness monitor, the deposition of $Ir(piq)_3$ is then carried out at the much higher temperature of 330°C. After the successful deposition of the three organic layers, the vacuum chamber is opened to place Alq_3 into the now empty graphite boat.

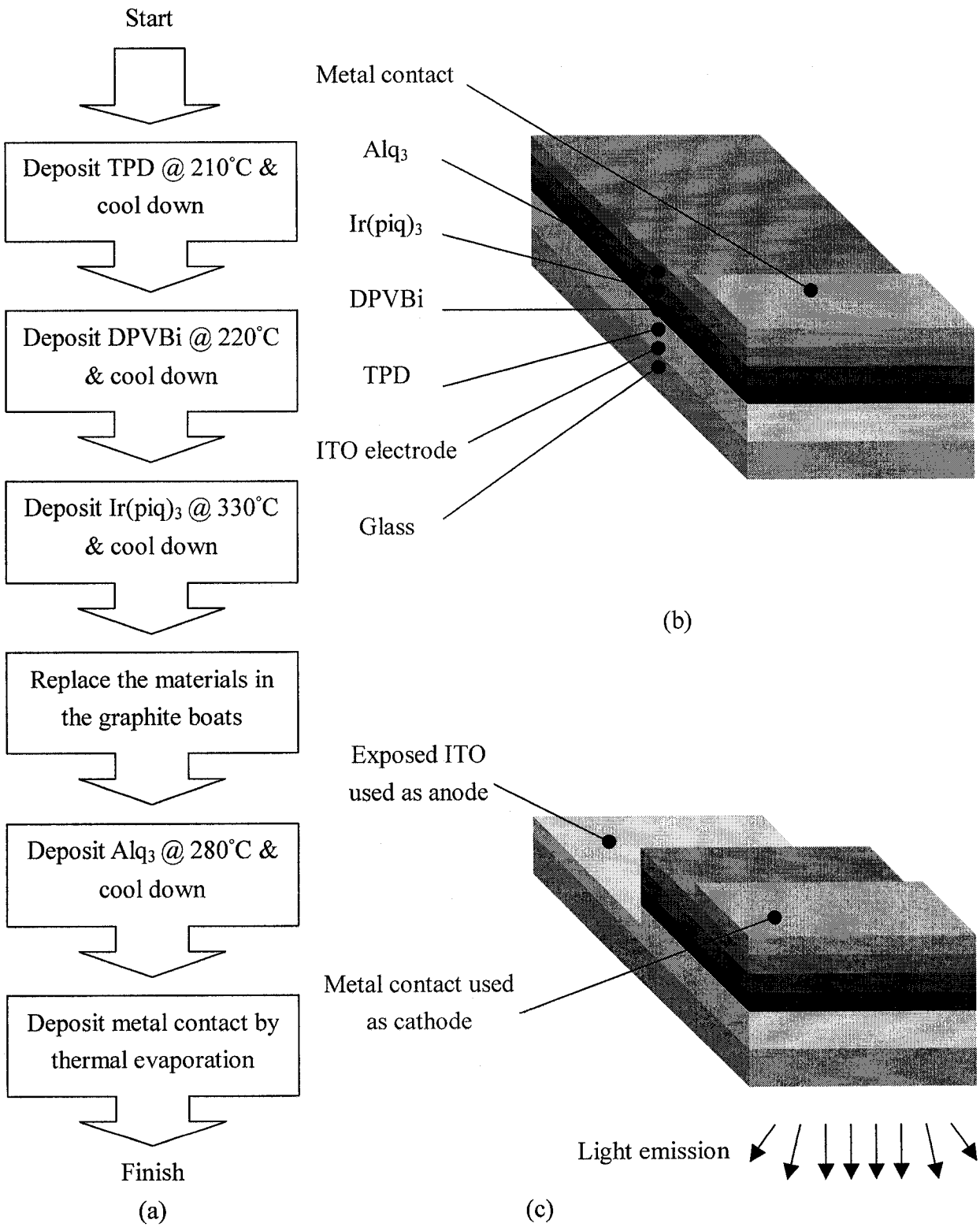

Figure 3-7: (a) a flow chart for organic material deposition process, (b)&(c) 3D diagrams showing the structural construct of the white OLED fabricated in this experiment.

Figure 3-7(b) is a 3D schematic diagram showing the structure of the white OLED fabricated in this experiment. The order of layer deposition is from bottom to the top and the metal contact is only partially covering the device due to the shadow mask used during the metal contact evaporation.

Figure 3-7(c) is also a 3D schematic diagram showing the structure of the white OLED fabricated in this experiment and ready for characterization. The diagram shows the exposed ITO layer, which is to be used as anode during device operation. A portion of the substrate not covered by the metal contact is exposed by using acetone on a cotton swab to wipe clean the organic layers. The exposed ITO then can be used as anode to compliment the top metal contact, which is used as cathode. The diagram also shows the direction of light generated by the fabricated OLED.

As discussed in chapter 2, both the device structure and individual layer thickness have substantial effects on OLED performance and OLED color. As a result, a series of white OLED samples of the same structure design proposed in chapter 2 with varying layer thicknesses are fabricated. The purpose is to investigate the effect of layer thickness on the device performances in a specific WOLED structure design.

3.3.5 Thermal evaporation of top metal contact

A dual metal layer consisting of a top silver and a bottom magnesium is used as the top metal contact for all devices fabricated in this study. As purchased, silver comes in under the form of thin sheets while magnesium comes as small lumps. The silver sheets are cleaned with acetone and DI water and then cut into small thin strips. The magnesium lumps are broken into smaller lumps in a quantity suited for each individual experiment. For deposition, both metals are placed into a Mo boat. The evaporation of the metals is performed at the base pressure of roughly $1x10^{-6}$ Torr. The magnesium is deposited first since this metal has a lower melting point than silver. This is desirable as the work function of magnesium is lower than silver, and the low work function material is needed for the cathode. Although the film thickness is monitored during deposition, the recorded layer thickness does not represent the real metal layer thickness as the thickness monitor sensor is not properly aligned to the Mo boat. Nevertheless, the real-time thickness monitoring during deposition is still useful in achieving consistent metal layer thicknesses among all samples – even though the exact thickness of the metal layer is not known. Shadow masking is also used to pattern the metal layers on the samples. During the pre-heating process of the Mo, the sample is shielded from the thermal radiation by a

metal mask. The deposition process typically lasts 2 to 3 minutes in order to provide sufficient metal layer thickness and avoid possible accidental over-heating of the sample. When the Mo boat is cooling down, the sample is again shielded from thermal radiation by the metal mask.

Table 3-3: Physical properties of metal contact and metal boat materials

Name	Element Symbol	Bulk material appearance	Metal Work function	Melting Point	Boiling Point
Silver	Ag	Sheet	4.26 eV	962°C	2162°C
Magnesium	Mg	Small chunks	3.66 eV	650°C	1090°C
Molybdenum	Mo	Sheet	4.6 eV	2623°C	4639°C

3.4 Summary

We presented an overview of the various fabrication methods for OLEDs. The adopted fabrication process uses vacuum deposition since the organic materials chosen for this work are of small molecule materials. The critical steps in this fabrication procedure are the cleaning of the ITO substrates, precise control of the deposition temperature, the precise control of the organic layer thickness, and the setting up of the various components in the vacuum deposition system.

[3-1] Joseph Shinar ed., *Organic light-emitting devices : a survey*, AIP Press, New York, **2004**.

[3-2] J.N. Bardsley, *IEEE Journal on Selected Topics in Quantum Electronics* **2004**, *10*, no. 1, 3.

[3-3] J.C. Carter, A. Wehrum, M.C. Dowling, M. Cacheiro-Martinez N.B. Baynes, *Proceedings of SPIE - The International Society for Optical Engineering* **2002**, *4800*, 34.

Chapter 4

Device Characterization

4.1 Overview

Following the selected small molecule material and selected device structure layout chosen in Chapter 2, multi-color organic light emitting devices (OLEDs) have been fabricated using the experimental setup described in Chapter 3. In order to study the performance of the fabricated OLEDs and more importantly to verify the emission color of the devices, two measurements including current-voltage characteristic measurements and optical emission spectrum measurements have been performed. From these two measurements, the device characteristics such as emission spectrum, luminescence intensity, luminous efficiency, external quantum efficiency, and CIE color coordinates were deduced. The definition and analytical framework of the various optical characterization techniques have been treated in details in other references [4-1, 4-2]. Brief discussions on each of the optical characteristics considered in this study are presented in this chapter. Furthermore, the effect of the organic layer thickness of each layer on the device performance has been investigated. The results provide the means of

fine-tuning the device performance and identifying the best-performing white OLED under the selected material and structure composition.

4.2 Measurement setup

The current-voltage characteristics measurements of all fabricated devices were performed by using a HP 4145A parameter analyzer. The ITO anode of the OLED is connected to the positive electrode while the metal cathode is connected to the negative electrode of the analyzer. The bias voltage is applied through the parameter analyzer source channel. The applied bias starts at 0 V and is ramped to 15 V using 0.1 V step increments. The corresponding current value flowing through the device at each voltage level is recorded by the parameter analyzer. In order to minimize the effect of any possible unwanted external photo excitation, the measurement was performed in a dark room. Figure 4-1 shows a schematic diagram of current-voltage characteristics measurement setup.

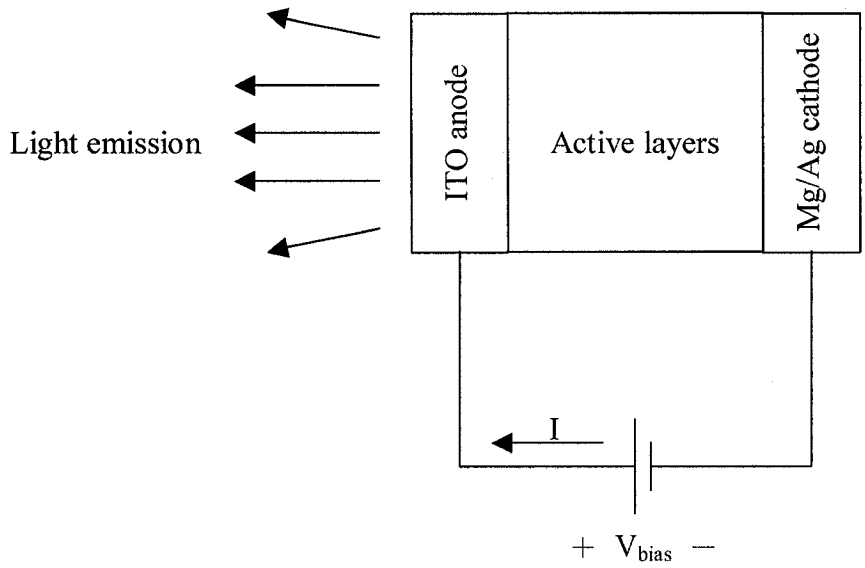

Figure 4-1: A schematic diagram of I-V measurement setup on the OLEDs.

The optical emission spectrum measurements of all fabricated devices were performed by utilizing a Photon Technology International (PTI) steady state spectrofluorometer system model QuantaMaster QM-4/2003 equipped with a R928PMT (190-900nm) detector. The detector reports back the measurement results in the format of photon counts per second across the designated spectral range. Due to the sensor sensitivity limitation, the maximum photon count per second limitation that can be measured by the detector is 3773590 photons per second. As a result, any spectral data showing peak intensity over the 3773590 photons per second limitation were disregarded in the report of device characteristics. The spectral measurement was taken at each voltage bias point in the 3 V to 15 V range with 1 V increment. The wavelength range for

the measurements is 300 nm to 850 nm with 1 nm increment, which range encompasses the visible range (380-780 nm). A schematic of the QM-4/2003 spectrofluorometer system is illustrated in Figure 4-2.

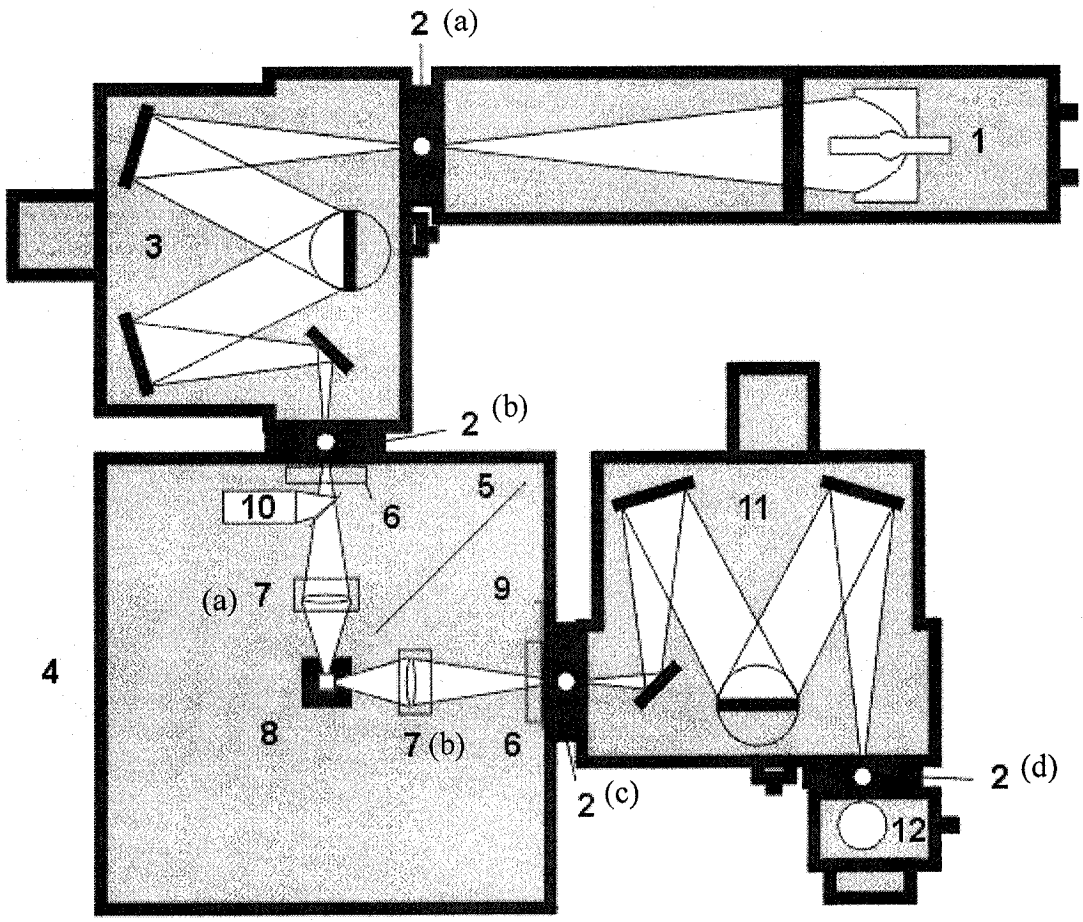

1 Lamp Housing
2 Adjustable slits
3 Excitation Monochromator
4 Sample compartment
5 Baffle
6 Filter holders
7 Excitation/emission optics
8 Sample holder
9 Emission port shutter
10 Excitation correction
11 Emission Monochromator
12 PMT detector

Figure 4-2: The setup of the PTI QuantaMaster QM-4/2003 spectrofluorometer system.

The OLED was placed and fixed to the sample holder at location 8, facing in the direction of the optic lens 7(b). The normal to the OLED emission area was aligned with the axis of the lens 7(b). During measurement, the adjustable slits at 2(a) and 2(b) were fully closed to prevent any possible light leakage from external sources. The adjustable slits at 2(c) and 2(d) were fully opened. The light transmission from the lens at 7(b) to the PMT detector at 12 is assumed to have the attenuation ratio, γ. This assumption implies that the photons count detected by the PMT detector is only a certain percentage of the photon count collected at the lens 7(b). The assumption is an important basis for OLED emission intensity calculation, which topic will be discussed later in this chapter.

For both electrical and optical measurements, a total of 6 different OLED configurations were investigated. All devices share the same standard device structure (ITO/TPD/DPVBi/$Ir(piq)_3$/Alq_3) discussed in chapter 2. The difference between each device primarily lies in the thickness of each organic layer - specifically both the DPVBi layer and $Ir(piq)_3$ layers and the slightly different effective active device area. The purpose of mix match different layer thickness parameter was to investigate their effects on the device performance and resulting device color. Thus, the best layer thickness parameters for producing a good performance white OLED can be identified. The layer thickness configurations of the fabricated OLEDs are shown in Table 4-1.

Table 4-1: Device layer thicknesses of the fabricated OLEDs. 1 Å = 1×10^{-10} m.

Device	OLED1	OLED2	OLED3	OLED4	OLED5	OLED6
Device Area	6 mm^2	6 mm^2	6 mm^2	6 mm^2	6 mm^2	5 mm^2
Alq_3 layer thickness	500 Å	450 Å	450 Å	450 Å	500 Å	500 Å
$Ir(piq)_3$ layer thickness	40 Å	40 Å	40 Å	20 Å	15 Å	25 Å
DPVBi layer thickness	100 Å	110 Å	90 Å	60 Å	75 Å	100 Å
TPD layer thickness	600 Å	600 Å	600 Å	600 Å	600 Å	500 Å
Total layer thickness	1240 Å	1200 Å	1180 Å	1130 Å	1190 Å	1125 Å

4.3 Current-voltage characteristics

The current-voltage characteristics of the device provide the information on the electrical properties of the device. Information such as injected current density at a given voltage and power consumption of the device can be obtained. Also, this provides the opportunity to combine the optical characteristics such as luminance and external quantum efficiency with the current density data as the optical data is measured against the specific bias voltages. Figure 4-3 to 4-4 shows the current-voltage characteristics of the device where figure 4-3 uses a linear scale while figure 4-4 uses a logarithmic scale.

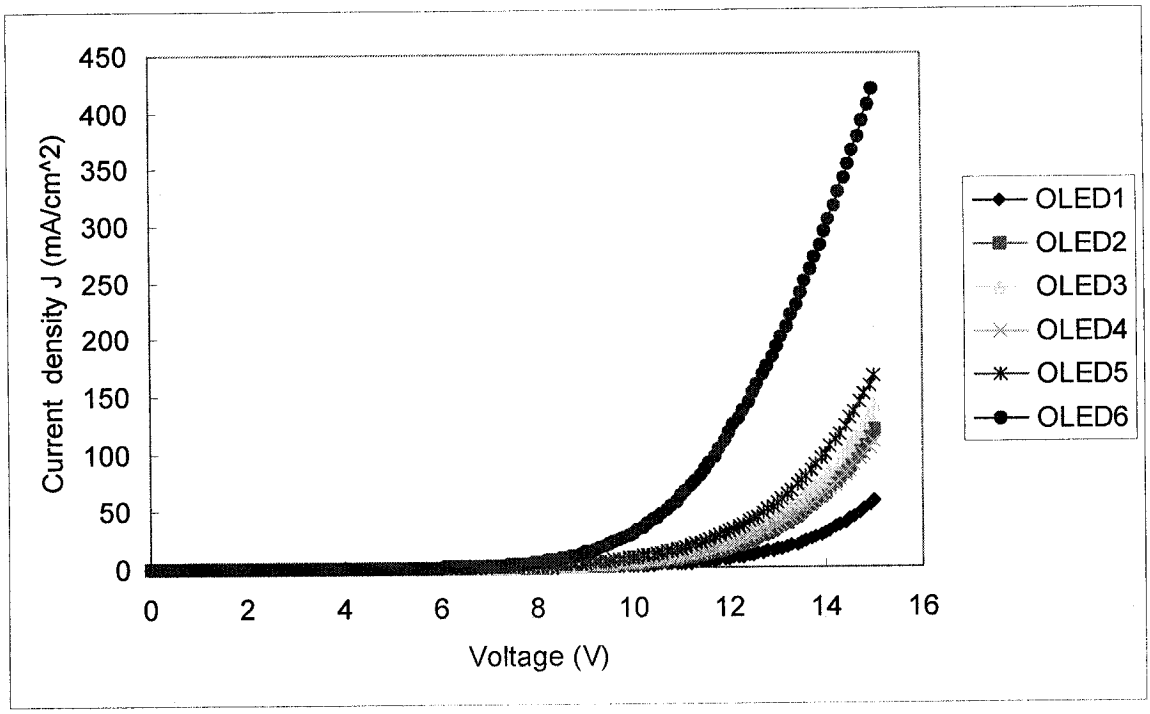

Figure 4-3: J-V characteristics of the fabricated OLEDs in linear scale.

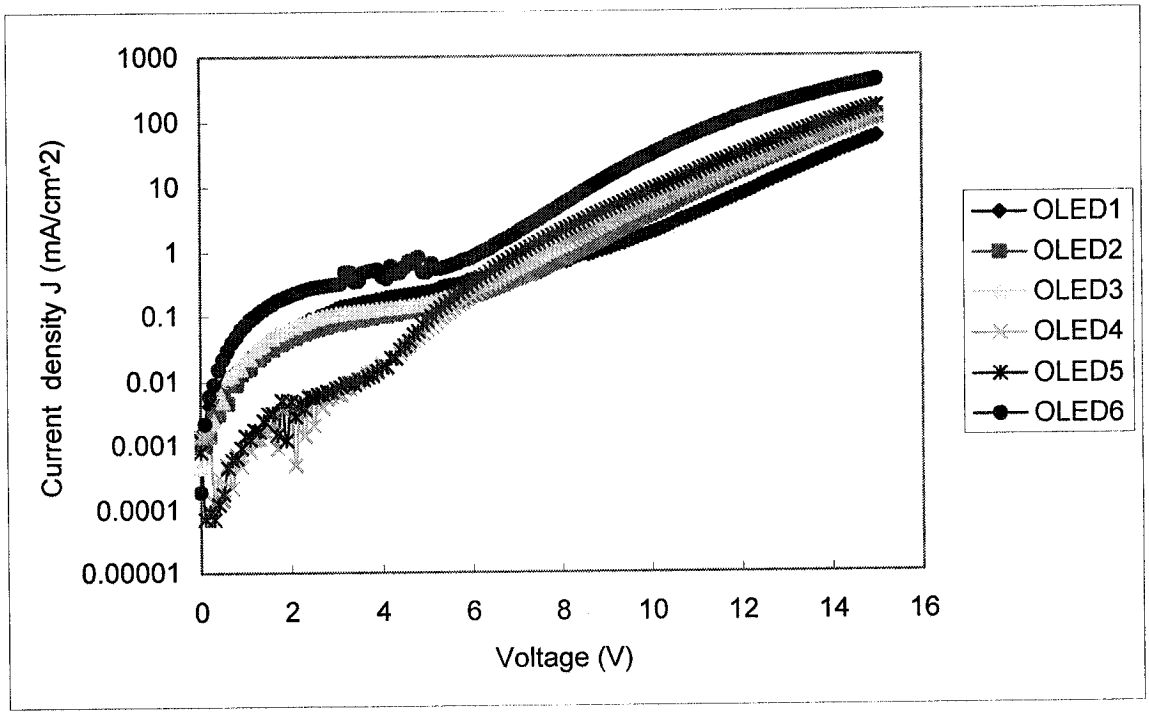

Figure 4-4: J-V characteristics of the fabricated OLEDs in logarithmic scale.

It can be clearly seen that the current density of the device is dependent on the total layer thickness of all layers where the largest total layer thickness (OLED1) corresponds to the lowest current density characteristic. Conversely, the smallest total layer thickness (OLED6) corresponds to the highest current density characteristics. This is due to the fact that organic materials used in OLED typically have low carrier mobility values and smaller layer thicknesses promote successful carrier injection and transport from one electrode to the other. It can also be seen that the injected current density is strongly dependent on the thickness of both hole transport layer and electron transport layer. The reduction of either the TPD layer thickness or the Alq_3 layer thickness leads to the increase in current density with the reduction of the TPD layer thickness having a more profound effect (see OLED6). The discrepancy in the lower current density values at a lower biasing voltage is likely due to the localized surface defects in both organic layers and electrodes. Localized defects such as pinholes can lead to possible localized shorting which affects the current-voltage behavior at low current densities. It can also be observed that the current density increases at a faster pace after above a threshold voltage of 5 to 6 V. This also corresponds to the voltage where the energy barriers between each layers can be overcome by the majority of the carrier. Thus, the energy barriers will no longer effectively confine the carrier transport on a large scale.

4.4 Device Luminance

4.4.1 Luminous flux

The measurement data obtained form the detector is the photon emission rate across the designated spectrum (300-850 nm) and the unit is in photon counts per second. In order to obtain the device characteristics such as luminous intensity, a series of calculation and transformation from the photon emission rate raw data must be performed. First, the spectral power distribution of the radiant flux, or sometimes referred to as radiant power, is calculated from the photon emission rate spectra. In radiometry, radiant power is defined as the measure of total power of electromagnetic radiation. The SI unit for radiant power is watt (W). Equation 4-1 illustrates the relationship between the energy of a photon, E, and its frequency, f, with its corresponding wavelength λ, where h = 6.626×10^{-34} J·s is Planck's constant and c=2.998×10^{8} m/s is the speed of light.

$$E = hf = h\frac{c}{\lambda} \qquad (4\text{-}1)$$

Thus, the total radiant power Φ(λ) at given wavelength is the photon emission rate N(λ) at the wavelength times the energy E(λ) of a single photon at the wavelength.

$$\phi(\lambda) = N(\lambda)E(\lambda) \qquad (4\text{-}2)$$

However, the spectral distribution of the luminous flux is different from the spectral

distribution of the radiant flux due to the fact that human perception of brightness is wavelength dependent. Human visual system is more sensitive to wavelengths in the middle of the visual spectrum and becomes less and less sensitive to light near the extremes of the visible spectrum. The CIE spectral luminous efficiency function, $V(\lambda)$, established in 1924, is a spectral weighting function used to describe the perception of brightness matches for photopic vision. Figure 4-5 shows the CIE photopic spectral luminous efficiency function $V(\lambda)$.

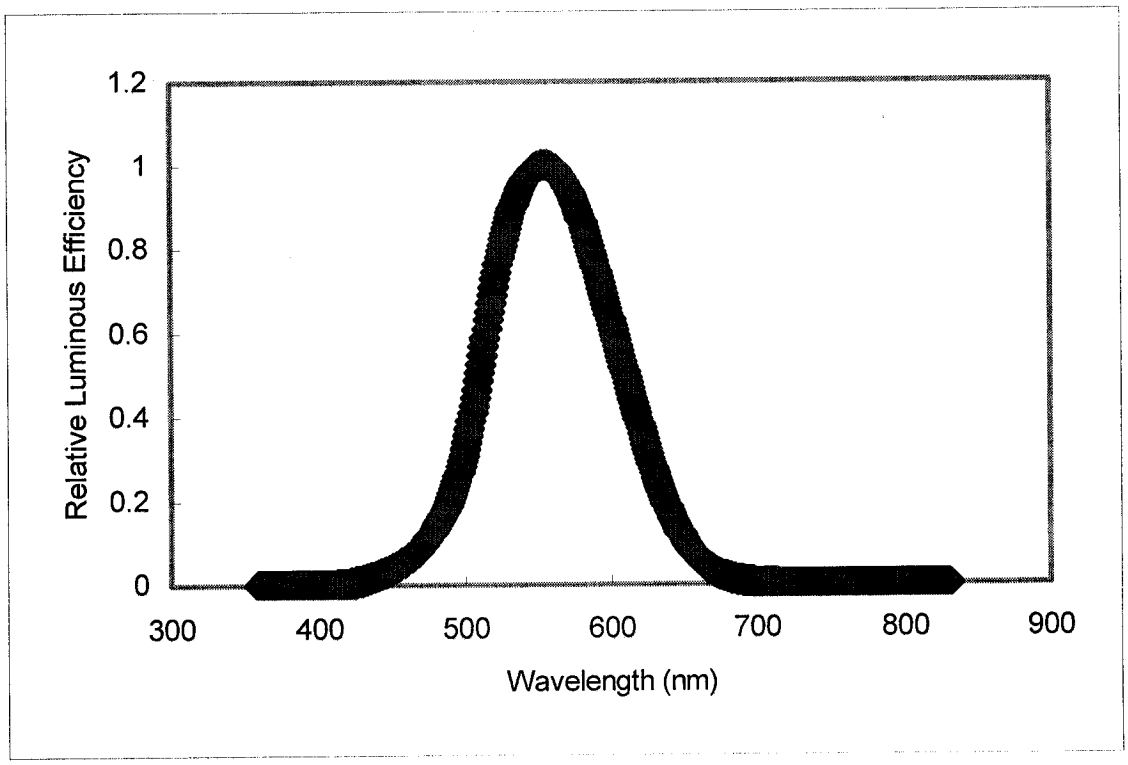

Figure 4-5: CIE photopic luminous efficiency function, $V(\lambda)$.

The conversion from radiant flux (radiometric quantity) to total luminous flux (photometric quantity) is achieved via spectral integration, as shown in Equation 4-3.

$$\phi_v = k \int_{\lambda} \phi(\lambda) V(\lambda) d\lambda \qquad (4\text{-}3)$$

Φ_v is the total luminous flux across the spectral band under consideration; $\Phi(\lambda)$ is the spectral distribution of radiant flux; $V(\lambda)$ is the CIE spectral luminous efficiency function; and k = 683 lumens/watt is the unit conversion constant between luminous flux and radiant flux. In photometry, luminous flux, or sometimes referred to as luminous power, is the measure of perceived power of light by human visual system. It differs from radiant flux in that the luminous flux is adjusted by the sensitivity of the human visual system. The SI unit for luminous flux is lumen (lm).

The electroluminescence intensity measurement in the format of photons emission rate reading taken directly from the detector does not represent the overall luminous power of the device or the luminous intensity of the device, but rather it represents only the fraction of total luminous power passing through optic lens 7(b) in Figure 4-1. For this reason, the overall emissive luminous power of the device and the luminous intensity with respect to the surface normal have to be calculated from combining knowledge of the light emission distribution profile of the device and the detector reading. In photometry, luminous intensity is defined as a measure of the perceived power of light by

human visual system from a light source in a particular direction. In short, luminous flux is the total luminous intensity in the pre-defined range of directions. The SI unit for luminous intensity is candela (cd).

4.4.2 Lambertian emission

Several authors have reported that the light distribution of OLED light emission is approximately Lambertian [4-2 and 4-3]. According to Lambert's law, the total radiant power observed from a Lambertian source is directly proportional to the cosine of the angle between observer's line of sight and the surface normal. In effect, for a Lambertian emission, the luminous intensity profile relationship is represented by Equation 4-4 and illustrated in Figure 4-6 (a), where I is the luminous intensity emitted at an angle θ with respect to the normal of the surface of the OLED and I_v is the luminous intensity emitted with respect to the surface normal.

$$I = I_v \cos(\theta) \qquad (4\text{-}4)$$

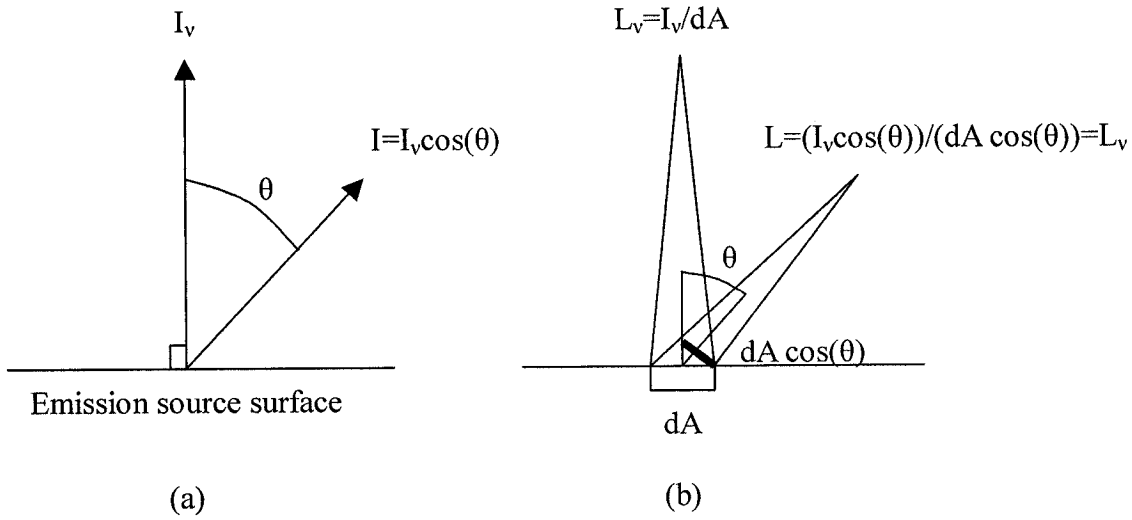

Figure 4-6: Lambertian emission (a) the relation between luminous intensity and the viewing angle; (b) the luminance is the same regardless of the viewing angle.

In terms of radiance, a Lambertian emitter is isotropic, which emits equal radiance into any solid angle within the first half space. This implies that the human perceived brightness, or luminance, a radiance quantity, will be the same regardless the viewing angle. Note that this is different from the relation between the luminous intensity, which is a radiant intensity quantity, and the viewing angle. The radiance quantity is measured as the density of the radiant intensity quantity while radiance quantity is the radiant intensity per unit apparent emission area. For viewing from an angle, although the luminous intensity is reduced by the cosine of the angle, the observed size of the apparent emission area is also reduced by the cosine of the angle. Thus, as illustrated in figure 4-6(b), the luminance is the same regardless of the viewing angle.

4.4.3 Luminous intensity

As discussed in section 4.2, the total electroluminescence intensity measurement is based on the assumption of lossy photon transmission with the attenuation ratio of γ where the photon count collected at the detector will only be a certain percentage, as defined by γ, of the photon count collected at the optic lens 7 in Figure 4-1. In effect, the effective detector area can be treated the same as the surface area of the optic lens with a specific scaling ratio of attenuation on radiant flux. This means that the total luminous flux measured by the detector will be a fraction of the total luminous flux passing through the optic lens. Figure 4-7 depicts the schematic of the source (OLED) and the optic lens in the electrofluorometer system setup, where S_a is the apparent surface area of the OLED; S_d is the surface area of the optic lens which is also equal to the effective detector area; D is the distance between the source and the optic lens; r is the radius of the optic lens; Ω_{lens} is the solid angle covered by optic lens; φ is the half angle at the apex such that $\tan(\varphi) = r/D$. While the surface area of the optic lens area is $\pi r^2 = 2.89\pi$ cm^2, the surface area of the OLED is around 6 mm^2. Therefore, the OLED is essentially a point source with respect to the optic lens area.

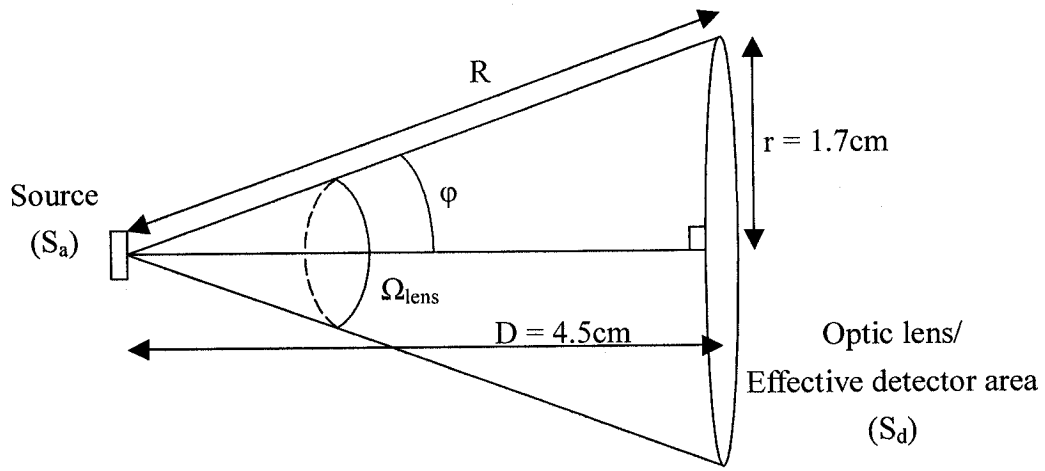

Figure 4-7: A schematic diagram of the source and the optic lens in the electrofluorometer system setup.

With the knowledge of both OLED being a nearly Lambertian source and the dimension of the setup, the total luminous flux or the total luminous power passed through the lens, Φ_{lens}, can be calculated by integrating the luminous intensity, $I = I_v\cos(\theta)$, over the solid angle covered by the optic lens area, Ω_{lens}. Equation 4-5 shows the calculation of total luminous flux passed through the lens.

$$\begin{aligned}\phi_{lens} &= \int_{\Omega_{lens}} I_v \cos(\theta) d\Omega \\ &= 2\pi I_v \int_0^{\varphi} \cos(\theta)\sin(\theta) d\theta \\ &= 2\pi I_v \int_0^{\frac{r}{R}} \sin(\theta)(d\sin(\theta)) \\ &= (\frac{r}{R})^2 \pi I_v = \frac{r^2}{r^2 + D^2} \pi I_v\end{aligned} \qquad (4\text{-}5)$$

Note that the solid angle Ω of a cone with the half apex angle θ is shown in Equation 4-6.

$$\Omega = 2\pi(1-\cos(\theta)) \qquad (4\text{-}6)$$

Essentially,

$$d\Omega = 2\pi \sin(\theta)d\theta \qquad (4\text{-}7)$$

The ratio of total luminous power measured by the detector, $\Phi_{detector}$, to the total luminous power passed through optic lens, Φ_{lens}, is defined by the attenuation ratio γ, as shown in Equation 4-8.

$$\phi_{detector} = \phi_{lens} \cdot \gamma \qquad (4\text{-}8)$$

From equation 4-5 and 4-8, the luminous intensity of the OLED in the direction of surface normal can be calculated using Equation 4-9.

$$\begin{aligned} I_v &= \phi_{lens}\left(\frac{r^2 + D^2}{\pi r^2}\right) \\ &= \frac{\phi_{detector}}{\gamma}\left(\frac{r^2 + D^2}{\pi r^2}\right) \end{aligned} \qquad (4\text{-}9)$$

4.4.4 Calculation of attenuation ratio γ

As discussed earlier, the attenuation ratio γ is defined as the percentage value of the photon count collected at the detector to the photon count collected at the optic lens 7 in Figure 4-1. In other words, the attenuation ratio defines the ratio between the quantitative value measured by the spectrofluorometer and the true quantitative value of the device

characteristic. The value of this ratio is essential to translate the detector reading into the device optical characteristics. To calculate this ratio, two sets of luminance measurements are carried out using the spectrofluorometer and a Delta OHM quantum photo radiometer model HD9021 with LP9021 luminance probe, respectively. The device luminance calculated from spectrofluorometer using the method discussed above is compared to the reading from the quantum photo radiometer and the attenuation ratio is then calculated. Table 4-2 shows the reference OLED luminance readings taken from two measurement methods and the calculated attenuation ratio.

Table 4-2: Luminance measurement data and the attenuation ratio.

Voltage	Luminance (spectrofluorometer)	Luminance (radiometer)	Ratio γ
12 V	5.182×10^{-3} cd/m^2	52 cd/m^2	1.03×10^{-5}
15V	5.33×10^{-4} cd/m^2	311 cd/m^2	1.67×10^{-5}

Taking the average from the two derived ratio values, the attenuation ratio is found to have the value of $\gamma = 1.35\times10^{-5}$.

4.4.5 Luminance

In photometry, luminance, or sometimes referred as luminosity, is defined as a

measure of the density of luminous intensity. It describes the amount of energy of light that passes through or is emitted from a particular surface area, and falls within a given direction. The SI unit for luminance is candela per square meter (cd/m^2). In practice, luminance is used to describe the brightness of the display per unit device area. As mentioned earlier in the chapter, for a nearly Lambertian emitter such as an OLED, the luminance is the same regardless of the viewing angle. Thus, luminance is a suitable measure of the display brightness regardless of the display size and viewing angle. Given the OLED device area is known, the luminance of the OLED, L_v, can be calculated by dividing the OLED luminous intensity, I_v, by total OLED emission area, S_a, as shown in Equation 4-10.

$$L_v = \frac{I_v}{S_a} \qquad (4\text{-}10)$$

4.4.6 Device Luminance

Figure 4-8 and Figure 4-9 illustrates the luminance characteristics of the fabricated OLEDs with respect to biasing voltage in both linear and logarithmic scales, respectively. As mentioned earlier, the detector of the spectrofluorometer has a maximum detectable photon count limitation, thus, any measured data exceeding the detector limit will not be

representative of the true device characteristics as the peak emission data will be capped at the detector limit. Thus, the data with peak photon emission rate exceeding the detector limit are discarded. Devices OLED3, OLED4, and OLED5 are such devices exceeding detector limitation at 11, 12, and 14 V respectively. As a result, these three devices have the accurate data only up to 10, 11, and 13 V, respectively, as shown. Figure 4-10 and Figure 4-11 illustrates the luminance characteristics of the fabricated OLEDs with respect to current density in linear and logarithmic scales, respectively.

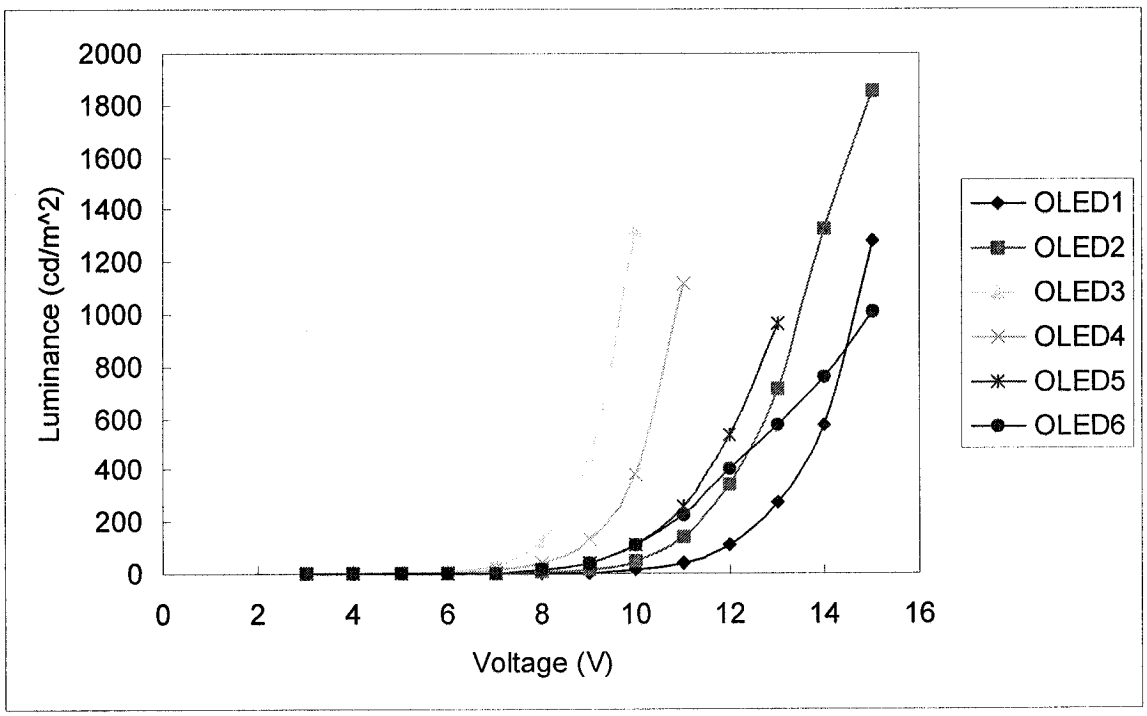

Figure 4-8: Device luminance characteristics with respect to voltage in linear scale.

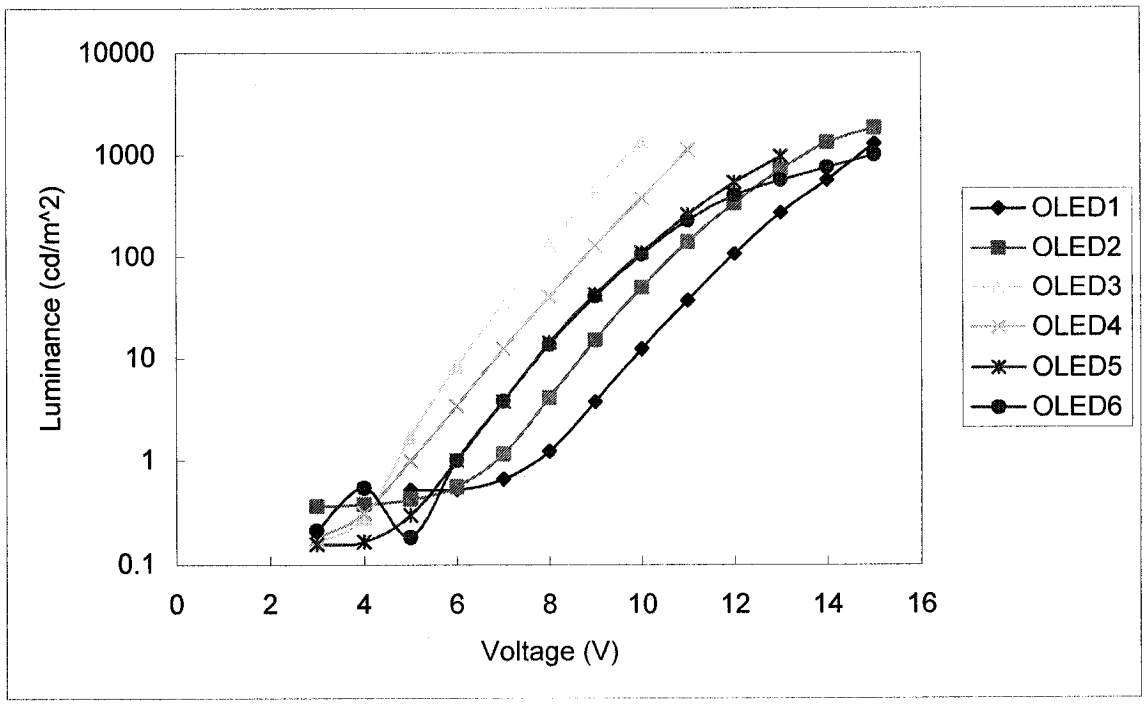

Figure 4-8: Device luminance characteristics with respect to voltage in linear scale.

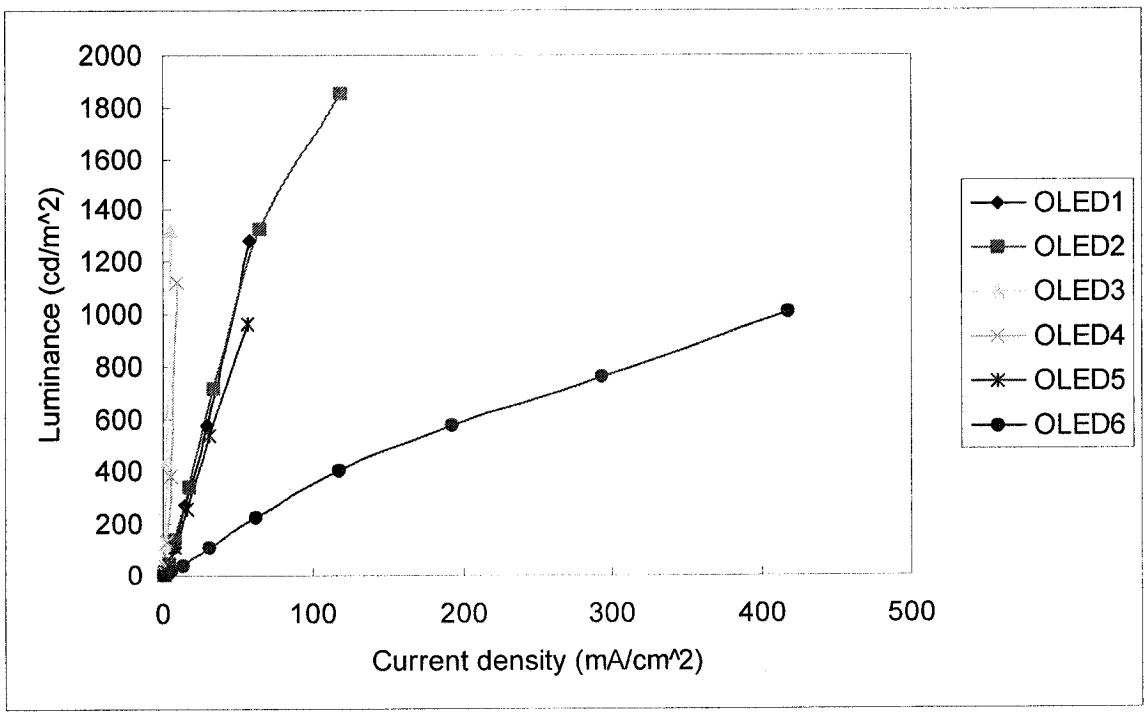

Figure 4-8: Device luminance characteristics with respect to current density in linear scale.

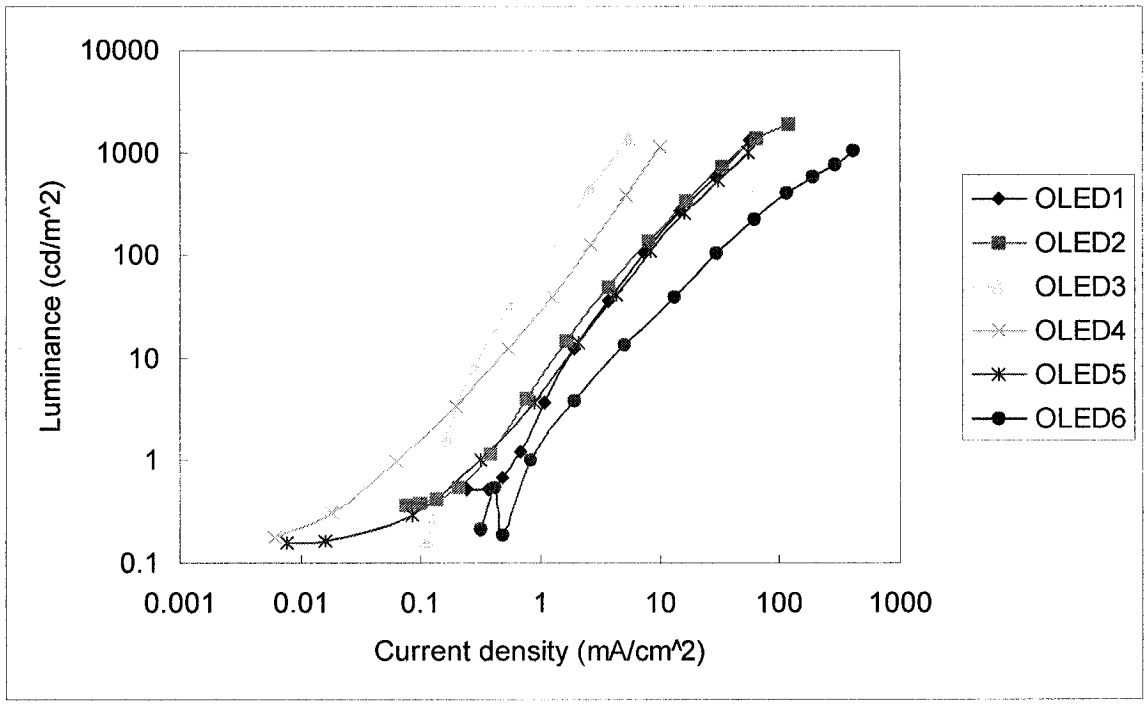

Figure 4-8: Device luminance characteristics with respect to current density in logarithmic scale.

Although the luminance characteristics of OLED3 and OLED4 are not available at higher current densities, it is expected that these devices will outperform the rest of the devices. For these two devices, a relatively high luminance value of close to 1000 cd/m^2 can be easily obtained at the lower operating voltage than any other devices at 10 and 11 V, respectively. To put it into context, a typical LCD monitor has the luminance value between 200 to 250 cd/m^2 when viewed from the front under normal viewing conditions. Thus, it could be concluded that OLED3 is the brightest device and OLED4 is a close second. For all devices except OLED6, the luminance value of 1000 cd/m^2 can be

obtained at the current density less than 60 mA/cm^2. Device OLED6 shows a quite different luminance-voltage characteristic from the rest of the devices. The difference can probably be attributed to the significantly smaller hole transport layer thickness in OLED6. A thinner hole transport layer tends to have worse interface surface morphology than the thicker hole transport layer so that thinner layer is more easily to be affected by localized defects. Also, the total light emitting layer thickness of OLED6 is almost identical to other devices and the thin hole transport layer thickness eases the carrier injection from anode at the same time. As a result, the possible maximum current density passing through the device is high but with low efficiency light emission. This is caused by the combination of both zero increase in possible emission region and the comparatively ease of carrier transport. The turn-on voltage of the devices defined as the voltage above which the luminance becomes higher than 1 cd/m^2, which should be visible under the condition of minimal amount of ambient light, range from 5 to 7 V. Both device OLED 3 and OLED 4 exhibit a significantly lower turn-on voltage than the others. The most efficient devices are also OLED 3 and OLED 4, which have the highest luminance at the lowest current density among all devices among the devices. The level off at the tail end of the L-J curve is a sign of possible emission efficiency stabilizing or falling off. A detailed discussion on emission efficiency of the devices will be covered in the later

sections.

4.5 Luminous Efficiency

For display applications, the luminous efficiency, η_L, is used as a measure of the emission efficiency. It describes the emission efficiency in which the amount of luminous intensity is compared against the amount of injected current. In many respects, luminous efficiency is analogous to the external quantum efficiency, which will be discussed in section 4.6. The difference is that luminous efficiency focuses on the emission luminance, where the photon emission rate is weighted to human perception of brightness. The unit for luminous efficiency is candela per amp. The mathematical definition of luminous efficiency is provided in Equation 4-11, where η_L is the luminous efficiency; S_a is the OLED total emission area; L is the luminance of OLED; I_{OLED} is the driving current; and J_{OLED} is the driving current density.

$$\eta_L = \frac{S_a L}{I_{OLED}} = \frac{L}{J_{OLED}} \qquad (4\text{-}11)$$

Figure 4-9 and 4-10 illustrates the luminous efficiency characteristics of the fabricated OLEDs with respect to current density in linear and logarithmic scales, respectively.

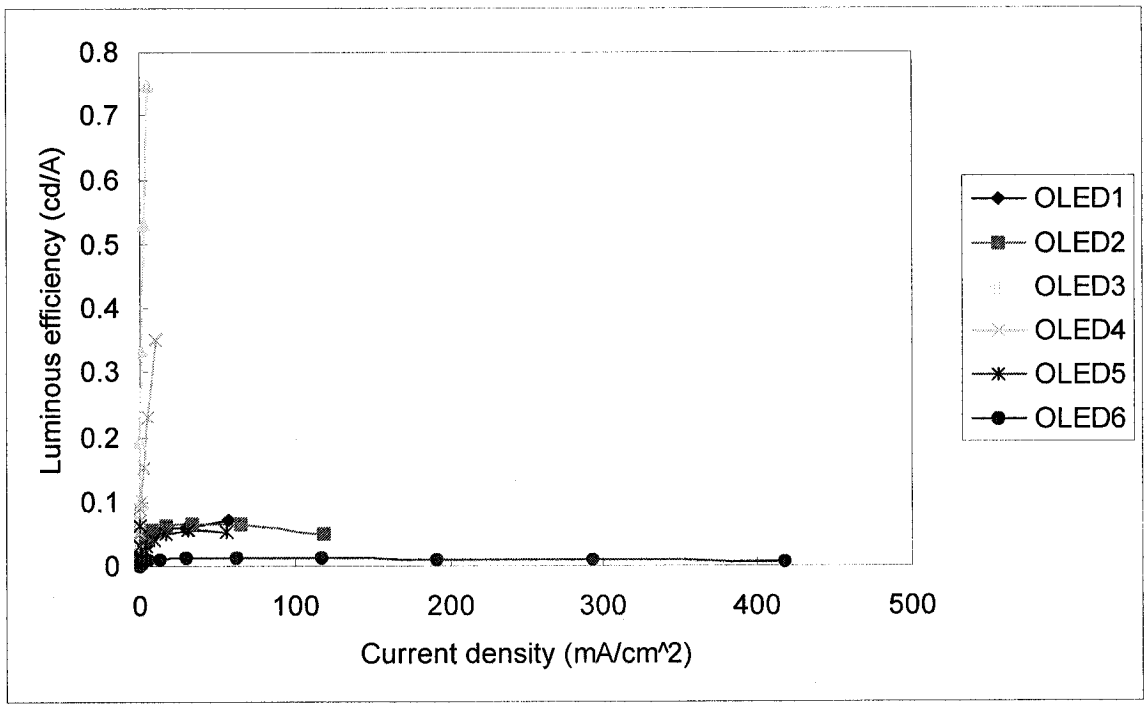

Figure 4-9: Device luminous efficiency characteristics with respect to current density in linear scale.

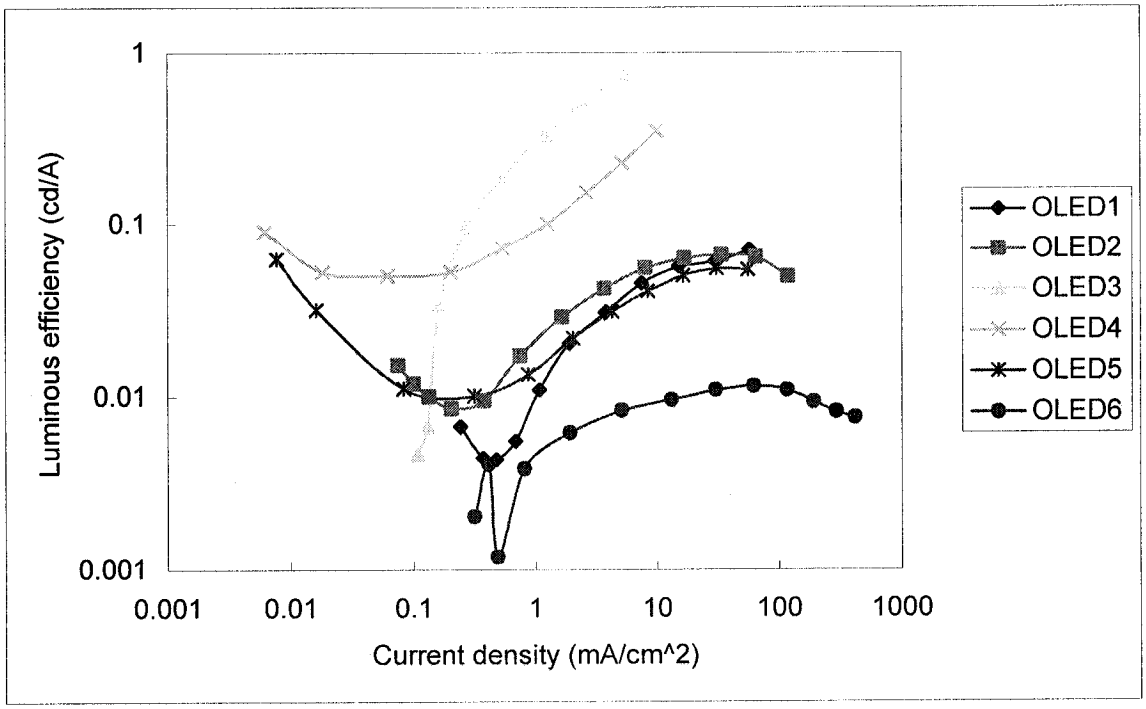

Figure 4-10: Device luminous efficiency characteristics with respect to current density in logarithmic scale.

As shown by the graphs, devices OLED3 and OLED4 both have significantly better luminous efficiency than other devices. Although the exact cause of such difference is not known, it can probably be attributed to two probable causes: strong emission contribution from the red phosphorescent emitting material, $Ir(piq)_3$, or the error in luminance intensity measurement. As discussed in chapter 2, phosphorescent light-emitting material is capable of breaking the 25% internal quantum efficiency limitation posed by the singlet exciton ratio. Thus, with Ir(piq) being the sole phosphorescent material in the OLED configuration for this work, it has the potential of raising the overall luminous efficiency by strongly contributing to the overall luminous intensity. Possible errors in the luminance intensity measurement can be resulted from any inaccuracy in the assumptions that the calculations are based on. As discussed earlier, the assumptions include that the device is perfectly aligned to the optic lens and the nearly Lambertian emission of OLED. It should also be noted that the luminous efficiency value of both OLED3 and OELD4 are still yet to attain the maximum value, which occurred at higher current density for the other devices, within the measured values. Also, the luminous efficiency is heavily influenced by the thickness of the $Ir(piq)_3$ layer and the charge balancing effect which is controlled by the layer thickness in other organic layers. The highest luminous efficiency is obtained with $Ir(piq)_3$ thickness between 20 Å to 40 Å along with 90 Å to 60 Å thick

DPVBi layer, 600 Å thick TPD layer, and 450 Å thick Alq_3 layer.

The decrease in the efficiency values at around J ≈ 90 mA/cm^2 can possibly be attributed to sample heating by current [4-4], triplet-triplet annihilation [4-5], or exciton quenching [4-6]. As discussed in the previous section on device luminance, the low efficiency value of OLED6 may be attributed to the fact that the total light emitting layer thickness of OLED6 is almost identical to other devices and to the fact that the thin hole transport layer thickness eases the carrier injection from the anode.

4.6 External Quantum Efficiency

For display applications, the external quantum efficiency, η_{ext}, is defined as the ratio of the number of photons emitted by the OLED into the viewing direction to the number of electrons ejected. Since the viewing direction of a typical OLED covers the front half plane of the OLED, the number of photons emitted from the front face of the OLED is used for the calculation of external quantum efficiency. In effect, external quantum efficiency provides the information on how many injected charge carriers actually contribute to the photon generation emitting toward the front half hemisphere. The definition of the external quantum efficiency is shown in Equation 4-12, where $N_{ext}(\lambda)$ is

the photon emission rate at the specific wavelength λ emitting into the front half hemisphere; $q = 1.6\times10^{-19}$ is the electronic charge; and I_{OLED} is the device current.

$$\eta_{ext} = \frac{q\int_{\lambda} N_{ext}(\lambda)d\lambda}{I_{OLED}} \qquad (4\text{-}12)$$

As discussed in the earlier section, the photon emission rate measured by the detector is only a fraction of the device total photon emission rate. Furthermore, the detector only measures a fraction of the photon emission flux passing through the optic lens as defined by attenuation ratio γ. Following the similar steps in the luminous intensity calculation, the total photon emission rate can be calculated from the detector reading. Equation 4-13 illustrates the calculation of photon emission rate per solid angle with respect to the surface normal, $n_0(\lambda)$, where $N_{lens}(\lambda)$ is the photon emission rate at the specific wavelength λ through the lens, Ω_{lens} is the solid angle covered by the optic lens area, and R,r,D are the physical equipment setup parameters as shown in Figure 4-7.

$$\begin{aligned} N_{lens}(\lambda) &= \int_{\Omega_{lens}} n_0(\lambda)\cos(\theta)d\Omega \\ &= 2\pi n_0(\lambda)\int_0^{\varphi}\cos(\theta)\sin(\theta)d\theta \\ &= 2\pi n_0(\lambda)\int_0^{\frac{r}{R}}\sin(\theta)(d\sin(\theta)) \\ &= (\frac{r}{R})^2\pi n_0(\lambda) = \frac{r^2}{r^2+D^2}\pi n_0(\lambda) \end{aligned} \qquad (4\text{-}13)$$

The total photon emission rate covering the forward half plane can then be

calculated by integrating the photon emission rate per solid angle, $n_0(\lambda)$, over the forward half plane, as illustrated by Equation 4-14.

$$\begin{aligned} N_{ext}(\lambda) &= \int_{1/2space} n_0(\lambda)\cos(\theta)d\Omega \\ &= 2\pi n_0(\lambda)\int_0^{\pi/2}\cos(\theta)\sin(\theta)d\theta \\ &= 2\pi n_0(\lambda)\int_0^1 \sin(\theta)(d\sin(\theta)) \\ &= \pi n_0(\lambda) \end{aligned} \qquad (4\text{-}14)$$

From Equation 4-13 and 4-14, $N_{ext}(\lambda)$ can be represented by $N_{lens}(\lambda)$

$$N_{ext}(\lambda) = \frac{r^2 + D^2}{r^2} N_{lens}(\lambda) = \frac{r^2 + D^2}{r^2} \cdot \frac{N_{detector}(\lambda)}{\gamma} \qquad (4\text{-}15)$$

Figure 4-11 to 4-12 show the quantum efficiency of the OLED emission as a function of current density.

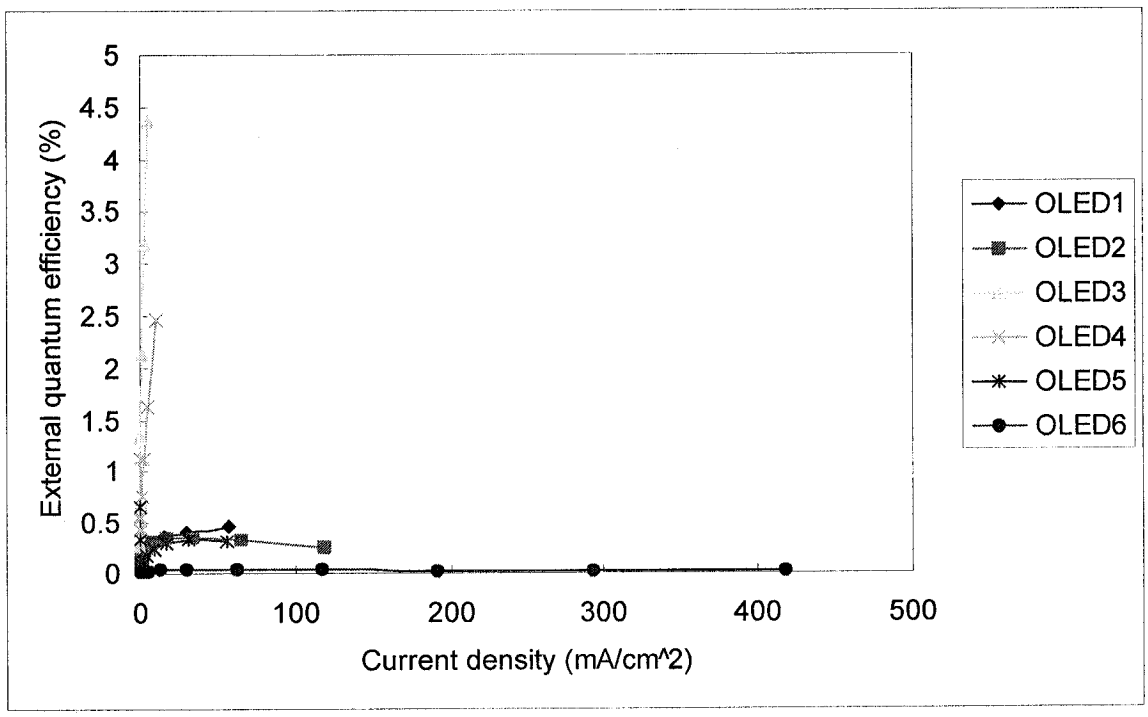

Figure 4-11: Device external quantum efficiency characteristics with respect to current density in linear scale.

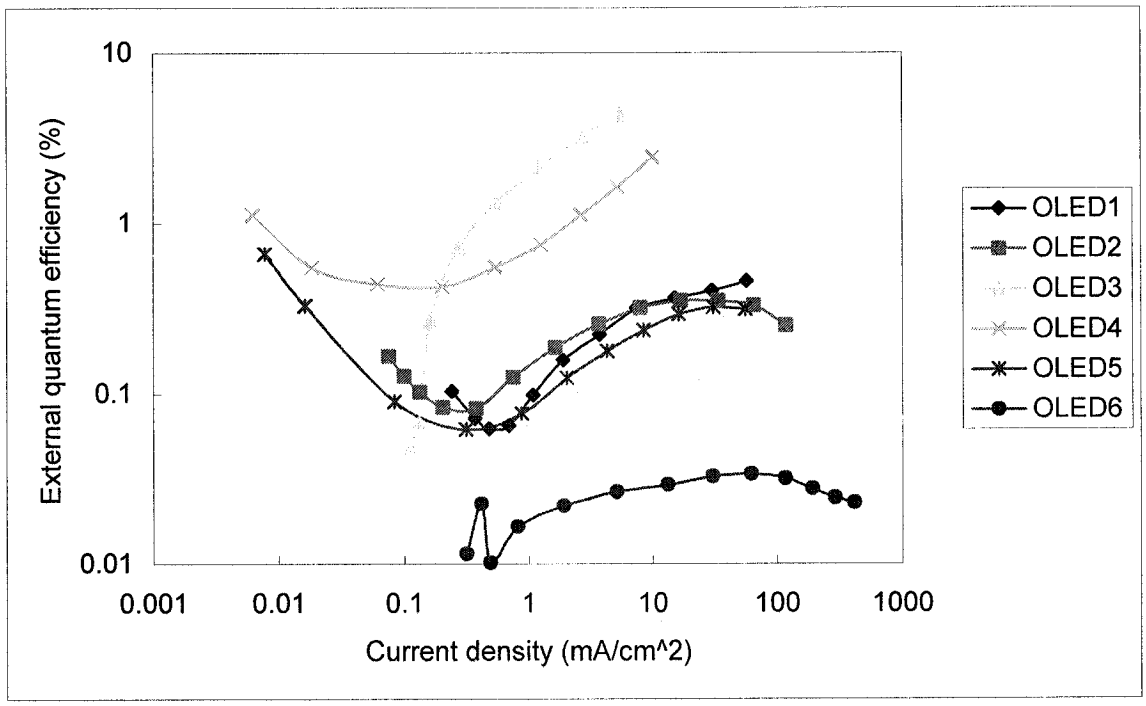

Figure 4-12: Device external quantum efficiency characteristics with respect to current density in logarithmic scale.

In a general sense, the external quantum efficiency of an OLED will be somewhat similar to its luminous efficiency. However, in an extreme case, a device could theoretically have good external quantum efficiency but mediocre luminous efficiency. For example, in two OLEDs with similar external quantum efficiency values, the one with its emission spectrum centered around the green light (≈550 nm) will have higher luminous efficiency value than the one with deep blue or deep red emission. This is due to the fact that human visual system is more sensitive to wavelengths in the middle of the visual spectrum. This particular phenomenon can be observed on the tail end of the

efficiency curve for devices OLED1, OLED2, and OLED5, where OLED2 has a higher luminous efficiency value than OLED1 but a lower external quantum efficiency value than OLED1. By inspecting the emission spectrum diagrams in section 4.4.7, it can be found that OLED1 has a higher overall photon emission rate, but OLED 2 has a stronger blue-green light emission.

Otherwise, the external quantum efficiency characteristic is very similar to the luminous efficiency characteristic discussed earlier, where devices OLED3 and OLED4 both have significantly better external quantum efficiency than other devices due to strong $Ir(piq)_3$ emission; the external quantum efficiency value of both OLED3 and OELD4 are still yet to attain the maximum efficiency value; and OLED6 has lowest external quantum efficiency value than any other. The probable causes for these particular characteristics are the same as the ones discussed earlier in section 4.5.

4.7 CIE Color Coordinates

The Commission Internationale de l'Eclairage (CIE) colorimetry system is a useful international standard for the specification of color matches for an average observer. The precise definition of colorimetry is in the primary reference, CIE Publication 15.2 (CIE,

1986) and colorimetry books such as *Color Appearance Model*, by M.D. Fairchild (1998) also provides a good introduction to the CIE colorimetry system [4-7].

4.7.1 Color-matching functions and XYZ tristimulus values

In 1931, the CIE system of colorimetry was established as a unified standard to describe color in the eyes of an average observer. The purpose of such system is that it could be used to specify when two stimuli match in color for an average observer. To develop this system of colorimetry, a basic concept is constructed based on the principles of trichromacy and Grassmann's laws of additive color mixture. This basic concept states that color matches can be specified in terms of the amounts of three additive primaries required to visually match a stimulus. The concept is illustrated in Equation 4-16 as follows:

$$C \equiv R(R^*) + G(G^*) + B(B^*) \qquad (4\text{-}16)$$

The above statement states that a color C is matched by R units of the R* primary, G units of the G* primary, and B units of the B primary. The term R*G*B* defines a particular set of primaries and the term RGB indicates the amounts of each primary required to match the color. These amounts are called tristimulus values. Since any color

can be matched by certain tristimulus values, if combining with a specific definition of the primary set, the specification of a color is allowed. This means that if two stimuli with different spectra can be matched using equal tristimulus values, then the colors of each stimulus also match each other when viewed under the same conditions.

Spectral tristimulus values for the complete spectrum are called color-matching functions. They are obtained by matching a unit amount of power at each wavelength with an additive mixture of three primaries. In essense, color-matching functions are spectral weighting functions that are used to describe the perception of each brightness match. Considering that any given stimulus spectral power can be treated as an additive mixture of various amounts of monochromatic stimuli, the tristimulus values for a stimulus can be obtained by multiplying the color-matching functions by the amount of energy in the stimulus at each wavelength and then integrating across the spectrum.

Spectral tristimulus values for the CIE RGB system of colorimetry with RGB primaries of 700.0nm, 546.1nm, and 435.8nm were established from the results of the experiments completed by Wright (1928-1929) using monochromatic primaries and Guild (1931) using broadband primaries. The spectral tristimulus values for the CIE RGB system of colorimetry are illustrated in Figure 4-13.

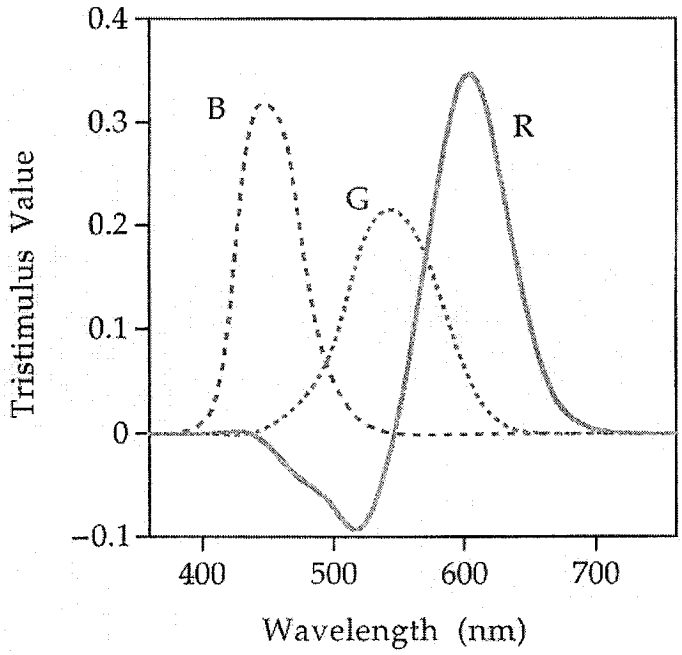

Figure 4-13: The spectral trimulus values of the color-matching functions for the CIE RGB system of colorimetry [4-7].

For convenience, the CIE decided to transform to another set of abstract primaries, the XYZ primaries, by eliminating the negative values in the RGB color-matching functions and to forcing one of the color-matching functions to equal the CIE 1924 photopic luminous efficiency function, $V(\lambda)$. As discussed earlier, the CIE photopic luminous efficiency function is a spectral weighting function used to describe the perception of brightness matches. The transformation installs two important properties to the CIE XYZ tristimulus values.

1. All tristimulus values are positive for all colors due to the fact that color-matching functions for XYZ primaries are all positive.

2. The X and Z tristimulus values have zero luminance response, therefore Y tristimulus value contains all luminance information. This is because color-matching function for primary Y is made equal to the CIE 1924 photopic luminous efficiency function, V(λ).

Figure 4-14 illustrates the spectral trimulus values/ color-matching functions of the CIE 1931 standard colorimetric observer.

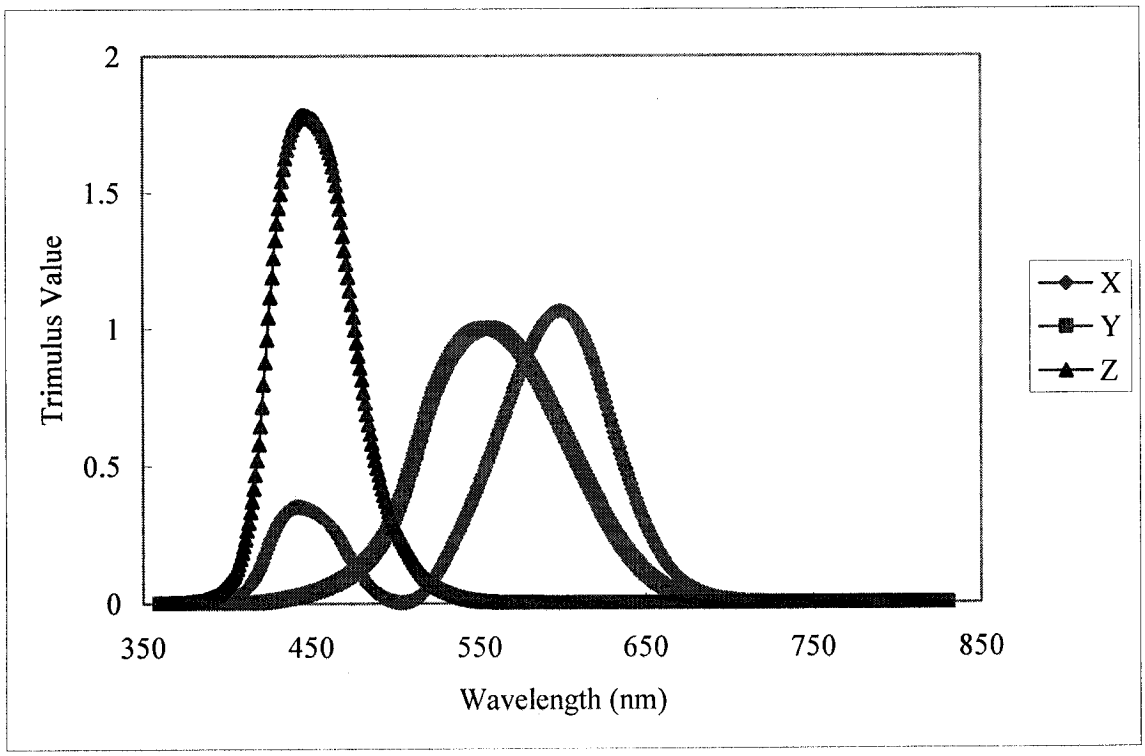

Figure 4-14: The spectral trimulus values of the color-matching functions for the CIE 1931 standard colorimetric observer.

XYZ tristimulus values for colored stimuli are calculated in the method described previously. The general equations for calculating XYZ trimulus values are illustrated in

Equations 4-17 through 4-19, where $\Phi(\lambda)$ is the spectral power distribution of the stimulus; $\bar{x}(\lambda)$, $\bar{y}(\lambda)$, and $\bar{z}(\lambda)$ are the color matching functions; and k is a normalizing constant.

$$X = k\int_{\lambda}\phi(\lambda)\bar{x}(\lambda)d\lambda \qquad (4\text{-}17)$$

$$Y = k\int_{\lambda}\phi(\lambda)\bar{y}(\lambda)d\lambda \qquad (4\text{-}18)$$

$$Z = k\int_{\lambda}\phi(\lambda)\bar{z}(\lambda)d\lambda \qquad (4\text{-}19)$$

If relative colorimetry is used to calculate the tristimulus values of a light source, the normalizing constant will be the raw Y tristimulus value so that the final Y tristimulus value is always equal to 100. For relative colorimetry measuring a light source, k is defined by Equation 4-20.

$$k = \frac{100}{\int_{\lambda}\phi(\lambda)\bar{y}(\lambda)d\lambda} \qquad (4\text{-}20)$$

If absolute colorimetry is used to calculate the trimulus values, the normalizing constant will be k = 683 lumens/watt, thus making the system of colorimetry compatible with the system of photometry. Note that the k = 683 lumens/watt is the same constant used in the calculation of luminous flux discussed earlier in the chapter, and resulting Y trimulus value represent the luminous power measured by the instrument.

4.7.2 CIE color coordinates

Chromaticity diagrams were developed to provide a convenient two-dimentional representation of colors. The transformation from the three tristimulus values to the chromaticity coordinates is accomplished through a normalization that removes luminance information. The transformation is defined by Equations 4-21 through 4-23, where x, y, and z are chromaticity coordinates; X, Y, and Z are XYZ trimulus values.

$$x = \frac{X}{X+Y+Z} \qquad (4\text{-}21)$$

$$y = \frac{Y}{X+Y+Z} \qquad (4\text{-}22)$$

$$z = \frac{Z}{X+Y+Z} \qquad (4\text{-}23)$$

Note that the sum of three chromaticity coordinates will always be unity. Since there are only two dimensions of information in the (x,y) chromaticity coordinates, the third chromaticity coordinate, z, can be obtained from the other two coordinates as follows:

$$z = 1.0 - x - y \qquad (4\text{-}24)$$

Since the luminance information is removed from chromaticity coordinates, the chromaticity coordinates can only provide the information on color but no information on luminance level at all. As such, a white color of CIE (x,y)=(0.33,0.33) can be anything between bright white, dim white, or close to dark white if no luminance level is specified.

4.7.3 CIE chromaticity diagram and CIE standard illuminants

The CIE has also established a number of spectral power distributions as CIE stanadard illuminants for colorimetry. The CIE illuminants are used as standards for illuminants, which include CIE illuminant A, C, D65, D50, F2, F8, and F11. From a purely mathematical point of view, the neutral white point has the coordinate of (0.333,0.333) in the chromaticity diagram. The chromaticity coordinates of these CIE illuminants along with the CIE 1931 chromaticity diagram are shown in Figure 4-15.

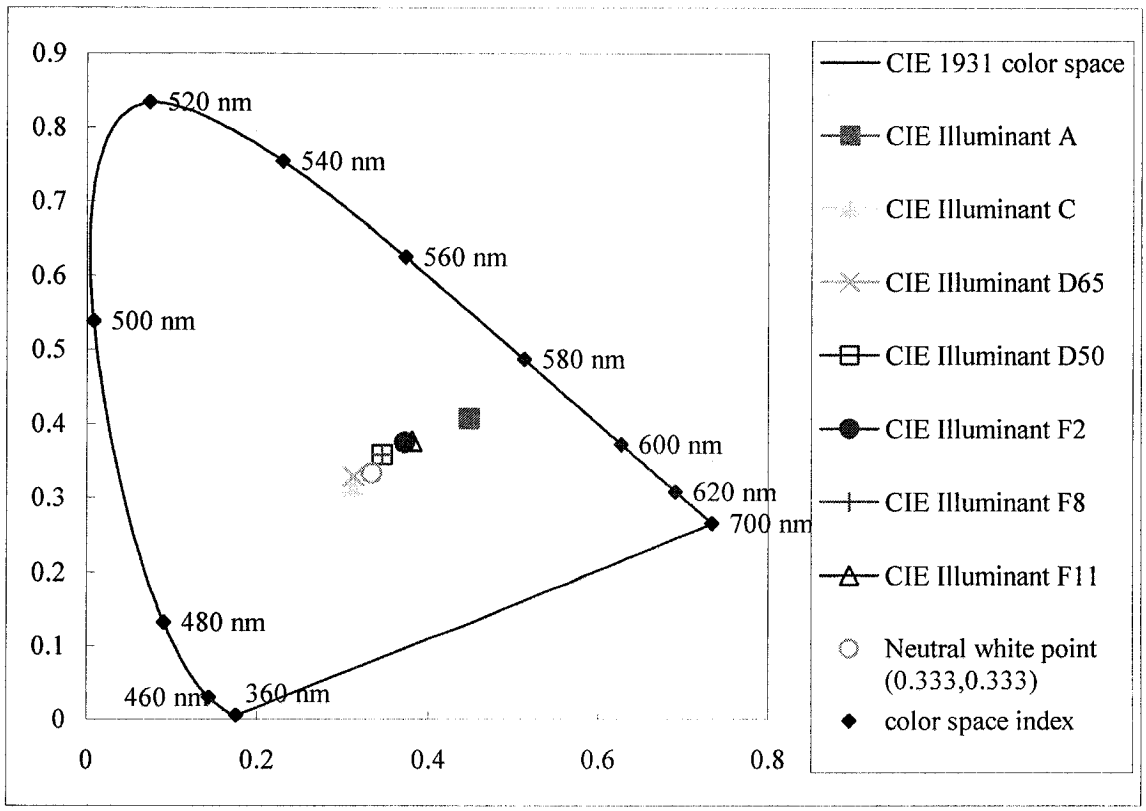

Figure 4-15: CIE chromaticity diagram with CIE 1931 color space and various CIE illuminant examples.

CIE illuminant A represents a Planckian radiator or a black-body radiator with a correlated color temperature (CCT) of 2,856 K. It is used for incandescent illumination such as a tungsten halogen light source. CIE illuminant C is the spectral power distribution (SPD) of illuminant A modified by particular liquid filters and it represents a daylight simulator with a CCT of 6,774 K. CIE D-series illuminants are defined based on measurements of different real daylight, in which CIE illuminant D65 represents an average daylight with a CCT of 6,504K and D50 represents an average daylight with a CCT of 5,003 K. CIE F-series illuminants represent typical spectral power distributions of fluorescent sources, in which F2 represents a cool-white fluorescent light with a CCT of 4,230 K, F8 represents a fluorescent D50 simulator with a CCT of 5,000 K, and F11 represents a tri-band fluorescent source with a CCT of 4,000 K. Table 4-3 includes some useful colorimetric data for the above-mentioned CIE illuminants, where XYZ values are trimulus values; xy values are CIE chromaticity coordinates; and CCT values are correlated color temperatures.

Table 4-3: Colorimetric data for some CIE illuminants [4-7].

CIE illuminants	A	C	D65	D50	F2	F8	F11
X	109.85	98.07	95.05	96.42	99.20	96.43	100.96
Y	100.0	100.0	100.0	100.0	100.0	100.0	100.0
Z	35.58	118.23	108.88	82.49	67.40	82.46	64.37
x	0.4476	0.3101	0.3127	0.3457	0.3721	0.3458	0.3805
y	0.4074	0.3162	0.3290	0.3585	0.3751	0.3586	0.3769
CCT	2,856 K	6,800 K	6,504 K	5,003 K	4,230 K	5,000 K	4,000 K

4.7.4 Device CIE color coordinates

An emission spectrum, a chromaticity diagram, and a table detailing CIE color coordinates at various voltages are presented for each OLED device fabricated. We follow with a discussion on the performance of each device. It should be noted that the CIE color coordinates presented in the chromaticity diagram include the data measured at all device luminance levels. Thus, at low luminance level $L < 1$ cd/m^2, even if the color coordinate is close neutral white color, the device will still appear to be extremely dim and close to dark. For this reason and in order to provide references, the tables detailing CIE color coordinates at various voltages also include the device luminance data measured at that specific operating voltage.

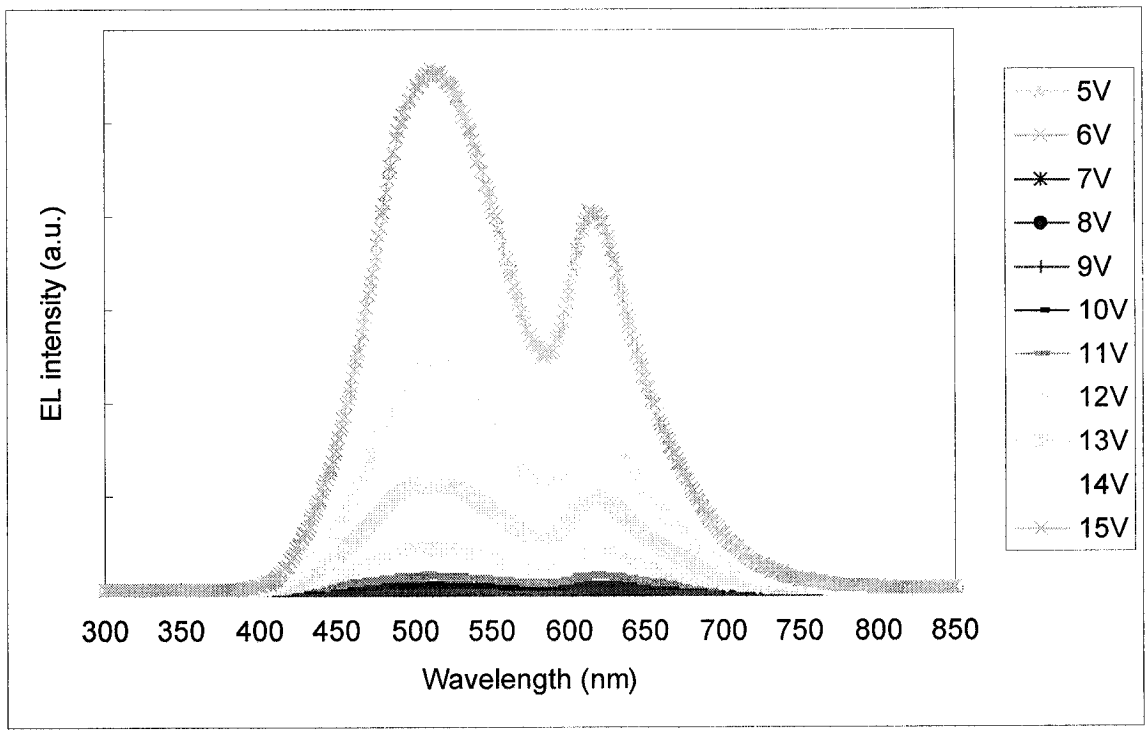

Figure 4-16: Electroluminescence emission spectra under different operating voltage for OLED1.

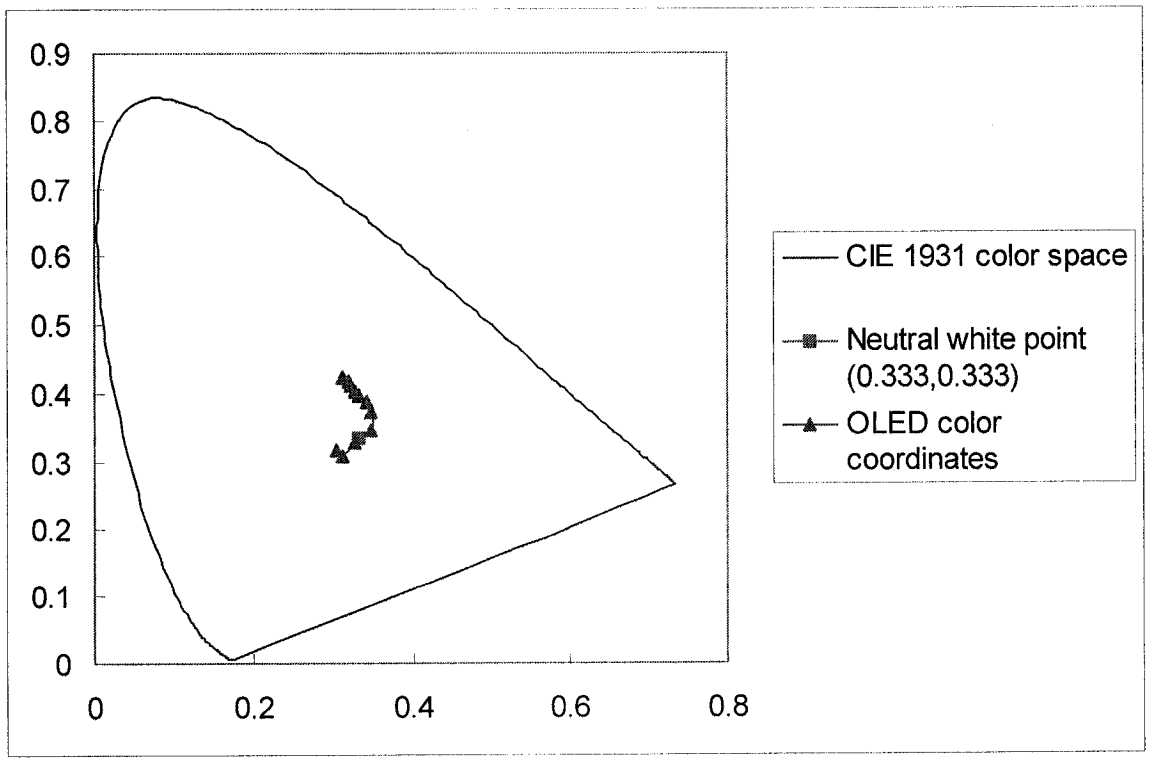

Figure 4-17: CIE color coordinates under different operating voltage for OLED1.

Table 4-4: CIE color coordinate and luminance with respect to voltage for OLED1.

Voltage	5	6	7	8	9	10	11	12	13	14	15
x	0.304	0.312	0.329	0.347	0.349	0.342	0.333	0.328	0.322	0.319	0.312
y	0.316	0.309	0.328	0.347	0.372	0.387	0.397	0.403	0.411	0.417	0.422
L (cd/m^2)	0.5	0.5	0.7	1.2	3.8	12.3	36.3	106.5	271.4	574.5	1282.9

Device OLED 1 has a close to balanced emission spectrum where the strong contributions from DPVBi, $Ir(piq)_3$, and Alq_3 can be clearly seen. The emissions from both DPVBi and Alq_3 contribute to the large emission peak centered around 510 nm. Although the color coordinates of OLED 1 shifts with increasing device brightness from (0.342,0.387) at 12.3 cd/m^2 to (0.312,0.422) at 1282.9 12.3 cd/m^2, the color shift is not extremely dramatic and OLED1 is one of the more color stable device among all devices fabricated. It can be clearly seen that the contributions to the emission from both DPVBi and Alq_3 increase slightly faster than the contribution from $Ir(piq)_3$, with respect to increasing brightness. Thus, the imbalanced emission spectrum growth causes the color to shift from yellowish to greenish. At the lower brightness levels, the color coordinates are still quite close to the neutral white light (0.333,0.333), but the color shifts further away from the neutral white with the increased brightness, which results in a visible green hue.

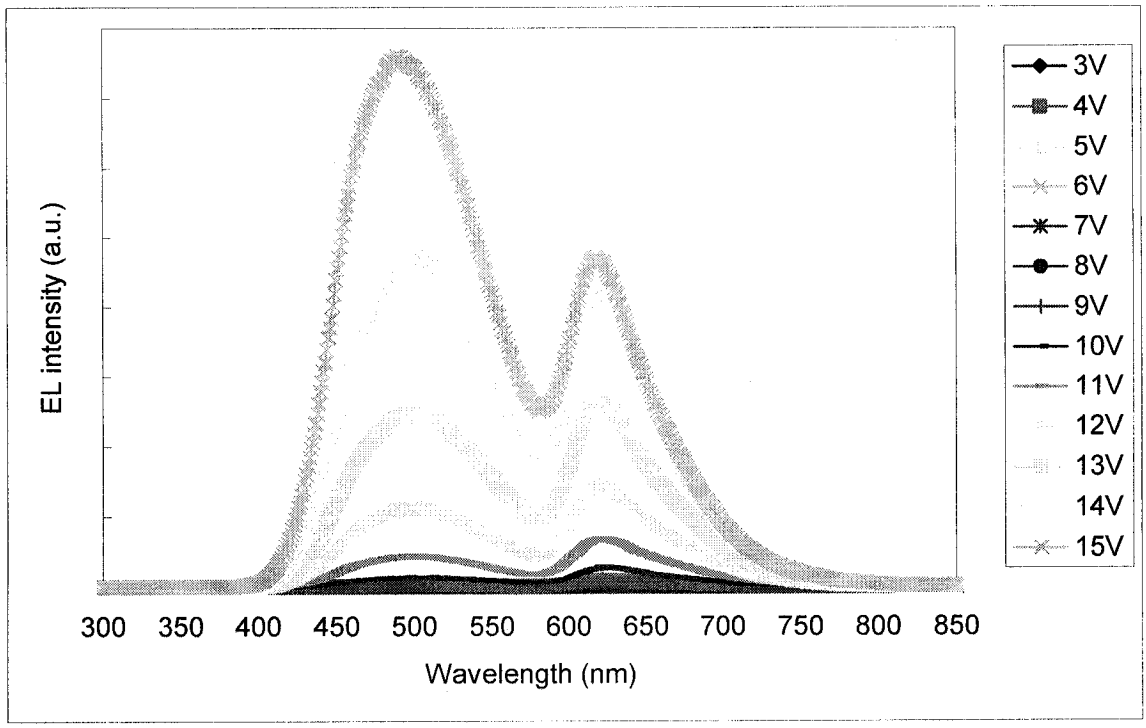

Figure 4-18: Electroluminescence emission spectra under different operating voltage for OLED2.

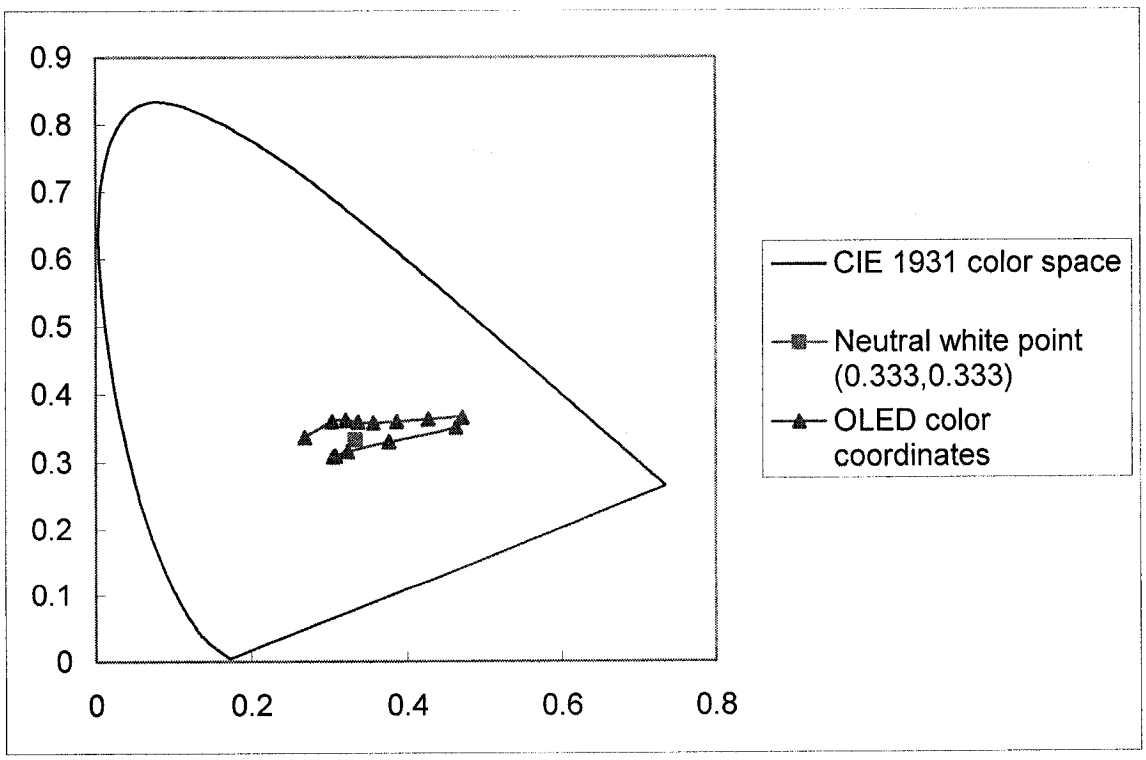

Figure 4-19: CIE color coordinates under different operating voltage for OLED2.

Table 4-5: CIE color coordinate and luminance with respect to voltage for OLED2.

Voltage	3	4	5	6	7	8	9	10	11	12	13	14	15
x	0.305	0.308	0.323	0.377	0.463	0.471	0.427	0.387	0.357	0.337	0.321	0.303	0.269
y	0.308	0.310	0.316	0.331	0.351	0.365	0.364	0.360	0.358	0.359	0.361	0.360	0.337
L (cd/m^2)	0.4	0.4	0.4	0.6	1.1	4.1	15.1	49.2	140.4	338.2	712.7	1321.7	1852.7

Device OLED 2 has a shifting emission spectrum depending on the brightness of the device. At lower brightness levels, the contribution from $Ir(piq)_3$ is stronger than the contribution from both DPVBi and Alq_3, thus resulting in an orange-red color at low luminance levels. As the device brightness is increased, the contributions from both DPVBi and Alq_3 become substantially more predominant and push the color back to white, and toward blue at highest brightness. Although a relatively dramatic shift in color coordinates creates color instability with respect to brightness, the color coordinates actually stay quite close to the neutral white point at the medium to high luminance level between (0.357,0.358) of 140.4 cd/m^2 to (0.303,0.360) of 1321.7 cd/m^2. The shift in color at the medium brightness levels is not as extreme as the color shift at the lowest and highest brightness levels. This relatively good white color stability in medium luminance levels should be beneficial for moderate white color lighting applications.

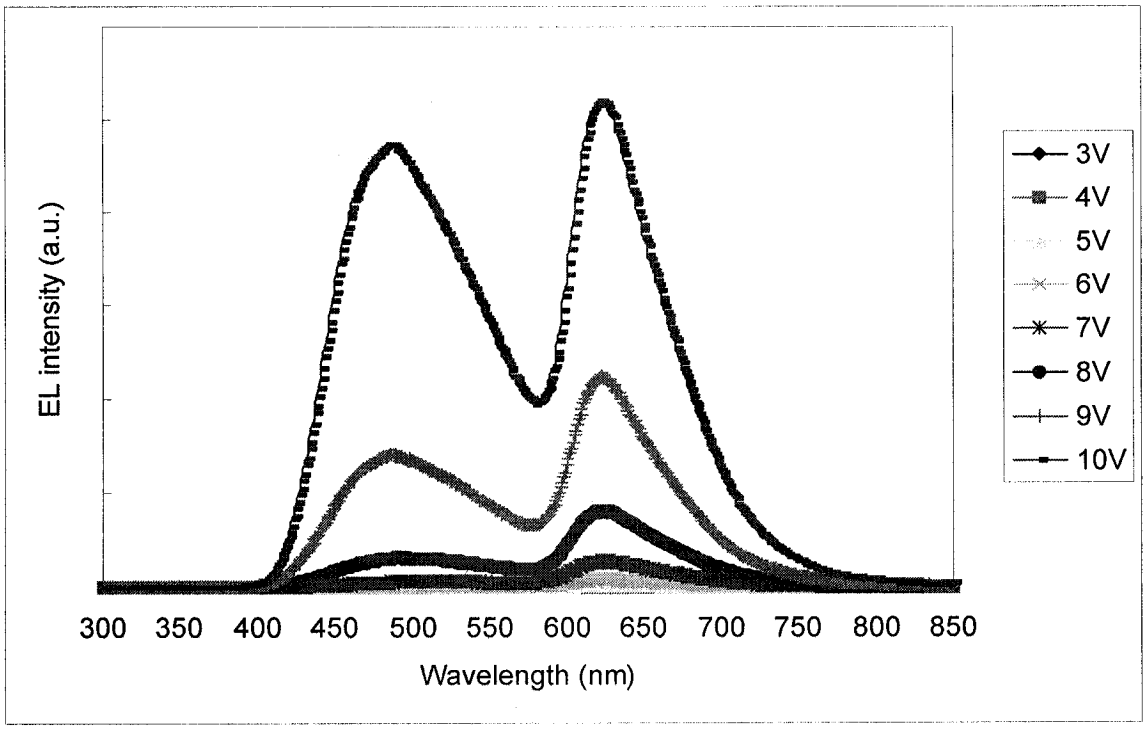

Figure 4-20: Electroluminescence emission spectra under different operating voltage for OLED3.

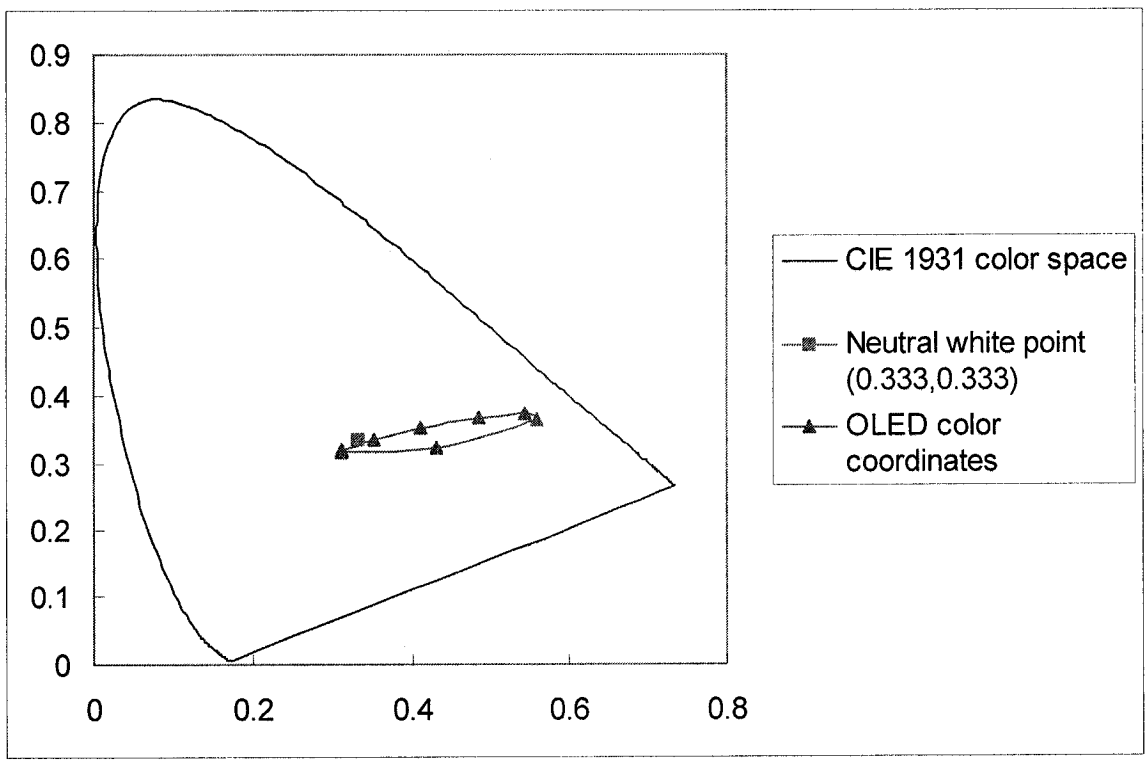

Figure 4-21: CIE color coordinates under different operating voltage for OLED3.

Table 4-6: CIE color coordinate and luminance with respect to voltage for OLED3.

Voltage	3	4	5	6	7	8	9	10
x	0.312	0.432	0.558	0.544	0.486	0.412	0.352	0.313
y	0.316	0.323	0.364	0.372	0.368	0.351	0.333	0.320
L (cd/m^2)	0.2	0.3	1.7	8.3	33.8	127.9	445.6	1320.2

Along with device OLED4, OLED 3 is one the most unstable devices in terms of color coordinate stability. From the spectrum, we see that the red emission from $Ir(piq)_3$ remains strong throughout the whole brightness range while the contributions from both DPVBi and Alq_3 change drastically with respect to device brightness and, eventually, nearly even the red light emission. The strong contribution from $Ir(piq)_3$ emission is probably due to the superior emission efficiency of $Ir(piq)_3$ when compared to the other two emission materials. Although the color stability is quite poor, at highest measured brightness level of 1320.2 cd/m^2, the emission color coordinate (0.313,0.320) is very close to the neutral white point. This provides a relatively good bright white light at high luminance level. It is not known whether the magnitude of the shifts in color coordinates will be reduced at even higher device brightness, though the results from other devices do hint at a more stable color at higher brightness.

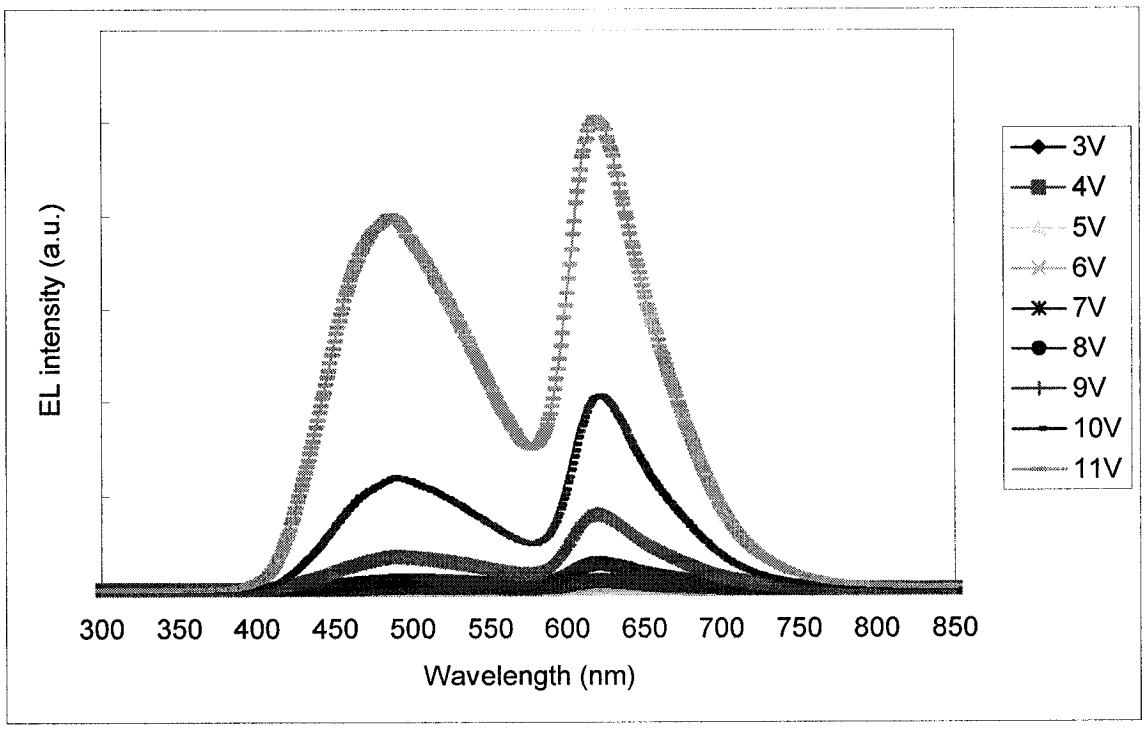

Figure 4-22: Electroluminescence emission spectra under different operating voltage for OLED4.

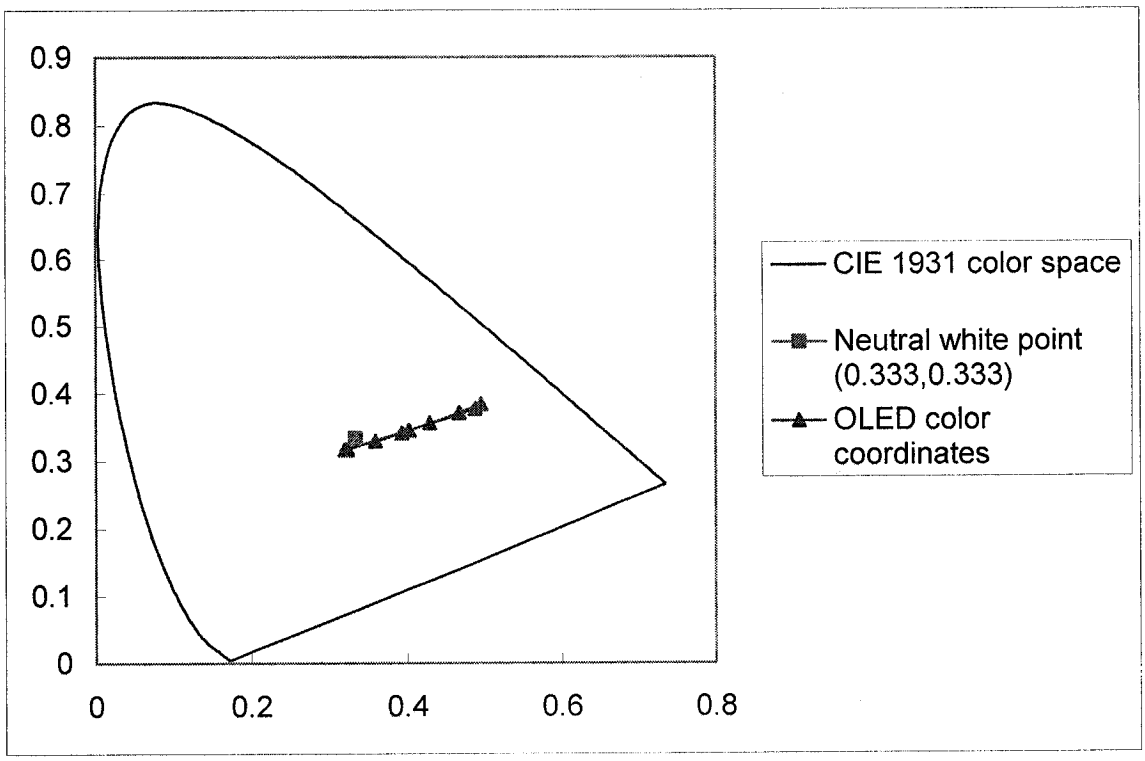

Figure 4-23: CIE color coordinates under different operating voltage for OLED4.

Table 4-7: CIE color coordinate and luminance with respect to voltage for OLED4.

Voltage	3	4	5	6	7	8	9	10	11
x	0.321	0.402	0.488	0.496	0.467	0.429	0.393	0.360	0.324
y	0.317	0.346	0.377	0.383	0.371	0.356	0.342	0.329	0.317
L (cd/m^2)	0.2	0.3	1.0	3.4	12.3	40.0	128.2	376.5	1117.3

Similar to device OLED3, OLED 4 is one the most unstable devices in terms of color coordinate stability. Also similar to OLED3, the red emission from $Ir(piq)_3$ remains strong throughout the whole brightness range while the emission contributions from both DPVBi and Alq_3 changes drastically with respect to device brightness and eventually close to even level with red emission. Although the color stability is poor, the highest measured brightness level of 1117.2 cd/m^2, the emission color coordinate (0.324,0.317) is very close to the neutral white point, which provides a good bright approximate white light at high luminance level. Same with OLED3, it is not known whether the magnitude of shifts in color coordinates will be reduced at even higher device brightness, though the results from other devices do hint at a more stable color at higher brightness. It should also be noted that both OLED3 and OLED4 have the strongest red emission contribution from $Ir(piq)_3$ among all devices.

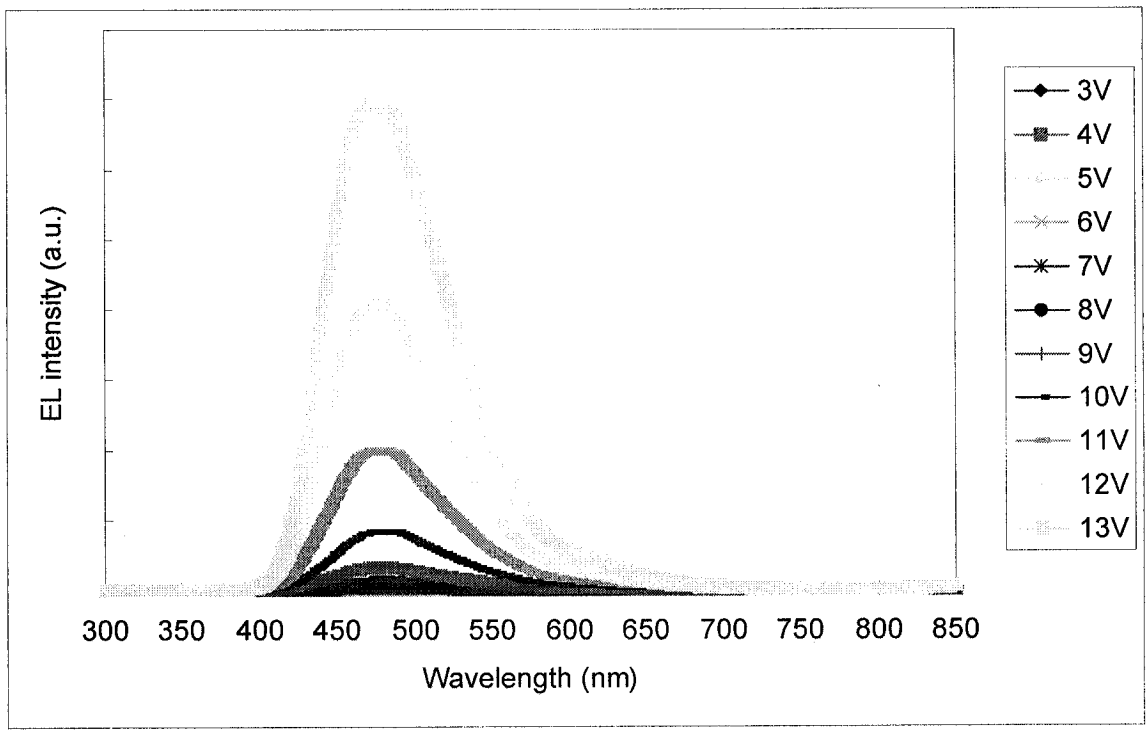

Figure 4-24: Electroluminescence emission spectra under different operating voltage for OLED5.

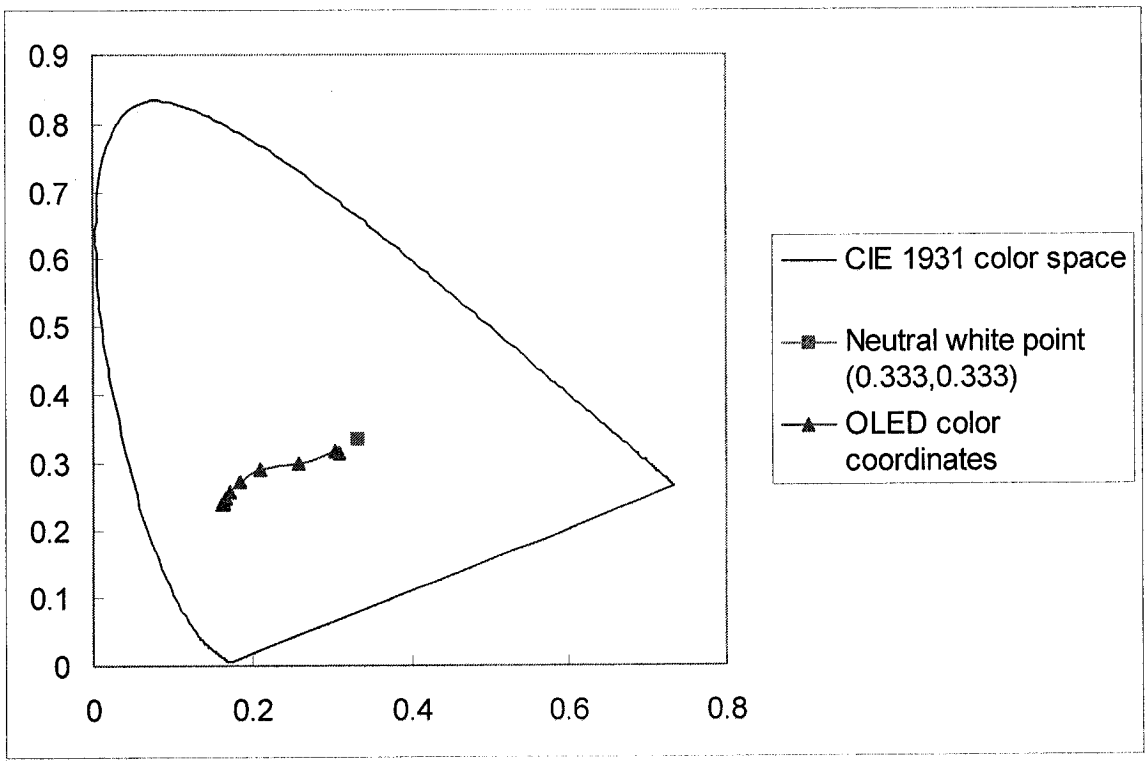

Figure 4-25: CIE color coordinates under different operating voltage for OLED5.

Table 4-8: CIE color coordinate and luminance with respect to voltage for OLED5.

Voltage	3	4	5	6	7	8	9	10	11	12	13
x	0.310	0.304	0.258	0.211	0.185	0.173	0.168	0.165	0.164	0.164	0.166
y	0.314	0.317	0.300	0.291	0.273	0.258	0.250	0.244	0.240	0.239	0.241
L (cd/m^2)	0.2	0.2	0.3	1.0	3.8	14.1	42.0	109.4	258.4	536.6	962.3

Device OLED5 is one of the most peculiar devices, where the emission contribution from $Ir(piq)_3$ is almost non-existent, thus causing the device to be lacking emission at longer wavelengths in the visible spectrum. Coincidentally, OLED5 is also the device with the thinnest $Ir(piq)_3$ layer of only 15 Å thick. The lack of red light emission in OLED 5 can probably be attributed to the failure of carrier confinement due to insufficient layer thickness. The insufficient layer thickness could possibly lead to the more frequent occurrence of tunneling effect. Thus, carriers move from either the DPVBi or the Alq_3 interface to another, bypassing the $Ir(piq)_3$ layer all together. Without the sufficient carrier density build-up in the $Ir(piq)_3$ layer, the electron-hole recombination becomes much less likely to occur in the $Ir(piq)_3$ layer and the probability of emission in $Ir(piq)_3$ is reduced. At visible brightness, the color coordinates are concentrated around the blue and cyan colors, thus making this OLED an unsuitable white light illuminant.

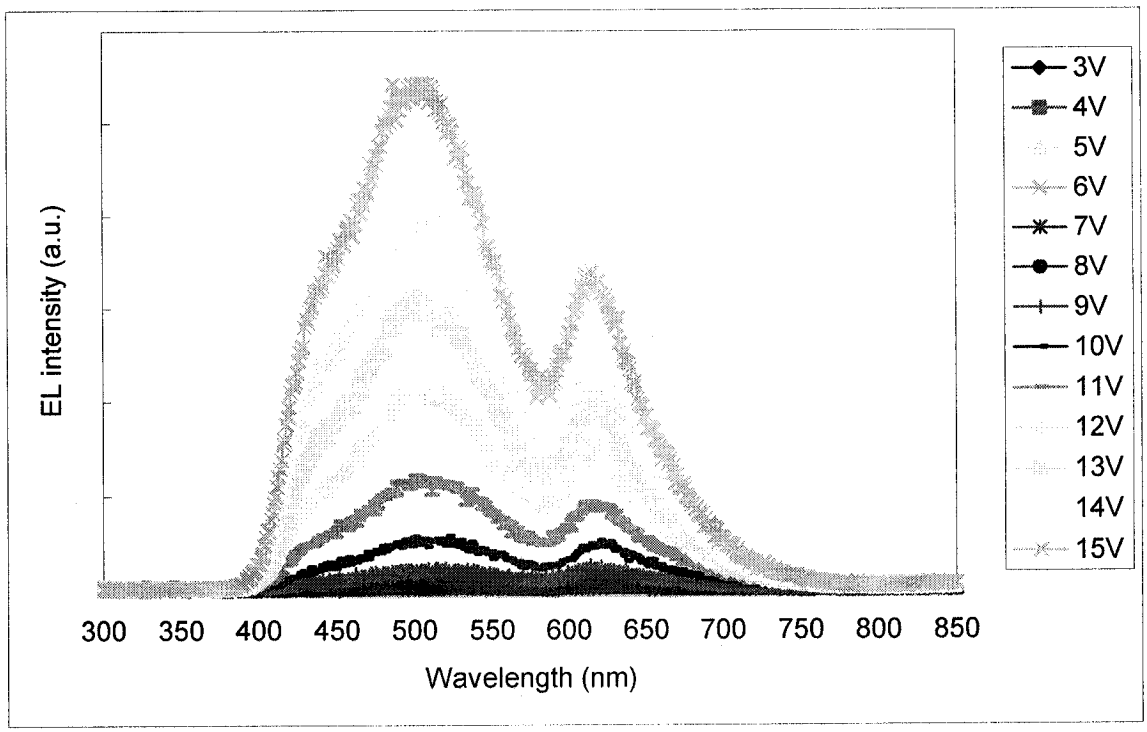

Figure 4-26: Electroluminescence emission spectra under different operating voltage for OLED6.

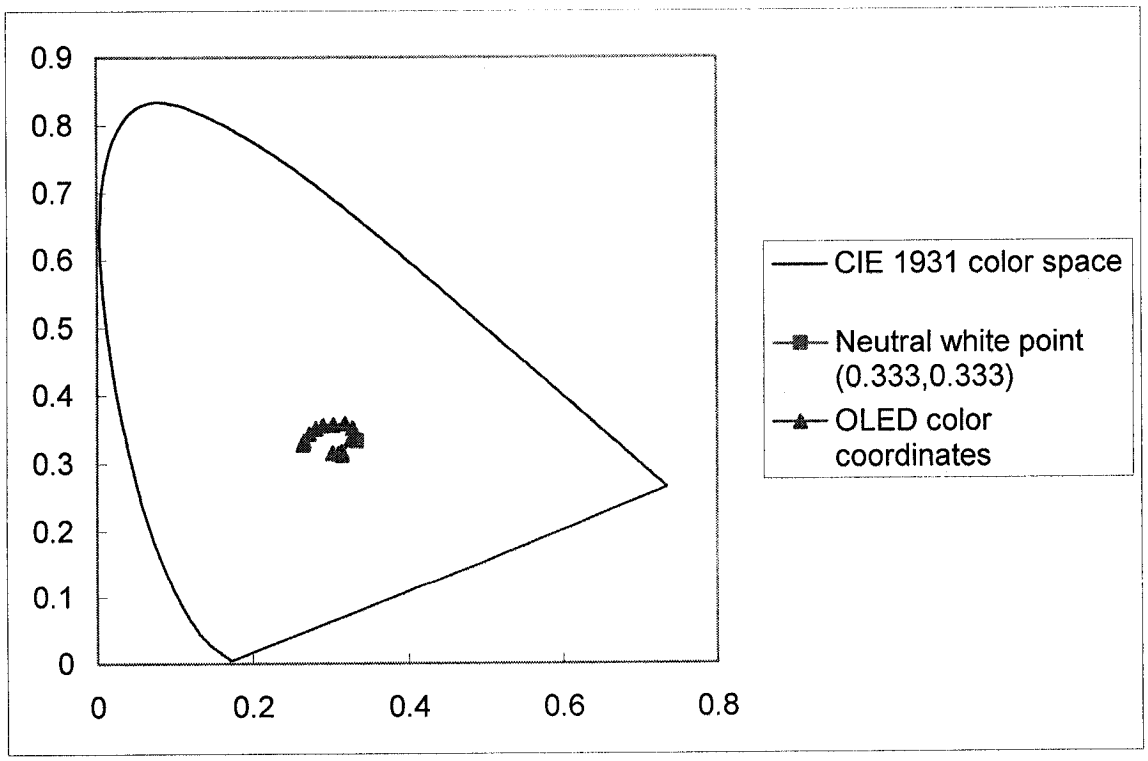

Figure 4-27: CIE color coordinates under different operating voltage for OLED6.

Table 4-9: CIE color coordinate and luminance with respect to voltage for OLED6.

Voltage	3	4	5	6	7	8	9	10	11	12	13	14	15
x	0.311	0.315	0.303	0.315	0.327	0.328	0.319	0.304	0.291	0.281	0.273	0.266	0.265
y	0.314	0.312	0.315	0.317	.0336	0.351	0.358	0.356	0.355	0.50	0.342	0.332	0.328
L (cd/m^2)	0.2	0.5	0.2	1.0	3.8	13.6	40.4	105.2	227.3	403.3	572.2	761.3	1008.1

Similar to device OLED1, OLED6 also has a close to balanced emission spectrum where the strong contributions from DPVBi, $Ir(piq)_3$, and Alq_3 can be clearly seen. The balanced spectrum emission throughout the device brightness level range makes OLED6 one of the more color stable device among all devices fabricated. It can be seen that the contributions from both DPVBi and Alq_3 slowly become more significant in the overall emission spectrum, causing the device color to shift toward blue and cyan color. It should also be noted that the color coordinate shifts of OLED6 is not as drastic as OLED3 or OLED4, ranging from (0.319,0.358) at 40.4 cd/m^2 to (0.265,0.328) at 1008.1 cd/m^2. At the low brightness levels, the color coordinates are still quite close to the neutral white light (0.333,0.333), but the color shifts further away from the neutral white with the increased brightness.

Figure 4-28 and Figure 4-29 shows photographs of a sample fabricated OLED in operation under both minimal ambient light condition and in a dark room. It should be noted that the color of the pictures differs from the actual device emission color where the picture gives a strong hue in purple color. The color difference between the pictures and what is seen by the eyes is likely due to the inadequacy of the white balance setting of the camera.

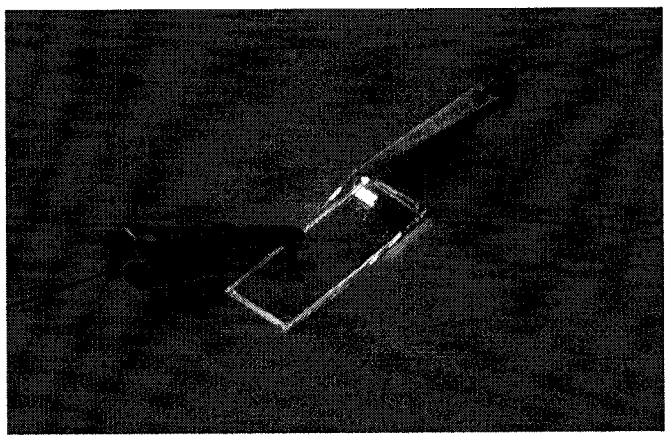

Figure 4-28: Photograph of a sample fabricated OLED in operation under minimal ambient light condition.

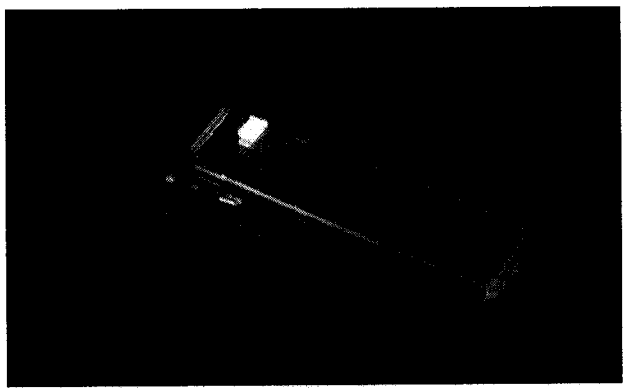

Figure 4-29: Photograph of a sample fabricated OLED in operation in a dark room.

4.8 Conclusions

The effects of organic layer thickness in 6 different overall device configurations on white OLED device performances have been investigated from both the electrical and optical perspectives. The electrical characterization includes current-voltage characteristic, while optical characterization includes luminance, luminous efficiency, external quantum efficiency, and the emission CIE color coordinate. The characteristics comparison between the 6 different device configurations is shown in Table 4-10.

Table 4-10: A comparison of device characteristics of the fabricated OLEDs

Device	OLED1	OLED2	OLED3	OLED4	OLED5	OLED6
Alq_3 layer thickness	500 Å	450 Å	450 Å	450 Å	500 Å	500 Å
$Ir(piq)_3$ layer thickness	40 Å	40 Å	40 Å	20 Å	15 Å	25 Å
DPVBi layer thickness	100 Å	110 Å	90 Å	60 Å	75 Å	100 Å
TPD layer thickness	600 Å	600 Å	600 Å	600 Å	600 Å	500 Å
Total layer thickness	1240 Å	1200 Å	1180 Å	1130 Å	1190 Å	1125 Å
Maximum measured current density	57.2 mA/cm^2 at 15 V	118.2 mA/cm^2 at 15 V	139.1 mA/cm^2 at 15 V	108.8 mA/cm^2 at 15 V	165.6 mA/cm^2 at 15 V	417.8 mA/cm^2 at 15 V

Device	OLED1	OLED2	OLED3	OLED4	OLED5	OLED6
Operating voltage when luminance exceeds 1000 cd/m^2	1282.9 cd/m^2 at 15V	1321.7 cd/m^2 at 14V	1320.1 cd/m^2 at 5.5 10V	1117.3 cd/m^2 at 11V	1470.6 cd/m^2 at 14V	1008.1 cd/m^2 at 15V
Maximum measured luminance	1282.9 cd/m^2 at 57.2 mA/cm^2	1852.7 cd/m^2 at 118.2 mA/cm^2	1320.1 cd/m^2 at 5.5 mA/cm^2	1117.3 cd/m^2 at 10.0 mA/cm^2	1470.6 cd/m^2 at 98.5 mA/cm^2	1008.1 cd/m^2 at 417.8 mA/cm^2
Maximum measured η_L	0.07 cd/A at 57.2 mA/cm^2	0.06 cd/A at 34.0 mA/cm^2	0.74 cd/A at 5.5 mA/cm^2	0.35 cd/A at 10.0 mA/cm^2	0.05 cd/A at 0.008 mA/cm^2	0.011 cd/A at 62.4 mA/cm^2
Maximum measured η_{ext}	0.46% at 57.2 mA/cm^2	0.35% at 34.0 mA/cm^2	4.36% at 5.5 mA/cm^2	2.45% at 10.0 mA/cm^2	0.66% cd/A at 0.008 mA/cm^2	0.033% at 62.4 mA/cm^2
Color stability	Good	Stable in the medium luminance level	Poor	Poor	Poor	Good
CIE color coordinate	Close to white at low luminance but shift to light green at high luminance level	Close to white at medium to high luminance level; shift away from white at low and very high luminance level	Only close to white at highest measured luminance; emits in orange-red region at low luminance level	Only close to white at highest measured luminance; emits in orange-red region at low luminance level	In the blue and cyan region; away from white	Close to white at low luminance but shift to blue/cyan at high luminance level

The configuration most suitable to be used as white color illuminant is found to be device OLED2 with the layer thickness of TPD (600Å)/ DPVBi (110Å)/ $Ir(piq)_3$ (40Å)/ Alq_3 (450Å). This particular configuration has the closest CIE color coordinates to the neutral white point (0.333,0.33) for the widest luminance level range, from (0.357,0.358) at 140.4 cd/m^2 to (0.303,0.360) at 1321.7 cd/m^2. Although this particular configuration does not provide the best luminous efficiency or external quantum efficiency, it is the best suitable for white light illumination application due to its close to white color emission and acceptable color stability with respect to device brightness.

The configurations of OLED3 and OLED4 provide the best performing OLED in all optical characteristics except emission color coordinates and color stability. Both devices have the highest luminance level at the lowest biasing voltage. Both devices also have significantly higher luminous efficiency and external quantum efficiency values than other devices. However, both OLED3 and OLED4 configurations suffer from severe color shift with respect to luminance level, thus making such configuration less suitable for white light illumination applications. With the OLED6 configuration, it is found that although the reduced hole transport layer thickness helps to promote the transport of carriers, the increased carrier density does not directly translate into an improvement of optical performances with the same emitting layer thickness.

Base on the optical characteristics of all device configurations, it is found that the layer thickness of the red phosphorescent emitting material, $Ir(piq)_3$, along with the charge balance controlled by the thickness of other organic materials, have critical effects in the emission performance of the $Ir(piq)_3$. When the layer thickness is sufficiently thin, ranging from 20 to 40 Å in OLED3 and OLED4, the $Ir(piq)_3$ emission is highly efficient and contributes greatly to the overall device photon emission. When the $Ir(piq)_3$ layer thickness is reduced to around 15 Å, the $Ir(piq)_3$ emission becomes almost non-existent compared to the emission from DPVBi and Alq_3.

[4-1] S.R. Forrest, D.D.C. Bradley, Mark E. Thompson, *Adv. Mater.* **2003**, *15*, No. 13, 1043

[4-2] D. Troadec, A. Moliton, B. Ratier, R. Antony, R.C. Hiorns, *J. Appl. Phys.* **2005**, *97*, 043103

[4-3] N.C. Greenham, R.H. Friend, D.D.C. Bradley, *Adv. Mater.* **1994**, *6*, 491.

[4-4] N. Tessler, N.T. Harrison, D.S. Thomas, R.H. Friend, *Appl. Phys. Lett.* **1998**, *73*, 732.

[4-5] C. Adachi, M.A. Baldo, S.R. Forrest, *J. Appl. Phys.* **2000**, *87*, no.11, 8049

[4-6] M.A. Baldo, D.F. O'Brien, Y. You, A. Shoustikov, S. Sibley, M.E. Thompson, S.R. Forrest, *Nature* **1998**, *395*, 151.

[4-7] Mark D. Fairchild, *Color Appearance Model*, Addison-Wesley, Reading, Massachusetts, **1998**.

Chapter 5

Conclusions and Future Work

5.1 Thesis Summary

In this thesis, organic light emitting devices (OLED) with a multi-layer stacking structure capable of producing light emission close to white color have been fabricated using the thermal vacuum deposition method. The organic materials used in the OLED consist of one hole transport material, *N*, *N*′-diphenyl-*N*, *N*′-bis(3-methylphenyl)-1, 1′-biphenyl-4, 4′-diamine [TPD], and three light emitting materials: 4, 4′-bis(2, 2′-diphenylvinyl)-1, 1′-biphenyl [DPVBi], tris-(1-phenylisoquinolinato-N) iridium (III) [Ir(piq)$_3$], and tris- (8-hydroxyquinoline) aluminium [Alq3]. Alq$_3$, in particular, not only serves as one of the light emitting materials, but also serves as electron transport material. The emission color from each light emitting materials corresponds to one of three primary colors, where DPVBi has emission spectrum in the blue region, Ir(piq)$_3$ in the red region, and Alq$_3$ in the green region. Six different layer thickness configurations have been implemented in order to investigate the effects of organic layer thickness on the overall device performance. Each configuration shared the same OLED structure of

ITO/TPD/DPVBi/Ir(piq)$_3$/Alq$_3$/Mg:Ag.

Aside from the selection of organic materials, an appropriate selection of electrode materials with proper energy level match-up with the organic materials is also required for the successful fabrication of OLEDs. Indium tin oxide (ITO), which is a transparent and highly conducting material, was selected as the anode material, while a dual metal layer composed of magnesium and silver was chosen for the cathode material.

The characterization of the device electrical and optical properties was performed and device display characteristics such as luminance, luminous efficiency, external quantum efficiency, and CIE color coordinates were derived and calculated from the measurements. In those calculations, it was assumed that the OLED emission is nearly Lambertian. The current-voltage characteristics of the fabricated OLEDs revealed that the injected current density is related to total device thickness, and that it is strongly dependent on the thickness of both hole transport layer and electron transport layer. The reduction of either the TPD layer thickness or Alq$_3$ layer thickness led to the increase in current density, with the TPD layer thickness having a more profound effect.

For all devices except one, a relatively high value of luminance of 1000 cd/m^2 can be obtained at a relatively low current density (less than 60 mA/cm^2). The operating voltage for the luminance value of 1000 cd/m^2 is also relatively low, which ranges from 9

to 15 V for different device configurations. Both the luminous efficiency and external quantum efficiency are heavily influenced by the thickness of the $Ir(piq)_3$ layer and the charge balancing effect which is controlled by the layer thickness in other organic layers. It was found that the proper $Ir(piq)_3$ layer thickness and charge balancing effect leads to the efficient emission from the $Ir(piq)_3$ layer, which in effect could possibly boost the overall device emission efficiency. Since $Ir(piq)_3$ is a phosphorescent material, its emission does not only result from singlet exciton but also from the triplet exciton. As a result, phosphorescent material such as $Ir(piq)_3$ is capable of higher emission efficiency than fluorescent materials such as DPVBi and Alq_3.

For OLEDs to be used in general solid-state lighting application, both CIE color coordinate and color stability are important criteria. CIE color coordinate is an international standard developed for the specification of color matches for an average observer. For white illuminants, the CIE color coordinates should be as close as possible to the neutral white point (0.333,0.333), which represents the pure white light. Color stability is described by the shift in CIE color coordinates with respect to luminance level. In order to provide consistent illumination color at all luminance levels, the shift in CIE color coordinates with respect to luminance level should be as small as possible. A particular OLED configuration with layer thickness of TPD (600Å)/ DPVBi (110Å)/

$Ir(piq)_3$ (40Å)/Alq_3 (450Å) was found be to capable of producing the CIE color coordinates close to the neutral white point (0.333,0.33) for the widest luminance level range, from (0.357,0.358) at the luminance level of 140.4 cd/m^2 to (0.303,0.360) at the luminance level of 1321.7 cd/m^2. In conclusion, a white OLED suitable for lighting application has been demonstrated by fine-tuning the device characteristics with the thickness alteration of the component organics layers.

5.2 Future Work

Despite the fact a particular configuration of the white-color OLED as an acceptable white light illuminant has been demonstrated in this work, there are still many methods that may lead to further device performance enhancement and may be explored in details in the future.

First, the morphology of the interface between each layer has been reported to have significant impacts on the device performances. Since the typical organic layer overall thickness of the OLEDs is less than 100 nm, the ITO surface morphology, in particular, plays a critical role in reducing the occurrence of localized defects such as pinholes. Also, the successful fabrication and investigation of ultra-thin layer devices will also heavily

depend on the surface morphology at each individual layer interface. Enhancements in device performance are possible through surface morphology improvement. The color stability and the luminous efficiency remain important issues for OLED before they can become suitable for solid-state lighting applications. Further enhancement of the color stability and luminous efficiency is possible by utilizing more complex structures and by the addition of extra organic materials. Finally, the lifetime and reliability of OLED also remain critical issues in the deployment of the OLED technology in display and lighting applications. Further analysis and enhancement of the lifetime and reliability may be explored in detail in the future.